Design characteristics and some applications of the ruby laser

Whitman, P.

DESIGN CHARACTERISTICS AND SOME APPLICATIONS OF THE RUBY LASER.

BY

P. WHITEMAN, DIP. TECH., A.INST.P.

A THESIS SUBMITTED IN CANDITURE FOR A DEGREE OF MASTER OF SCIENCE.

UNIVERSITY OF DURHAM.

NOVEMBER 1966.

A B S T R A C T.

This thesis is concerned with the solid state ruby laser, and the determination of the optimum design parameters upon which its performance is dependent.

The voltage, current and light output characteristics of the linear xenon flashtubes used for excitation are measured for different discharge circuit conditions, and the efficiency of laser operation is related to these different operating conditions. It is shown that two factors affect the coupling efficiency of the cylindrical ellipse which is used to transfer the radiation emitted by flashtube to the ruby rod: its geometric shape and the reflectivity of its walls. The theory describing the coupling efficiency of the single elliptical cavity is extended for the case of multiple section elliptical cavities, and experimental measurements of laser output energy and efficiency are made for both single and double cavities which are found to agree with theoretical predictions. A theory relating the optimum laser mirror reflectivity to the ruby dimensions and pump energy is developed, for which laser output energy measurements made with ruby rods from 2" to 6½" in length are found to be in agreement. This work also enables the total internal loss of each ruby to be determined and thus gives a method of assessing their quality. It is also demonstrated that the laser efficiency

TEMPERATURE AND THE LASER OUTPUT ENERGY IS MEASURED AT
is strongly dependent upon the ruby temperatures of up to 50° C above ambient conditions.

The last chapter is concerned with a theoretical and practical assessment of the application of the ruby laser for machining and welding.

A C K N O W L E D G E M E N T S.

The author wishes to thank Dr. J. S. Thorp for his help and guidance and for the considerable amount of time which he has spent to bring this work to completion; also the Directors and Research Manager of the International Research and Development Co. Ltd., for their co-operation and financial assistance.

C O N T E N T S.

C O N T E N T S (CONTD)

Chapter 1. Introduction.

1.1 Historical Background.

As early as 1917 Einstein advanced the idea of the stimulated emission of radiation. The use of stimulated emission for microwave applications was developed by WEBER (1959), GORDON et al (1955) and BASOV (1955). A natural development of this work was its extension to the optical region. This was mainly due to SCHAWLOW and TOWNES (1958) and (1960), and it led to the development of laser which is derived from Light Amplification by the Stimulated Emission of Radiation.

The first workers to observe spectral narrowing and a reduction in lifetime due to an inverted population in the optical region was MAIMAN (1960) using ruby. These observations were extended by COLLINS et al (1960) who demonstrated the coherence and directionality of the stimulated radiation and who also observed the now characteristic relaxation oscillations in the output radiation.

About the same time as Maiman was developing the ruby laser, JAVAN (1961) made the first gas laser. He excited a mixture of helium and neon in a discharge tube and obtained stimulated radiation the spectral purity, directionality and coherence of which were far superior to the ruby laser light. This is almost entirely due to the gas being an almost perfect optical medium, in contract to solids such as ruby which exhibit various inhomogeneities. Laser action has now been observed for many different gas systems and output wavelengths from the ultra-violet to the infra-red have been generated.

Another important advance in 1962 was the development of the semiconductor laser by HALL (1962), NATHEN (1962) and QUIST (1962), by injecting a high current density in a gallium ARSENIDE p-n junction. They demonstrated line narrowing for output radiation at about 0.84μ.

Both gas and semiconductor lasers are outside the scope of this thesis which only considers solid state laser systems, and in particular the ruby laser system.

L.2 Solid State Lasers.

Before discussing different laser media it is necessary to divide the actual materials into two main groups, three-level and four-level systems; see figures 1a and 1b.

A four-level system is characterised by a laser terminal level which is greater than kT above the ground state level, where k is BOLTZMANN'S constant and T the absolute temperature. A rapid rate of spontaneous transition from the terminal to the ground state is required for laser action to be maintained. Examples of this type of laser include the rare earth doped materials such as neodymium in glass.

With the three-level system, the laser terminal state is less than kT above the ground state, and in particular for ruby the ground state is the laser terminal state, see figure 1b.

The necessary requirements for laser action are:-

1. At the laser frequency the active medium should have little absorption.
2. The metastable upper laser LEVEL should terminate in a radiative

process.

3. The laser material should possess absorption at the pump frequency.

4. Should be of a high optical quality such that scattering by optical inhomogeneities does not shorten the lifetime of the upper laser level. Although the question of material preparation is not considered here it should be noted that the need for high optical quality material, particularly ruby, has prompted much work on perfecting crystal growing techniques.

To excite the laser material and achieve a population inversion necessary for laser action (see section 2.2) high energy density radiation of the correct wavelength must be incident on it. Most solid state laser materials require excitation radiation in the visible region of the spectrum and such novel techniques as exploding wires STEVENSON et al (1963) and HALL and CHURCH (1963), the use of the sun's radiation KISS et al (1963) and KECK et al (1963), and the plasma pinch COLGATE (1961) have been investigated.

However two main pumping arrangements have arisen. First, the use of a helical flash tube contained in an reflecting cylinder, the laser material being placed inside the flash tube helix. Second, a linear flash lamp arranged on an elliptical reflector, the laser material being at one focus and the flash lamp at the other. Both these systems are equally effective in exciting laser material, except that the helical flash tube system has a higher threshold energy requirement, CONGLETON et al (1964). However, this disadvantage is

compensated by the fact that they can dissipate considerably more electrical energy because of their much longer discharge tube length.

The linear flashtube arrangement is the one considered in this thesis.

1.3 The Ruby Laser.

The laser radiation is due to 3d electronic transitions of Cr^{3+}. The Cr is contained in a matrix of Al_2O_3 to the concentration of about 0.05%.

The ruby crystals are usually manufactured in cylindrical form in sizes up to 13" long and 1" diameter. The ends are polished flat to $\lambda/10$ and parallel to within 2 seconds of arc. The laser optical cavity is formed by reflecting multilayer dielectric coatings which are deposited on the ruby end faces or which are held external to these faces but aligned parallel to them. In the Fabry-Perot cavity so formed the laser oscillations are amplified and part of the radiation in this cavity is extracted by making one of the reflectors partially transmitting (see sections 2.2 and 2.3).

Figure 2 shows a typical trace of laser radiation against flashtube excitation. Fluorescence begins immediately after the pumping radiation starts but typically stimulated emission does not begin until half to one millisecond later.

The irregularity of the laser pulses and their lack of reproducibility is due to a number of factors. One is that the laser is a multimode resonater for which the oscillations rise and decay at different rates for the different modes.

Also the crystal does not receive uniform pump light and thus the stimulated emission does not start at the same time and rate in all portions of the laser crystal.

The wavelength of the ruby radiation is 6943A° at 300°K and 6934A° at 77°K. From published data, LENGYAL (1966), the wavelength where T is in °C in the range 20°C to 80°C is given.

$$\lambda = [6943.25 + 0.068\ (T-20)]\ \text{A}^\circ \qquad (1.1)$$

The polarization of the laser beam depends on the crystal orientation, NELSON & COLLINS (1961). The output is unpolarized for 0° orientation ruby for which the optic axis of the ruby is parallel to cylinder axis. The output is plane polarized for 90° orientation ruby, when the E vector is perpendicular to the plane defined by the cylinder rod axis and optic axis of the material.

The beam divergence is typically found to be about 5 milliradians, but this figure is very dependent on the optical quality of the ruby crystal. This figure is much greater than that expected from diffaction theory which would define a beam divergence of

$$\frac{1.22\lambda}{d} \quad \text{radians} \qquad (1.2)$$

where d is the system aperture which can be taken as the diameter of the ruby. For a laser rod of diameter d = 1 cm, the theoretical beam divergence would be about 0.1 milliradians at λ = 6943A°.

1.4 Solid State Lasers other than Ruby.

The only ion, other than Cr^{3+} in ruby, which lases due to 3d electronic transitions is nickel in magnesium fluoride, JOHNSON et al (1963).

There is a very large group of four-level systems from which the laser radiation is due to unpaired electrons in 4f shells of the rare earth metals. Laser action has been observed for the following trivalent ions, erbium, europium, gadolinium, holmium, neodymium, praseodymium, thulium and ytterbium and for the following divalent ions samarium, thulium and dysprosium.

The most important of these is neodymium which has been observed to exhibit laser action in many host materials such as borosilicate glass and calcium tungstate; in each case the neodymium substitutes for divalent calcium. The principal laser wavelength is 1.06μ, but the linewidth of the transition can be as great as 100A$^{\circ}$. This is due to the splitting of the upper and terminal levels (The latter being 2000cm^{-1} above the ground level), and arises principally because of the local unbalance of charge caused by the substitution of a trivalent ion in a divalent lattice. This local charge imbalance at each neodymium site can be neutralised in a variety of ways, e.g. by calcium vacancies, interstitial oxygen atoms and the pairing of neodymium ions. Thus each neodymium ions give rise to its own spectrum and thus the complete spectrum from any material is very complex.

The only laser radiation which arises from 5f electronic transitions is from trivalent uranium in either calcium, strontium or barium fluoride.

1.05 Q-Switching.

This technique was first suggested by HELLWARTH (1961) and has made it possible to generate single, time controlled pulses of short duration. Pulses with half peak widths as short as 10 nano-seconds

and of peak powers of up to several gigawatts have been generated. These results may be compared with uncontrolled laser oscillations which are usually of about a millisecond duration and of about 100 kilowatts peak power.

The laser can be considered as a cavity resonator which is characterised by a particular value of Q and gain. If during the pumping period a loss is induced into the system, the Q is reduced and the gain can be made to approach a much higher value before laser oscillations occur. In this high gain condition the system is quickly switched to its original low loss state. Now the gain is much higher than for the uncontrolled laser oscillator and thus the laser pulse develops much more rapidly and in principle all the energy stored in the crystal can be extracted in a single short duration pulse.

Figure 3. shows a series of oscilloscope photographs which compare the uncontrolled and 'Q' switched laser pulses. Trace 1 is the uncontrolled pulse on a time base of 200μ second per division which is expanded on a time base of 5μ second per division on Trace 2. Trace 3 is the 'Q'-switched laser pulse on a time base of 200 μ second per division which is expanded on Trace 4 on a time base of 1μ second per division.

Methods of increasing the loss normally involve the interruption of the path between the reflecting mirrors forming the optical cavity. The following are some of the effects which have been used: Faraday rotation in glass, HELFRICH (1963); ultrasonic diffraction, DEMARIA (1963), mechanical devices HELLWARTH (1961); Kerr and Pockel cells,

McCLUNG & HELLWATH (1962); and passive bleachable dyes such as the phthallocyanines, KAFALAS et al (1964).

Q-switching has developed into a specialised study of its own and it is not included in this work.

1.6 Uses of the Ruby Laser.

The development of the laser and the generation of coherent light has made it possible to study multiphoton processes, e.g second harmonic generation, the theory pertaining to which was first formulated by LAX (1962) and KLEINMANN (1962). The first workers to observe the phenomena were FRANKEN et al (1961) who produced light at 3472A° from ruby radiation at 6943A°. The most efficient materials for harmonic generation are lithium niobate, and potassium or ammonium dihydrogen phosphate, and for maximum efficiency the orientation of the crystal should be such that the phase velocities of both the fundamental and second harmonic wave are the same. This is termed an index matched condition and the refractive index of the crystal is thus the same for both waves. By using high power Q-switched pulses efficiencies as high as 20% have been reported by TERHUNE et al (1963).

Another application for which the Q-switched laser is used is rangefinding or pulsed optical radar. The principle is that the time for an emitted laser pulse to travel to the target and to be scattered back to a photomultiplier detector is measured and used to determine the distance of the target. Apart from the obvious military uses this technique may find use for other applications such as the continuous monitoring of cloud base height for aviation control at

airports. A more recent meteorogical application is for the study of atmospheric scattering due to air turbulence, dust particles, and cloud, for which measurements have been made up to heights of 100Km, NORTHEND et al (1966).

Ruby laser light at 6943A° is in the transmission region of the clear media of the eye. Because of this one immediate application has been the treatment of retinal detachments by photocoagulation. Before the laser, the common method of treatment was by a high power xenon arc lamp. However the reaction of the patient to the application of the extremely bright arc light is to move the eye, and as the application may be of a few seconds duration, a local anaesthetic is required. The situation with the laser is very different since sufficient energy to coagulate the choroid can be delivered in about one millisecond and the patient experiences no sensation of heat or pain, VERNON-INGRAM et al (1965). The laser photocoagulator is now being used in many hospitals and standard equipment is available for purchase.

The ruby laser is also being used in the field of photography for a number of applications. These include high speed photography, McEWAN (1966) for which a Q-switched pulse is used to freeze a fast moving event; ~~Schleirlen~~ SCHLIERIN photography, OPPENHEIM (1966), which is now being used for the observation of the electric breakdown of spark gaps for which a source considerably brighter than the arc is required. Ruby lasers have also been used for pulsed holography. BROOKS et al (1966) with the possible application of recording and measuring stress and vibration in complex structures and for other

inspection procedures.

The high peak power, easily focussed and directed, laser radiation is also finding application for both micromachining and microwelding operations. This subject is considered in detail in chapter 9.

TABLE 1.

PRINCIPLE SOLID STATE LASER MATERIALS AND OPERATING WAVELENGTHS.

Active Ion	Host	Wavelength (μ)
Cr^{3+}	Al_2O_3	0.6943
Nd^{3+}	GLASS	1.06
	$CaWO_3$	1.06
Ho^{3+}	$CaWO_3$	2.05
Er^{3+}	$CaWO_3$	1.61
Pr^{3+}	$CaWO_3$	1.05
Eu^{3+}	Y_2O_3	0.6113
Tm^{3+}	$CaWO_3$	1.91
Gd^{3+}	GLASS	0.3125
Yb^{3+}	GLASS	1.015
Sm^{2+}	CaF_2	0.708
Dy^{2+}	CaF_2	2.36
Tm^{2+}	CaF_2	1.116
Ni^{2+}	MgF_2	1.622
U^{3+}	CaF_2	2.24

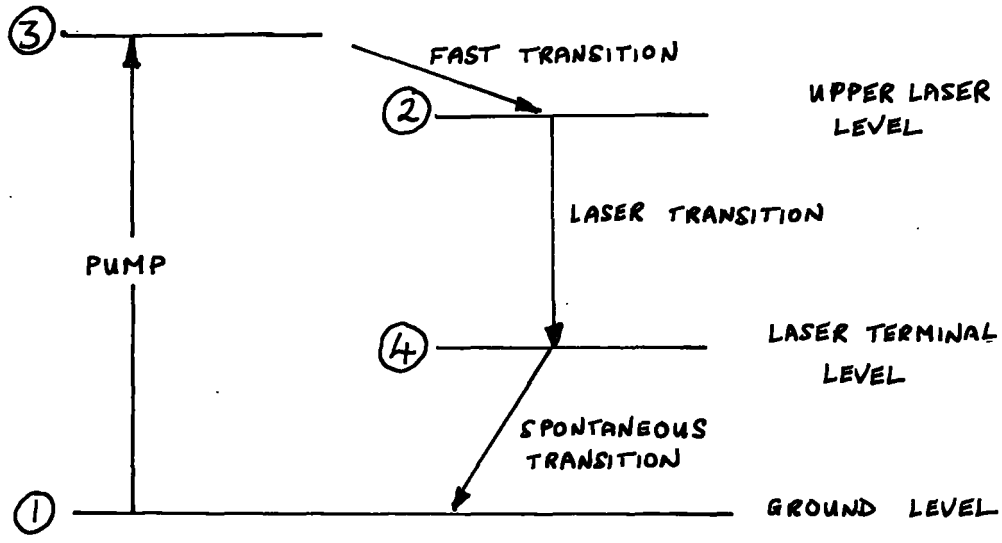

FIG 1a SIMPLIFIED 4-LEVEL SYSTEM

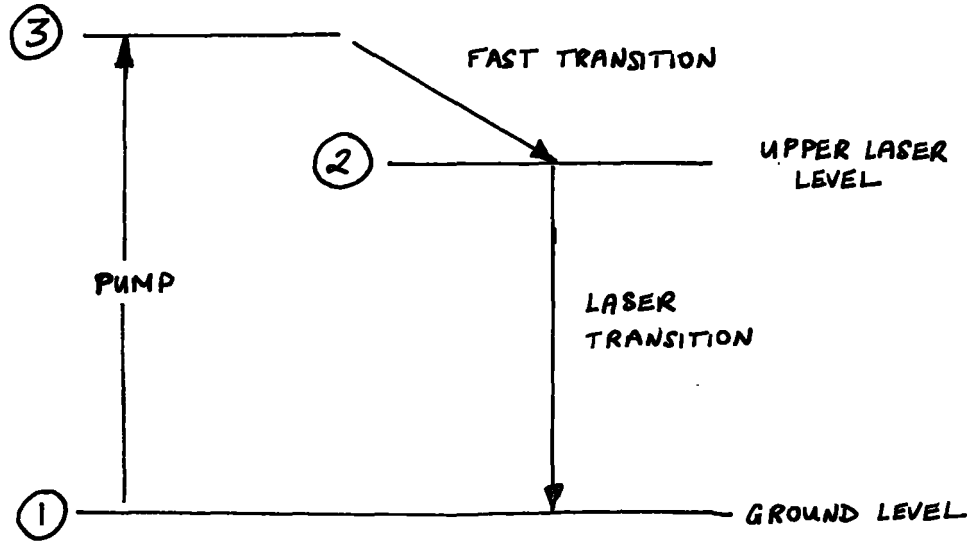

FIG 1b SIMPLIFIED 3-LEVEL SYSTEM

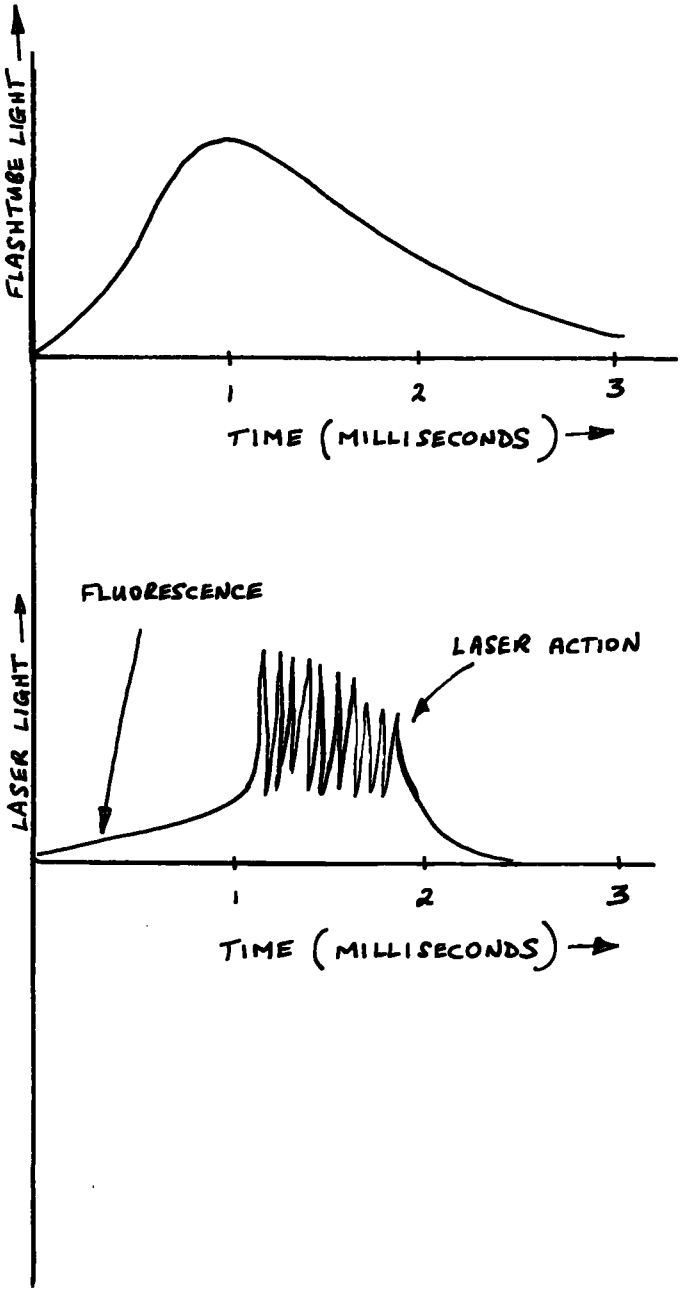

FIG 2. RELATIONSHIP BETWEEN FLASHTUBE LIGHT AND LASER LIGHT

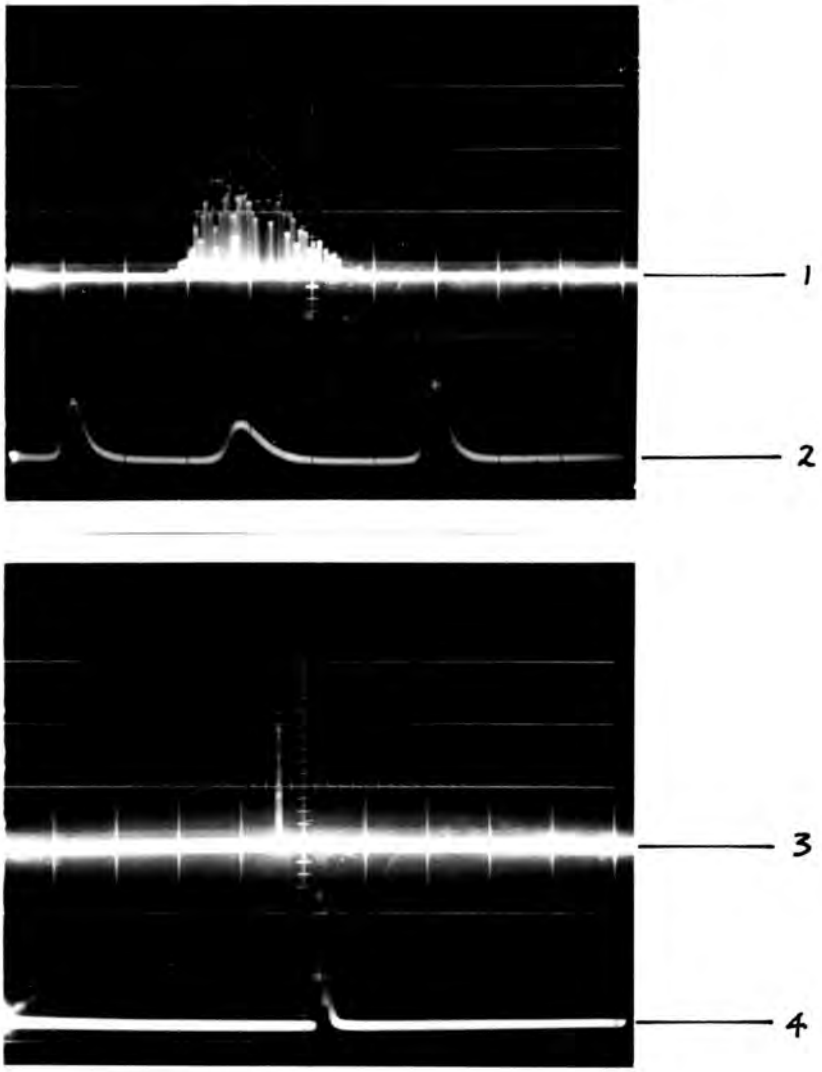

FIG 3. UNCONTROLLED AND Q-SWITCHED LASER OSCILLATIONS.

Chapter 2 Theoretical Background

2.1 Emission and Absorption of Radiation

Atoms and ions can exist in stationary states each of which corresponds to a definite energy level and which is characterised by a set of quantum numbers. When two or more states have the same energy the level is called degenerate and the number of states with the same energy is the multiplicity of the level. Transitions between stationary states can occur with either the emission or absorption of radiation according to Bohr's frequency criterion:-

$$h\nu = E_n - E_m \qquad (2.1)$$

where ν is the frequency of the radiation, h is Plank's constant and E_n and E_m are the energies of the two levels.

The lowest energy level is termed the ground level and an atom in the ground level can only absorb radiation. When the atom is in an excited energy level it may change to a lower level with the emission of radiation without any external cause. This phenomena is termed spontaneous emission, and the probability that an atom in level n will spontaneously change to a lower level m is denoted A_{nm}. If the number of atoms in level n is N_n, the total number of transitions per second is $N_n A_{nm}$. Spontaneous emission will emerge from the collection of atoms in random phase which will therefore act as an incoherent source.

Transitions can also take place under stimulation by electromagnetic radiation. This is termed stimulated emission. The probability that an atom in level n will be stimulated to change

to level m is denoted $u_\nu B_{nm}$, where u_ν is the radiation density at the frequency $\nu = \nu_{nm}$ defined by equation (2.1) The number of stimulated transitions per second is:-

$$[u_\nu B_{nm} N_n] \tag{2.2}$$

An atom can also absorb energy in moving from level m to level n . The probability of such an event is $u_\nu B_{mn}$ and the number of atoms excited per second is

$$[u_\nu B_{mn} N_m] \tag{2.3}$$

where N_m is the number of atoms in level m .

The relations between the A's and B's were first derived by EINSTEIN (1917) and they are

$$g_n B_{nm} = g_m B_{mn} \tag{2.4}$$

where g_m and g_n are the multiplicities of the levels m and n respectively and

$$A_{mn} = \frac{8\pi h\nu^3 \eta^3}{c^3} B_{mn} \tag{2.5}$$

where η is the refractive index of the absorbing medium and c the velocity of light.

The spontaneous emission is independent of the incident radiation, whereas the stimulated emission is phase coherent with it. For amplification to occur, the energy given out by the induced emission must be greater than the energy absorbed. From equations (2.2), (2.3) and (2.4) it is seen that for this to occur $\frac{N_n}{g_n} > \frac{N_m}{g_m}$ This is termed a population

inversion, since under thermal equilibrium conditions the distribution of atoms would be given by Boltzmann's equation.

$$\frac{N_m}{g_m} = \frac{N_n}{g_n} \exp\left[\frac{E_n - E_m}{kT}\right] \qquad (2.6)$$

and since $E_n > E_m$ then $\frac{N_n}{g_n} < \frac{N_m}{g_m}$

If the energy levels m and n were perfectly sharp the emitted radiation would have a frequency of exactly $\nu_o = \nu_{mn}$, however the levels are not exactly sharp so the radiation is spread about this frequency. The line width may be estimated using the Heisenburg Uncertainty Principle. The spread in energy of an excited state is ΔE defined by

$$\Delta E \cdot \Delta t \approx \frac{h}{2\pi}$$

Δt is the average time spent by an atom in an excited state which is the inverse of the spontaneous emission probability A_{nm}. Thus the spread in energy of the emitted radiation can be written as:-

$$\Delta E \approx \frac{hA_{nm}}{2\pi}$$

so that the line width in terms of frequency is:-

$$\Delta\nu \approx \frac{A_{nm}}{2\pi} \qquad (2.7)$$

The exact shape of the line is dependent upon the mechanism which shortens the lifetime of the excited state. Processes limiting lifetime include the collision of the radiating atom with the lattice which gives a Lorenztian line shape. Other line shapes

may occur, e.g. the Gaussian line shape may arise from mechanisms which create a distribution of atomic frequencies such as the random variation in the distribution of atoms in a solid. The mechanism of line broadening in solids has been extensively received by DEXTER (1958). For the purpose of calculation, a Lorenztian line shape is usually assumed. This gives a normalised line shape factor of, LENGYAL (1966):-

$$S(\nu,\nu_o) = \frac{\Delta\nu}{2\pi}\left\{\frac{1}{(\nu-\nu_o)^2 + (\Delta\nu/2)^2}\right\} \qquad (2.8)$$

such that $\int_{-\infty}^{+\infty} S \, d\nu = 1$

and the peak value of $S(\nu,\nu_o)$ is:-

$$\frac{2}{\pi\Delta\nu} \qquad (2.9)$$

When light of constant intensity Io, but variable frequency is incident upon a medium, the intensity of the light at frequency ν at a depth x is :-

$$I = Io \exp(-b_\nu x) \qquad (2.10)$$

The curve of I against ν is shown in Figure 4. The absorption coefficient, b_ν, against frequency is shown in Figure 5 and is a maximum value b_o at the centre frequency ν_o. The relationship between the total area under curve shown in figure 5, and the Einstein coefficients, and the atomic distribution in the levels m and n is known as the Fuchtbauer and Ladenburg equation which gives:-

$$\int b_\nu \, d\nu = C \left[N_m - \frac{g_m}{g_n} N_n \right] \qquad (2.11)$$

where $$C = \frac{\lambda_0^2 A_{nm}}{8\pi\eta^3} \frac{g_n}{g_m}.$$

If the ratio $\frac{Nn}{Nm}$ is small, i.e. unexcited material then

$$\int b_\nu' \, d\nu = C N_0 \qquad (2.12)$$

Where N_0 is the total number of atoms in the system being considered (which equals N_m for unexcited material and equals $N_m + N_n$ for excited material). The constant C is termed the integrated absorption cross-section per atom and the quantity $\sigma_\nu = \frac{b'_\nu}{N_0}$ the unexcited absorption cross section per atom. At the centre frequency $\nu = \nu_0$, $b'_\nu = b'_0$, the peak value of $\sigma_\nu = \sigma_0 = \frac{b'_0}{N_0}$, which from equation (2.9) can be written.

$$\sigma_0 = \frac{2C}{\pi \Delta\nu N_0} \qquad (2.13)$$

For solid state ruby the experimental value of σ_0 is 2.5×10^{-20} cm^2. MAIMAN (1961)

2.2 Threshold Condition.

When population inversion occurs for the levels m and n, then equation (2.11) gives a negative value of the integrated absorption cross-section coefficient. In a material under this condition an incident light wave grows according to equation (2.10), since b_ν is negative then

$$I = I_0 \exp (b_0 x) \qquad (2.14)$$

and thus amplification will occur.

The laser is a device which consists of a pair of parallel mirrors, between which is placed a piece of material, e.g. ruby, that is in this state of population inversion and negative absorption due to the absorption of the excitation light at the pumping wavelength. The device is represented schematically in figure 6. In order to obtain a power output from the laser material one of the mirrors is made partially transmitting while usually the other mirror is as near 100% reflecting as possible. The transmittance T, reflectivity R and loss Q are related by $R + Q + T = 1$. When good quality dielectric mirrors are used Q may be neglected (about 0.1%) and $R + T = 1$.

As a result of the spontaneous and stimulated emission in the laser optical cavity light is generated in the laser material. Light that does not pass through the sides travels the length of the laser material and is reflected back and forth between the reflecting mirrors. At each reflectance the fraction $(1 - R)$ of the energy is lost. Oscillations will only be maintained in the system if the gain is sufficient to compensate for the energy loss at the end of the laser material. If the reflection coefficients at the ends of the rod are R_1 and R_2, the gain in the rod is defined by equation (2.14); then during a double pass of the laser material the system gain will be given by

$$G = R_1 R_2 \exp (2b_0 L)$$

where L is the length of the laser rod. This may be written as

$$G = \exp 2 (b_\nu L - \gamma)$$

where $\gamma = -\log (R_1 R_2)^{\frac{1}{2}}$. When $G<1$ oscillations will die out, when $G>1$ oscillations will grow. The condition $G=1$ is termed the threshold condition and this occurs when

$$b_o = \frac{\gamma}{L} \qquad (2.15)$$

where b_o is the maximum value of b_ν for excited material. Since the maximum value of b_o only occurs over a very narrow spectral range, the output of the laser will be sharply peaked. From equations (2.11) and (2.12).

$$\frac{b_o}{b_o'} = - \left[\frac{N_m - g_m/g_n N_n}{N_o} \right]$$

Thus

$$\frac{\gamma}{L} = - \sigma_o \left[N_m - g_m/g_n N_n \right] \qquad (2.16.$$

The usual form of ruby laser is for $R_1 = 1$ and $R_2 = R$. As mentioned in section 1.2 ruby is a three level system. State m, the ground state will in future be called state 1; and state n, the upper laser state will be called state 2. The total number of atoms is No which equals $N_1 + N_2$, Since the life-time of the pump level 3 is very short. Also for ruby, as will be discussed in Section 2.4, $g_1 = g_2$. Equation (2.16) then reduces to

$$N_2 = \frac{No}{2} - \frac{\log R}{4 \sigma_o L} \qquad (2.17)$$

Equation (2.17) is known as the THRESHOLD CONDITION. It is seen that for no losses ie. R = 0, then $N_2 = {}^{No}/_{2}$. This means that at least 50% of the ground state atoms must be pumped to the upper laser level for the minimum threshold population inversion to be exceeded.

2.3 Emission Line Structure.

The field within the laser Fabry-Perot cavity may be regarded as the superposition of plane waves travelling back and forth, see figure 6. The plane waves that travel perpendicular to the mirrors form a standing wave pattern which leads to reinforcement when the distance between the mirrors L' is an integral multiple of half wavelengths. This occurs when $n\lambda = 2L'\eta$ where n is an integer. This gives frequency separation of

$$\Delta\nu_1 = \frac{c}{2L\eta} \qquad (2.18)$$

between different axial resonant modes.

This is a simplified picture since the laser material is three dimensional and the phase conditions of the other dimensions must also be considered. For a cylindrical laser resonator the resonant frequencies are found from, LENGYAL (1966).

$$\left[\frac{\chi_{\ell m}}{r}\right]^2 + \left[\frac{\pi n}{L'}\right]^2 = \left[\frac{2\pi\nu\eta}{c}\right]^2 \qquad (2.19)$$

where .r. is the radius of the rod and $\chi_{\ell m}$ is the m^{th} zero of the Bessel Function of order ℓ . The axial modes, equation (2.18)

are obtained for χ_{00} which is zero. The modes for which χ_{lm} is not zero are called transverse modes. From equation (2.19) the separation of the first transverse mode , χ_{01} = 2.4, from the axial mode, $\chi_{00} = 0$, is given by

$$\Delta\nu_2 = \frac{\chi_{01}\, c^2}{8\pi^2 r^2 \eta^2 \nu} \qquad (2.20)$$

For a typical ruby, L^1 = 15 cms, r = $\frac{1}{2}$ cm, η = 1.76 and λ = 6943A° equations (2.18) and (2.20) give $\Delta\nu_1 = 10^9$ cps and $\Delta\nu_2 = 10^5$ cps. Since the fluorescent line width of ruby is about 3×10^{10} cps, COLLINS AND WHITE (1963), a large number of both axial and transverse modes can be simultaneously amplified.

2.4 Spectroscopy of Ruby.

The ground level of the free Cr^{3+} ion is characterised by the spectroscopic symbol ^4F, this level is a quartet as indicated by superscript 4 and its multiplicity is 28. The next lowest group of states is the ^2G which has a multiplicity of 18.

In ruby the chromium ion is surrounded by a crystal field of nearly octohedral symmetry McCLURE (1959), which causes the splitting of the levels of the free ion. The ground state of the free Cr^{3+} ion splits into three levels, these are termed the $^4F_1$, $^4F_2$ and $^4A_2$ of multiplicates 12, 12 and 4 respectively. The next level, the ^2G, splits into four sub-levels are termed $^2A_1$, $^2F_2$, $^2F_1$ and ^2E with multiplicates of 2, 6, 6 and 4 respectively.

The relevant levels for the stimulated emission of ruby are shown in figure 7. The ^2E, which constitutes the level 2 in the

simplified energy level diagram figure 1b, is actually split into two closely spaced levels, the $^2E(A)$ and $^2E(E)$. These levels are only 29 cm^{-1} apart so at room temperature they are nearly equally populated.

The absorption of ruby is shown in figure 8. The peaks of the absorption curves correspond to the $^4F_2$ and $^4F_1$ levels which jointly constitute the level 3 in the simplified energy level diagram figure 1b.

Fluorescence of ruby consists of the R_1 and R_2 lines from the $^2E(E)$ and $^2E(A)$ levels respectively. Ordinarily laser action takes place only for the R_1 line because the transition probability is greater for this line. The ratio of transition probabilities corresponding to R_1 and R_2 lines is 7 to 5, McCLURE (1962).

For the R_1 line the following data is applicable at room temperature $b^1 = 0.4\ cm^{-1}$. $\sigma_o = 2.5 \times 10^{-20}\ cm^2$ and the lifetime of the level is 3 milliseconds.

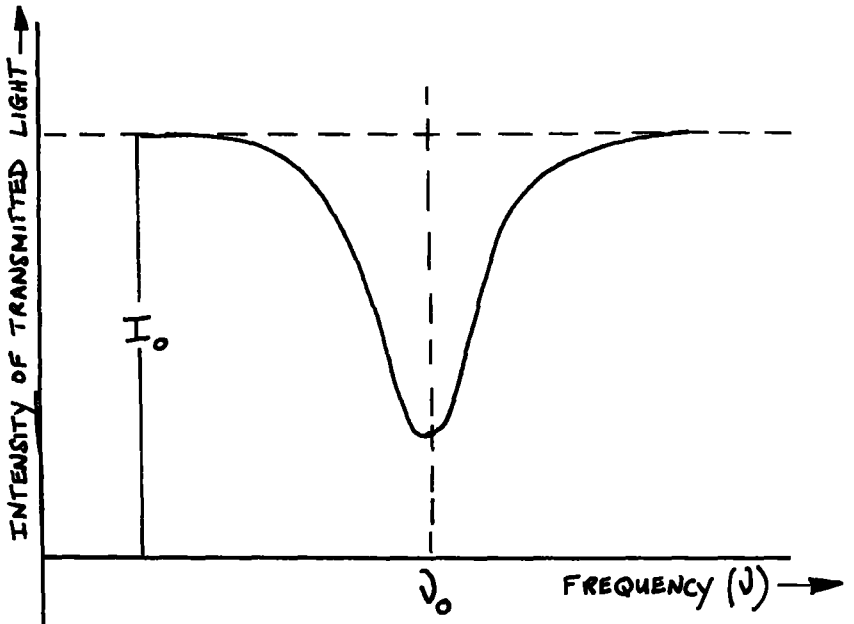

FIG 4. FREQUENCY DEPENDENCE OF THE TRANSMITTED LIGHT

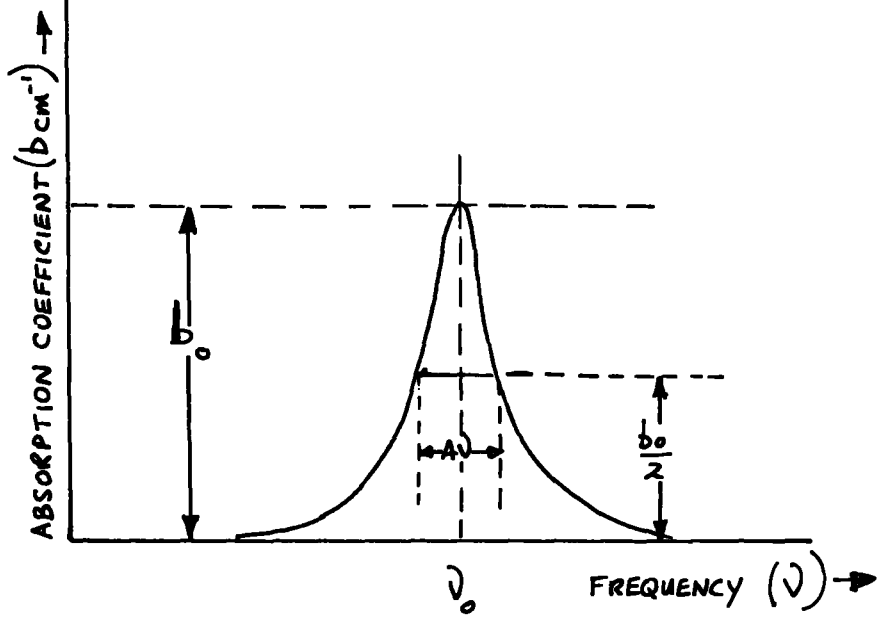

FIG 5. VARIATION OF ABSORPTION COEFFICIENT WITH FREQUENCY.

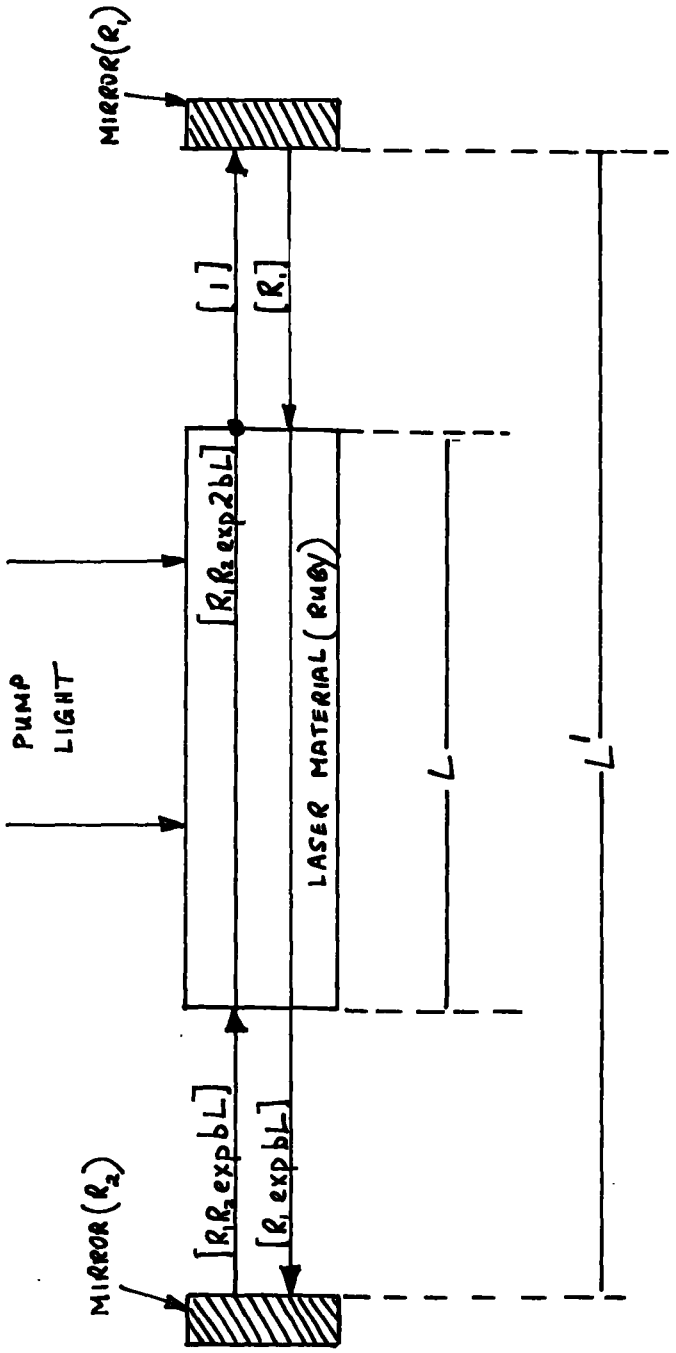

FIG 6. LASER AS A CAVITY RESONATOR

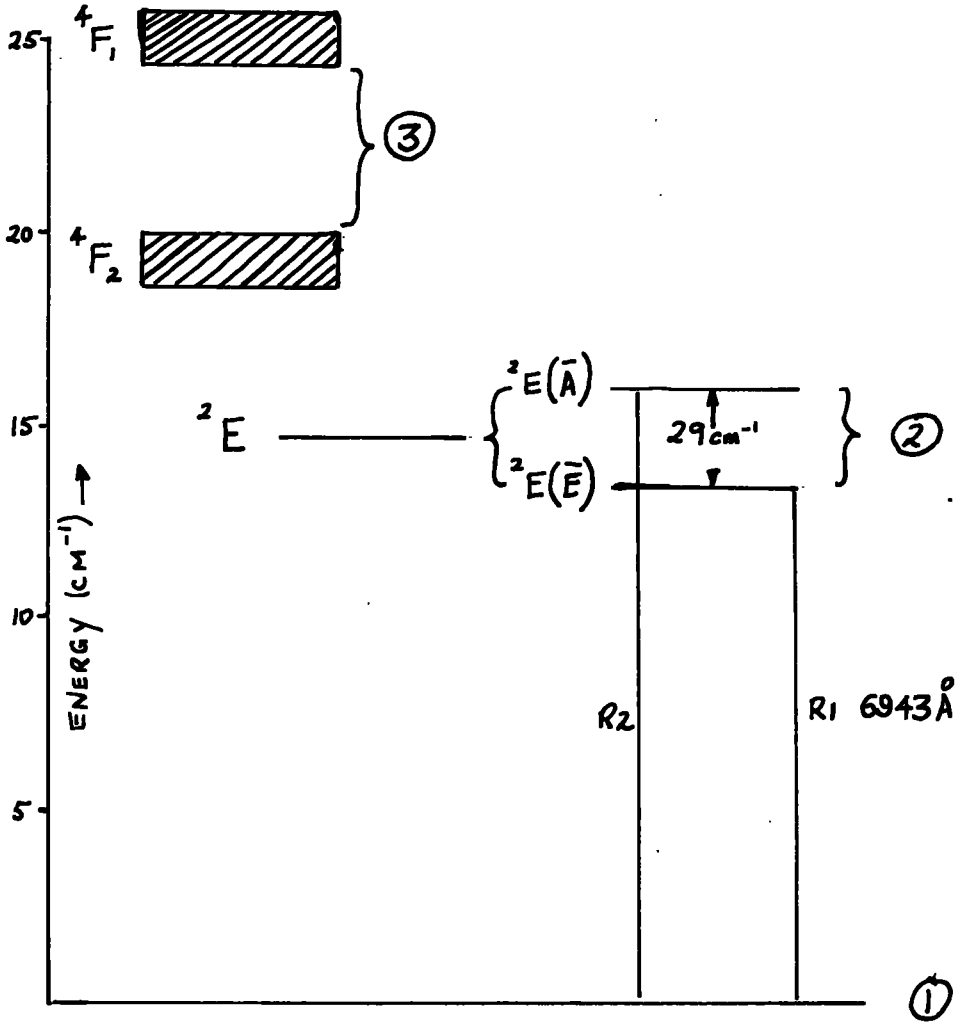

FIG 7 ENERGY LEVEL DIAGRAM OF RUBY.

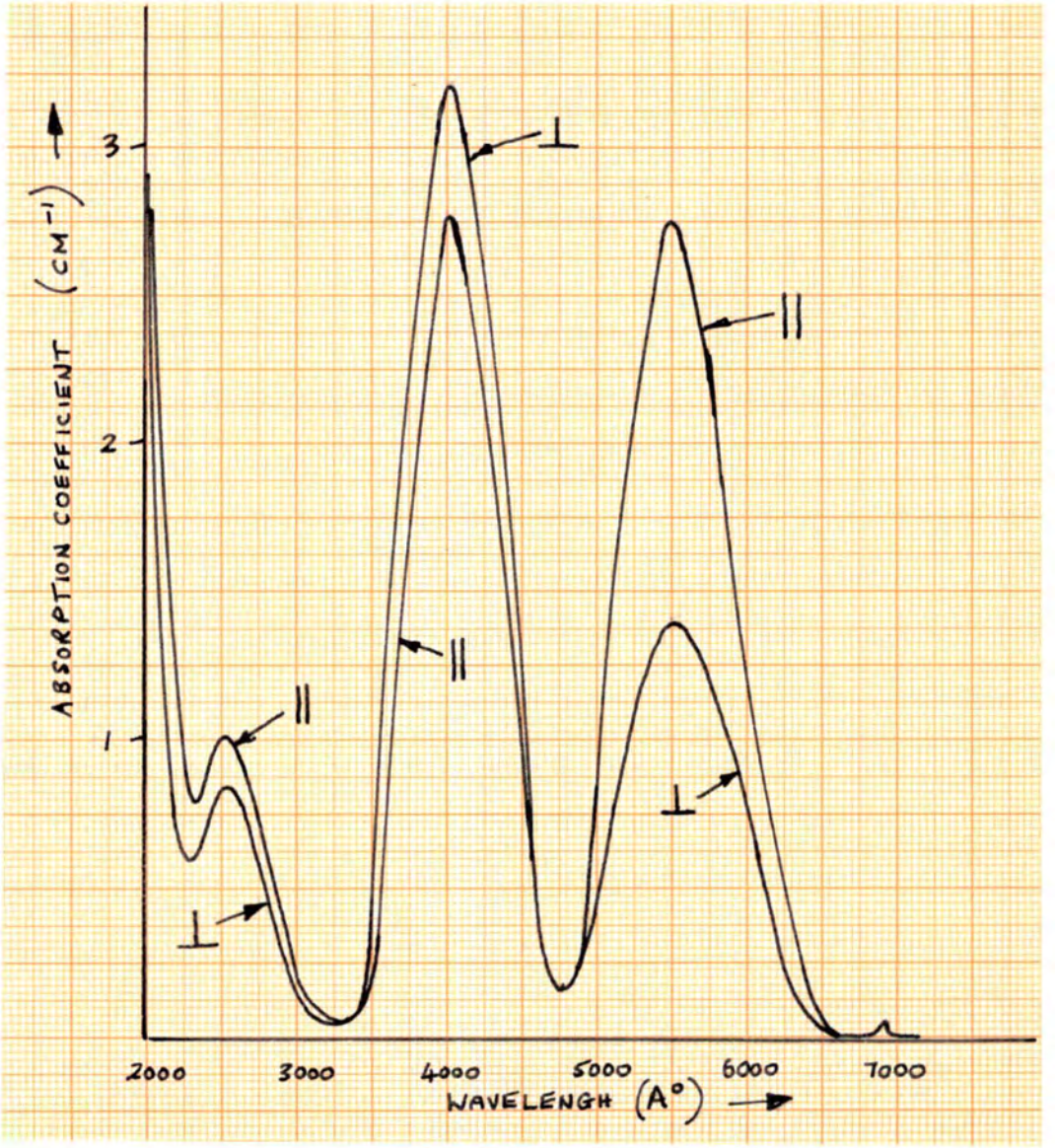

FIG 8 ABSORPTION COEFFICIENT OF RUBY FOR LIGHT INCIDENT PARALLEL TO AND PERPENDICULAR TO THE OPTIC AXIS

Chapter 3.

General Design Characteristics.

The solid state ruby laser is a device which amplifies light by means of stimulated emission of radiation. Its performance is dependent on several design parameters which are now summarised. These are discussed in greater detail in the subsequent chapters.

The laser configuration to be discussed consists of a cylindrical sample of ruby located at one line focus of a polished eliptical cylinder which acts to focus the light emitted from a linear flashtube which is positioned at the other line focus. The light generated by the ruby is amplified in the optical cavity which is formed by the ruby and two reflecting mirrors. One of the mirrors is partially transmitting so that some of the radiation is emitted from the optical cavity.

The linear flashtube is energised by discharging a capacitor bank through it, A series inductance is also placed in the circuit to limit the peak current. An exact calculation of the discharge characteristics is difficult to make since the component of series resistance due to the flashtube is a non-linear function of the discharge current. Capacitance values as high as several thousand microfarads are used. Supply voltages are generally in the range 1 - 2 kilovolts and the flashtube is triggered by a pulse transformer which supplies a high peak voltage, in addition to the standing voltage across the flashtube. Values of series inductance are typically a few hundred microhenries. The circuit is arranged

~~is arranged~~ so that the discharge is overdamped and the energy is dissipated in one current pulse which usually has a half peak duration of half to several milliseconds. An oscillatory discharge is avoided since the light output then consists of a series of pulses of twice the oscillating discharge frequency. A low value of series inductance is used to give a high peak current and thus high peak light output. At the same time the lifetime of the tube must be considered and operating conditions are usually arranged so that a reasonable compromise is achieved between long lifetime which is achieved by underrunning at low discharge currents, and more efficient operation which is achieved by overrunning at high discharge currents. Also, for efficient operation it is essential that maximum energy be dissipated in the flashtube, and thus a small residual circuit resistance is advisable to minimise Joule losses.

The spectrum of the light emitted by the flashtube corresponds roughly to a black body continuum of about 5000°K. It is simple to calculate that only about 10% of the total light output is in the two ruby pump bands. Despite this inefficiency the high pressure xenon filled flash lamp is still the only effective method of pumping ruby solid state lasers.

The efficiency of the focussing ellipse is dependent on several factors. Generally high efficiency is obtained for low eccentricity, but the physical dimensions of the ruby and flashtube elements determine the minimum foci separation and thus the minimum eccentricity. A highly polished specular reflecting inner surface is also required to produce a good image of the flashtube at the

ruby. Because the maximum energy capacity of a linear flashtube is about 10 kilojoules, high energy systems usually incorporate multiple cavity arrangements. With one such arrangement two cavities are superposed by removal of part of the wall sections so that one foci from each elliptical cylinder are coincident with each other; the ruby is placed at this position with one flashtube at each of the foci on either side. In a similar way three and four flashtubes can be used.

The reflecting mirrors that form the laser optical cavity are normally composed of multilayer dielectric coatings, which can be made to have a high peak reflectance in the required spectral region and which also have small scattering and absorption losses of about 0.1%. Silver mirrors are sometimes used but these are unsuitable for high power lasers since they absorb about 3 - 5% of the incident radiation. Apart from this loss of energy from the cavity, the energy absorbed causes disruption of the silver mirrors which occurs at much lower power levels than for damage of the dielectric mirrors. The value of the reflectivity enters into the threshold condition. A high reflectance results in a low threshold and in a high radiation density in the ruby, but little output energy is extracted. A low reflectance increases the thresholds and reduces the radiation density in the ruby. For efficient operation it is essential to determine the optimum reflectance for maximum energy output.

It is not essential to have the reflecting mirrors coincident with the ruby end faces. However, when external mirrors are used it is essential to ensure that they are in accurate alignment with

the end faces of the ruby, and in some cases it is required to anti-reflection coat the ruby end faces or polish the ruby end to a Brewster angle to minimise reflection losses. Other possible arrangements include the use of external 90° roof edge prisms, alternatively the ruby itself can be polished to a 90° wedge. Instead of multi-dielectric or silver mirrors, it is sometimes possible to use single pieces of quartz or glass with flat and parallel faces. By accurately lining up several of these plates it is possible to construct resonant reflectors with high reflection coefficients, however these are difficult to construct and are not widely used.

The performance of the system is also dependent on the ruby temperature. With increasing temperature the line width of the R_1 transition increases, therefore the peak absorption coefficient decreases and the energy required to attain threshold increases, and thus the efficiency of the laser decreases. For accurate and reproducable results it is essential that the ruby be cooled to maintain a low and constant temperature.

Some of the design parameters discussed in this chapter were selected for further study. Chapter 4 is concerned with the flashtube and describes an experiment to determine its characteristics. Chapter 5 is concerned with the effect of the geometric shape of both single and multiple focussing ellipses. Chapter 6 also deals with the focussing ellipse, but only with the effects of its surface reflectance. Chapter 7 deals with the reflecting mirrors that form the laser optical cavity, and discusses the conditions for optimum reflectance and their alignment with the ruby end faces. Chapter 8 is concerned with the

effect of ruby temperature on energy output. Chapter 9 is solely concerned with the application of the solid state ruby laser to machining and welding.

Chapter 4. Excitation Source.

4.1 Experimental Arrangement.

Knowledge of the flashtube discharge characteristics is essential for the efficient design of pulsed ruby lasers, and this work describes an experimental programme carried out to determine this information.

The characteristics measured were the peak discharge current, the voltage at peak current, the peak power dissipated, and peak light output. These measurements were made over a wide range of series inductance and for different energy inputs to the flashtube. Finally, measurements of the laser output energy were made, which were then related to the flashtube characteristics.

Two types of flashtube were selected, the T/E6/79/2 and T/E6/94/2 manufactured by Thermal Syndicate Ltd., Wallsend. The former being rated at 10 Kilojoules maximum input and of 16.5 cm length and 1.3 cm diameter. The latter being rated at 5 kilojoules maximum input and of 16.5 cm length and 1 cm diameter. Both were filled with Xenon to about 400 mm Hg pressure.

The capacitor bank was manufactured to a given specification by Clive Courtney Ltd., Dorking, Surrey. It consisted of eight capacitor trays giving a total of 3,696 microfarads, and a 30 amp dive unit. The charging voltage was continuously variable in the range 0 to 2.5 kilovolts and it was also possible to preset the required voltage before the charging cycle was initiated. The maximum energy storage was 12 kilojoules at 2.5 kilowatts. Initiation of the

discharge was simply effected by a push button on the front panel of the drive unit; this discharged a 1 microfarad capacitor charged to about 200 volts through a Ferranti Type PT60 pulse transformer. This pulse transformer was situated adjacent to the flashtube and gave a peak voltage of about 15 kilovolts on to a nickel trigger wire wrapped round the exterior wall of flashtube. The drive unit also included dumping resistors and a safety switch which only permitted the switching of the capacitor links if the mains voltage was switched off. A photograph of the complete unit is shown in figure 9.

Heavy duty P.V.C. 60 amp cables were used to connect the bank to the series inductance and flashtube. Two types of series inductance were used, which are shown in figure 10. First a solenoid inductance was wound; it consisted of about 250 turns of 16 s.w.g. insulated copper wire wound on a $2\frac{1}{2}$" diamater bakalised paper tube. The measured inductance and resistance valves were:-

TABLE 2

INDUCTANCE AND RESISTANCE OF SOLENOID WINDING

L(μH)	R(Ω)
164	0.150
250	0.225
345	0.300
425	0.375

At an early stage in the experiments it was evident that the series resistance of this inductance was too large for efficient flashtube operation, so a second low resistance inductance was constructed. This was made from 60 lb of 1/2" x 1/8" insulated copper strip, 56 turns were spirally wound on a 3" centre former and six tappings were taken off. This was then potted in about 2 lb of araldite and boxed in plywood. The calculation of the inductance was done by the method described by GROVER (1947). Measured and calculated values were within 5%; the measured inductance and resistance values were:-

TABLE 3

INDUCTANCE AND RESISTANCE OF SPIRAL WINDING

L(uH)	R(Ω)
237	0.012
340	0.014
431	0.017
536	0.019
629	0.022
727	0.024

A reflecting aluminium cavity was constructed of the same form as that used for a solid state ruby laser (see figure 11); (the

details of the construction are described in Chapter 5). The flashtube was assembled in the cavity and thus the operating conditions expected to be met in actual laser operation were simulated.

The discharge circuit arrangement is shown in figure 12. The flashtube voltage was measured across a 88 : 1 step down resistor chain and the total shunt across the flashtube was 5 megohms. The current was measured as the voltage across a 0.001 Ω registor in series with the flashtube. The light output was recorded with a BPY 10 photodiode placed at a fixed distance of 5½ ft from a 1/8" diameter hole in the wall of the aluminium cavity. A Sir Howard Grubb Parsons' general purpose green filter which had a 1% bandwidth at 5500A° was placed in front of the detector so that the light intensity measurements were relevant to the pump band of ruby. The voltage signals corresponding to the current, voltage and light output were displayed on a double beam Tetronik 585 oscilloscope. Since only one oscilloscope was available each discharge condition had to be repeated to enable all three parameters to be measured. All discharges were made at 15 minute intervals to ensure that the flashtube was at ambient temperature before recording.

For the 5 kilojoule flashtube measurements of the discharge parameters were made with both types of series inductance. The flashtube and a 6" x 5/8" ruby with a 90° wedge (shown figure 13) were then assembled in a polished elliptical laser cavity and measurements of the laser output energy were made for 5 kilojoules flashtube input energy. From these results it was apparent that the spiral was more efficient than the solenoid inductance. Because of this the solenoid

inductance was discarded and measurements with the 10 kilojoule flashtube were only made with the spiral inductance.

For both types of flashtubes used, no attempt was made to optimise the other laser components. The 6" x 5/8" ruby was operated with only the 7% ruby/air interface as the reflecting mirror. This and all other conditions were maintained constant so that a comparison could be made between the different flash tube operating conditions.

Laser energy measurements were made with a T.R.G. Thermopile Type 100. Its calibration was 232 microvolts per joule; the output voltage was measured with a Type GM6020 Philips valve voltmeter.

4.2 Results and Discussion.

Table 4 gives the peak current I kiloamps, the voltage at peak current, V kilovolts, the peak power W = V.I. megawatts, and the arc resistance at peak current $r = V / I$ ohms for the 5 kilojoule flashtube.

Table 5 gives the laser output energy E joules, the peak light output as recorded by the oscilloscope in millivolts, mv., and the half peak width of the discharge waveform T milliseconds, for the 5 kilojoule flashtube. The variation of laser output energy with different conditions of series inductance is shown graphically in figure 14.

Tables 6 and 7 gives measurements of V, I, W, .r., E and T for the 10 kilojoule flashtube for 5, 7.5 and 10 kilojoules energy input.

From the laser output energy measurements, it is apparent that

over the ranges of inductance used, the smaller the value of series inductance the more efficient is the laser operation. The minimum value of inductance permissible for a tube lifetime of at least 1,000 discharges can be calculated from the makers instructions which state that the average wall loading defined as

$$\frac{\text{DISCHARGE ENERGY}}{\text{WALL AREA} \times T}$$

should not exceed 45 kilowatts/cm^2.

For the 10 kilojoule flashtube at 10 kilojoule input, it can be calculated from the data in Table 7 that the minimum value of L is about 536 microhenries, and this value was selected for all further experiments.

For the 5 kilojoule flashtube at 5 kilojoule input, it can be calculated from the data in table 5 that the minimum value of L is about 340 microhenries, and this value was selected for all further experiments.

The arc resistance r. is plotted as a function of the discharge current I in figure 15 for both flashtubes. For the 5 kilojoule flashtube the empirical relation is:-

$$r = 15.5\, I^{-1/2} \text{ ohm} \qquad (4.1)$$

for the 10 kilojoule flashtube the empirical relation is:-

$$r = 13.5\, I^{-1/2} \text{ ohm} \qquad (4.2)$$

Equations (4.1) and (4.2) are in agreement with the work of GONCZ (1965) who showed that the plasma resistivity, ℓ , of a xenon filled flashtube was :-

$$\ell = 1.13\, j^{-1/2} \text{ ohm cm} \qquad (4.3)$$

where j is the current density

Since $r = \rho \frac{l}{\pi d^2}$, where l cm is the discharge length and d cm the tube diameter, equation (4.3) becomes

$$r = Ro\, I^{-1/2} \qquad (4.4)$$

where $Ro = 1.3 \left(\frac{l}{d}\right)$ For the 10 kilojoule flashtube, the calculated and measured values of Ro are 16.5 and 13.5 respectively. For the 5 kilojoule flashtube, the calculated and measured values of Ro are 21.5 and 15.5 respectively.

These measurements are in good agreement with recent results by PERLMAN (1966) who gives Ro = 16.5 for a 16.5 cm long 1.3 cm diameter EG and G FX47 flashtube.

TABLE 4

5 KILOJOULE FLASHTUBE.

Energy Input Joules	L uH	R Ω	I Kilamps	V Volts	W Megawatts	r Ω
5000	629	0.022	2.6	800	2.1	0.31
	536	0.019	2.7	840	2.3	0.31
	431	0.017	3.1	880	2.7	0.28
	340	0.014	3.5	930	3.3	0.27
	237	0.012	4.6	1000	4.6	0.22
6000	425	0.375	2.2	700	1.5	0.32
	345	0.300	2.5	750	1.9	0.30
	250	0.225	3.2	840	2.7	0.26
	164	0.150	3.6	910	3.3	0.25

TABLE 5

5 KILOJOULE FLASHTUBE.

Energy Input Joules	L uH	R Ω	T MILLISECONDS	Peak Light mV	E Joules
5000	629	0.022	3.2	1.8	3.0
	536	0.019	2.9	1.9	3.2
	431	0.017	2.6	2.1	4.1
	340	0.014	2.3	2.2	4.8
	237	0.012	2.0	2.5	5.0
5000	425	0.375	2.6	1.2	2.4
	345	0.300	2.4	1.4	3.0
	250	0.225	2.2	1.6	3.2
	164	0.150	1.8	1.7	3.6

TABLE 6.

10 KILOJOULE FLASHTUBE.

Energy Input Joules	L uH	R Ω	I Kilamps	V Volts	W Megawatts	r
5000	727	0.024	3.6	800	2.9	0.22
	629	0.022	3.8	850	3.2	0.22
	536	0.019	4.6	910	4.1	0.20
	431	0.017	5.2	950	5.0	0.18
	340	0.014	5.6	980	5.5	0.17
7500	727	0.024	5.2	950	4.9	0.18
	629	0.022	5.5	1000	5.5	0.18
	536	0.019	6.2	1040	6.4	0.17
	431	0.017	6.9	1090	7.5	0.16
	340	0.014	7.3	1130	8.3	0.15
10000	727	0.024	6.3	1030	6.5	0.16
	629	0.022	6.5	1080	7.0	0.17
	536	0.019	7.2	1150	8.3	0.16
	431	0.017	8.0	1200	9.6	0.15

TABLE 7

10 KILOJOULE FLASHTUBE

Energy Input Joules	L uH	R Ω	T Millisecs	Peak Light mv	E Joules
5000	727	0.024	3.2	2.3	2
	629	0.022	3.1	2.5	3
	536	0.019	2.8	2.6	3
	431	0.017	2.6	2.7	4
	340	0.014	2.4	3.0	6
7500	727	0.024	3.5	2.5	10
	629	0.022	3.4	2.9	12
	536	0.019	3.1	3.0	12
	431	0.017	2.8	3.1	13
	340	0.014	2.6	3.3	14
10,000	727	0.024	3.7	3.2	17
	629	0.022	3.5	3.3	19
	536	0.019	3.2	3.4	21
	431	0.017	2.9	3.5	22

FIG 9. 12 KILOJOULE CAPACITOR BANK AND DRIVE UNIT

FIG 10. SOLENOID AND SPIRAL INDUCTANCES

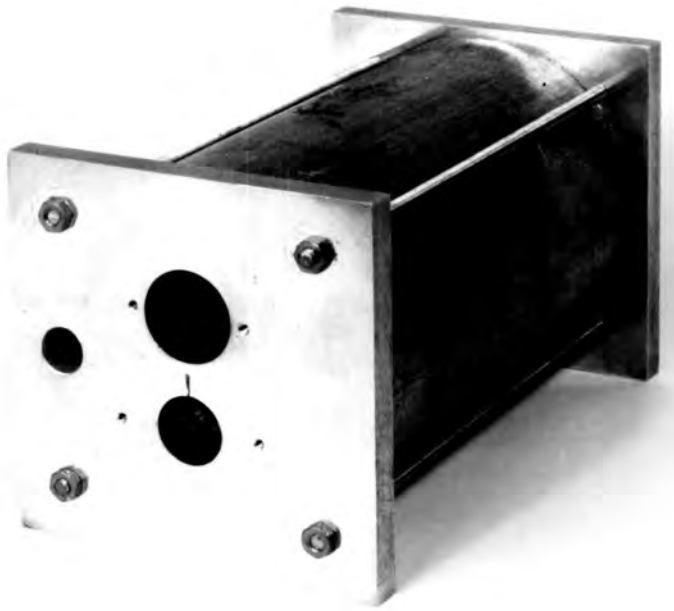

FIG 11 ALUMINIUM LASER CAVITY

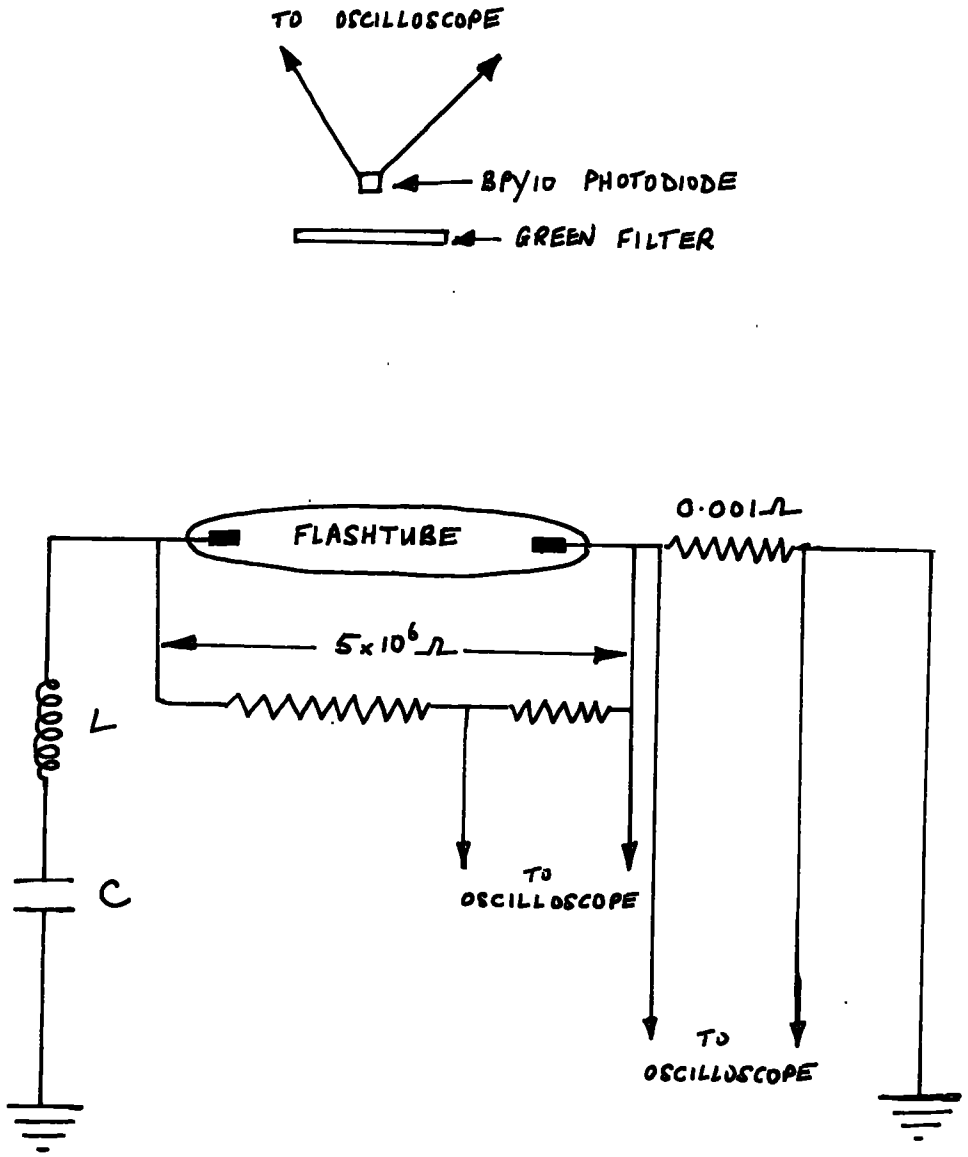

FIG 12. DISCHARGE CIRCUIT ARRANGEMENT

FIG 13 FLASHTUBE AND RUBY.

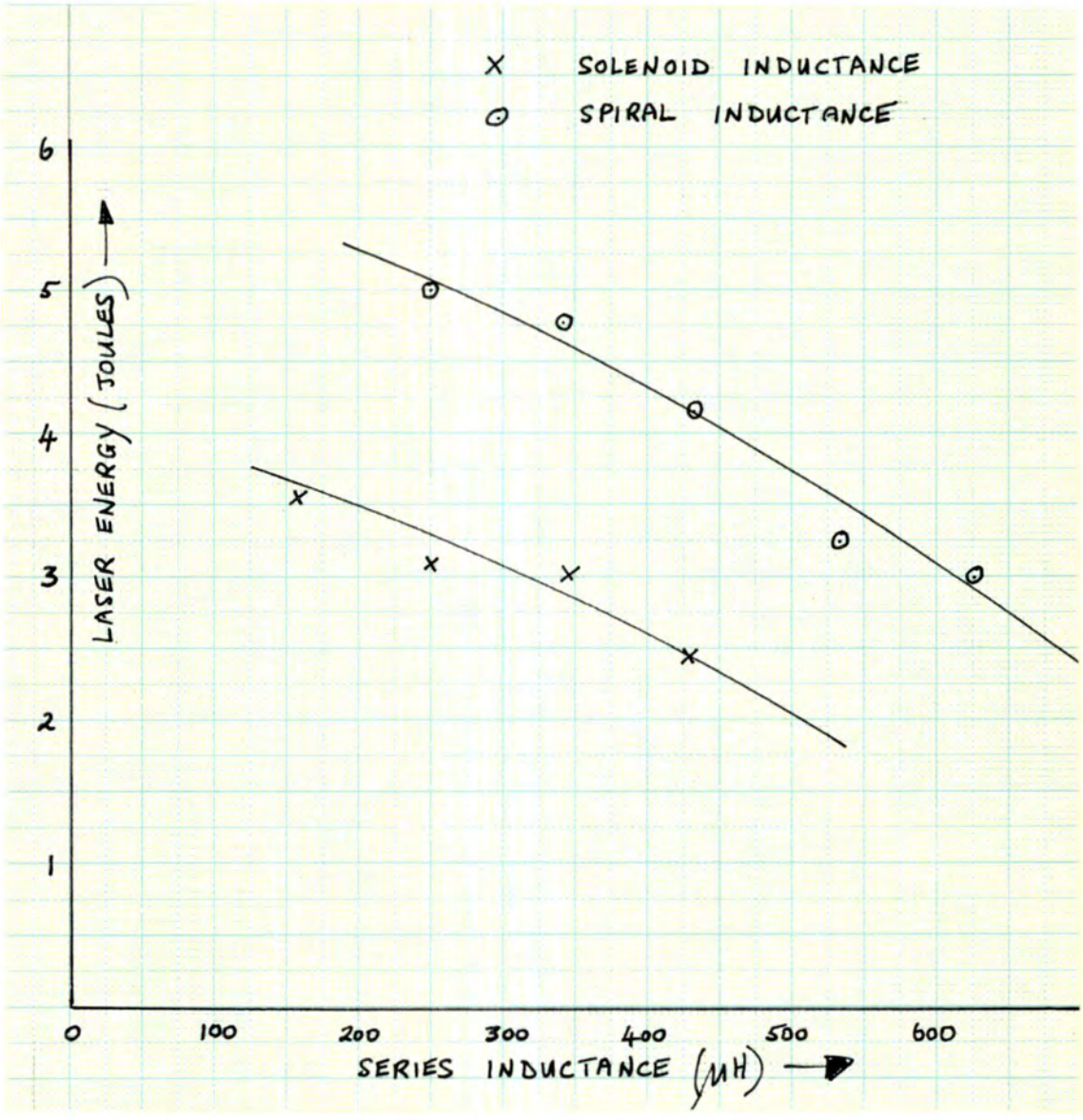

FIG 14. LASER OUTPUT ENERGY FOR A 5 KILOJOULE FLASHTUBE AS A FUNCTION OF SERIES INDUCTANCE

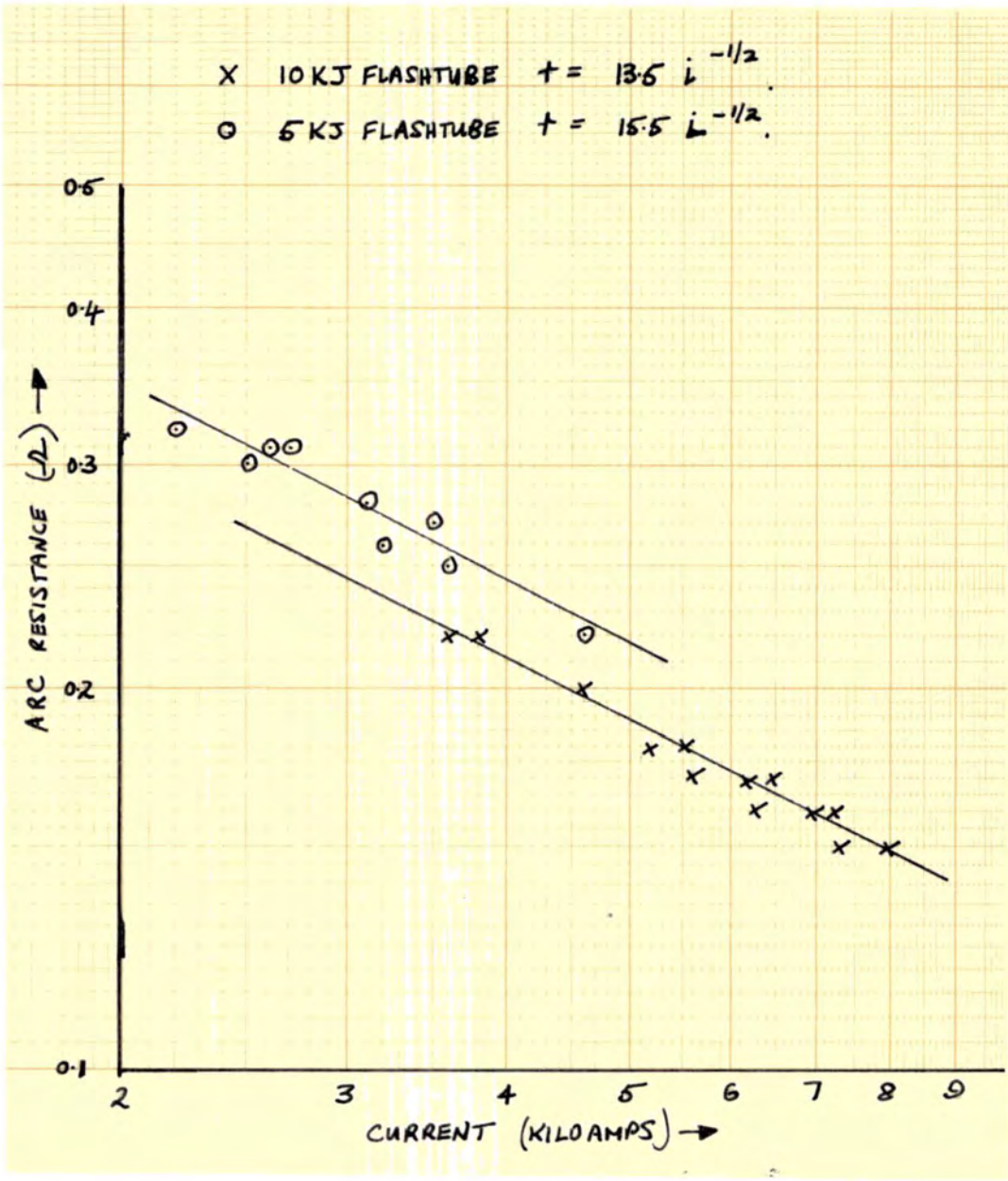

FIG 15 PEAK ARC RESISTANCE AS A FUNCTION OF PEAK DISCHARGE CURRENT

CHAPTER 5

Coupling System I

Geometric Shape of Focussing Ellipse.

5.1 Theory

Elliptical reflectors, which were first proposed by CIFTON (1961), can be made with relative ease and they are now commonly used for transfering pumping radiation from the cylindrical flashtube to active laser medium.

The purpose of this work is to obtain some idea of the pumping efficiency which in turn permits the optimum design of reflector to be chosen for any given lamp and crystal diameter. Generally the efficiency is the greatest when the source and laser material are close together; however this leads to large diameter reflectors and it is essential to know how the efficiency is reduced by reducing the diameter of the ellipse. Also, the effect of the relative size of the source and ruby is important. Maximum efficiency is obtained when the laser material is of large diameter as compared to flashtube diameter. However this is contrary to the laser pumping requirement of a high flux density which implies a small diameter laser rod and a large diameter flashtube. It is thus important to know if the increased power obtainable by increasing the flashtube diameter is nullified by a loss of coupling efficiency.

The case of a single elliptical cylinder reflector, see Figure 16 was first treated by SCHULDT and AAGARD (1963). The following assumptions were made

1) Perfect reflection at the cavity walls.

2) An infinitely long cylindrical cavity and source; thus the distribution of the light rays entering the laser is the same for any cross section through the elliptical cavity. The condition of an infinitely long cavity is met in practice by enclosing the ends with plane highly reflecting plates placed normal to the cylinder axis.

3) The laser material absorbs all light incident on it i.e. no second traverses of the light through it are allowed. The precise absorption pattern within the laser material has been studied by DEVLIN (1962) and McKENNA (1963) and is extremely complex.

4) The energy distribution of the flash tube is Lambertian i.e.

$$I(\beta) = \frac{\cos\beta}{4\pi} \qquad (5.1)$$

Referring to Figure 16 the coupling efficiency of the cavity was calculated as follows. Any light ray can be considered as originating from the centre of the flash lamp of radius R1 intersects the cavity wall at point P, and is focussed through the centre of the laser rod of radius R2 The two limiting rays from P which are tangential to the laser rod are defined by α and β, which are both functions of θ. Any light path can be denoted by a weight function $G(\alpha\beta)$, where $G(\alpha\beta) = 1$ if the light ray intersects the laser rod and $G(\alpha\beta) = 0$ if the light ray does not interesect the laser rod. The pumping efficiency F is then defined

by

$$F = 4 \int_0^{T} d\alpha \int_0^{\pi/2} I(\beta)\, G(\alpha\beta)\, d\beta \qquad (5.2)$$

where $I(\beta)$ is defined from equation 5.1. If $G(\alpha\beta) = 1$ for all rays then $F = 1$.

This integral was evaluated by SCHULDT and AAGARD (1963) and the solution obtained was:

$$F = \left\{1 - \frac{T}{\pi}\right\} + \frac{2}{\pi}\frac{R_2}{R_1}\left[\tan^{-1}\left(\frac{1-\varepsilon}{1+\varepsilon}\right)\tan\frac{T}{2}\right] \qquad (5.3)$$

WHERE R_2 and R_1 ARE THE RADII OF RUBY AND FLASHTUBE RESPECTIVELY, where ε is the eccentricity of the ellipse, and T is defined by

$$T = \begin{cases} 0 & \cdots\cdots \left(\frac{R_2}{R_1}\right) > \left(\frac{1+\varepsilon}{1-\varepsilon}\right) \\ \cos^{-1}\left\{\frac{\frac{R_2}{R_1}(1-\varepsilon^2) - (1+\varepsilon^2)}{2\varepsilon}\right\} & \cdots\cdots \left(\frac{1-\varepsilon}{1+\varepsilon}\right) \leq \left(\frac{R_2}{R_1}\right) \leq \left(\frac{1+\varepsilon}{1-\varepsilon}\right) \\ \pi & \cdots\cdots \left(\frac{1-\varepsilon}{1+\varepsilon}\right) > \left(\frac{R_2}{R_1}\right) \end{cases}$$

Equation (5.3) has been evaluated for single elliptical cavity for both $R2/R1 = 1$ and $R2/R1 = 2$ and F as a function of the eccentricity ε is plotted in Figure 17.

Since the energy which can be delivered to a linear flashtube is limited, multiple partial elliptical sections having one common axis at which the laser material is placed, have proved a useful design. Since each section is identical, the efficiency of any section is also the efficiency of the full assembly.

The above theory can be simply applied to calculate the pumping efficiency of the partial multiple sections, by allowing the limits of θ in equation 5.2 to very from 0 to ϕ instead of from 0 to π . The angle ϕ is defined by the edge of the partial elliptical section, the line centre of the flashtube and the major axis of the ellipse as shown in Figure 18.

It is then found that the pumping efficiency F is

$$\left.\begin{aligned} F &= \left\{\frac{\phi}{\pi}-\frac{T}{\pi}\right\}+\frac{2}{\pi}\frac{R_2}{R_1}\left[\tan^{-1}\left(\frac{1-\varepsilon}{1+\varepsilon}\right)\tan\frac{T}{2}\right] \cdot \phi > T \\ F &= \frac{2}{\pi}\frac{R_2}{R_1}\left[\tan^{-1}\left(\frac{1-\varepsilon}{1+\varepsilon}\right)\tan\frac{\phi}{2}\right] \cdot \phi < T \end{aligned}\right\} \quad (5.4)$$

For a 2-section elliptical cavity

$$\begin{aligned} w &= \pi/2 \\ x+y &= 2a \quad (\text{THE MAJOR AXIS OF THE ELLIPSE}) \\ V &= 2a\varepsilon \\ \tan\gamma &= \tan(\pi-\phi) = \frac{1-\varepsilon^2}{2\varepsilon} \end{aligned} \quad (5.5)$$

For a 4-section elliptical cavity

$$\begin{aligned} w &= \pi/4 \\ x+y &= 2a \\ V &= 2a\varepsilon \\ \tan\gamma &= \tan(\pi-\phi) = \frac{1-\varepsilon^2}{2\sqrt{2}\,\varepsilon-\varepsilon^2-1} \end{aligned} \quad (5.6)$$

From equations (5.4), (5.5) and (5.6), the coupling efficiencies of both 2 and 4-section elliptical cavities were calculated. These are shown in figures 19 and 20 for

$R2/R1 = 1$ and $R2/R1 = 2$ in each case.

For a n-section elliptical cavity, as $\mathcal{E} \to 0$ the limiting angle of ϕ is $\frac{\pi}{n}$ and the limiting angle of T is π and for the case of $\frac{R2}{R1} = 1$, the maximum efficiency is

$$F = \frac{2}{\pi} \cdot \tan^{-1}\left(\tan \frac{\pi}{2n}\right) = \frac{1}{n}$$

and thus each flashtube can only couple a maximum of $\left(\frac{1}{n}\right)^{th}$ of the total energy of the flashtube.

This result is in agreement with the laws of thermodynamics. If the flashtube and laser rod are considered as black body emitters and absorbers of radiation, the temperature of the absorber cannot be hotter than the emitter (i.e. the energy density of the image cannot be greater than its source) and under the most ideal conditions they can only be equal. With the single elliptical cavity this condition can only be realised if the flashtube and laser rod are coincident i.e. $\mathcal{E} = 0$ and thus $F = 1$. For the multiple elliptical cavities, if $F > \frac{1}{n}$, then the total energy absorbed by the laser rod given by nF per unit flashtube energy, would be greater than one.

This does not mean that the use of multiple elliptical cavities offers no advantage. For the condition $R_2/R_1 = 1$ it can be seem from Figure 21 that the total energy incident on the laser rod

which is defined by Fn, increases with n for any value of $\mathcal{E} > 0$; however, the advantage is only slight.

However, a much greater advantage is obtained when $\frac{R_2}{R_1} > 1$ because it is then possible for $F.n > 1$; as is shown in Figure 22 for $\frac{R_2}{R_1} = 2$.

For the single elliptical cavity the maximum efficiency of 100% is maintained to $\mathcal{E} \approx 0.35$ and the maximum energy supplied to the laser rod is 1 unit. For the 2-section multiple ellipse, the maximum efficiency is 70% at $\mathcal{E} \approx 0.4$ and the maximum energy supplied to the laser rod is 1.4 units. For the 4-section multiple ellipse the maximum efficiency is 50% at $\mathcal{E} \approx 0.45$ and the maximum energy supplied to the laser rod is 2 units.

In practice it is difficult to attain high values of $\frac{R_2}{R_1}$ by simply increasing the ruby diameter as the cost is prohibitive. A common practice to increase R_2 is to surround the laser material with a dielectric sheath of refractive index η. This increases the effective diameter of the ruby since it has been shown, DEVLIN(1962) and McKENNA (1963), that all light absorbed by the sheath of radius R is ultimately focussed through a smaller internal cylinder of radius R/η. Methods of achieving this effect can be simple. e.g. by surrounding the laser material with a water cooling sheath or by filling the whole cavity space with water.

5.2 EXPERIMENTAL ARRANGEMENT.

The reflecting elliptical cavities were made from 99% commercial purity aluminium tube of 3.85" internal diameter and 0.1" wall thickness. The elliptical cross-section was formed by compressing the circular cylinder along one diagonal until a small permanent deformation of the required amount was obtained. The accuracy of the ellipse was checked in three ways:-

(i) By measuring the major and minor axis. It was found that the extension of one diagonal was only slightly smaller than the ~~comparison~~ COMPRESSION of the diagonal at right angles to it. The actual measurements for three cylinders are given in Table 8 which also gives the calculated values of ε and focal separation $2a\varepsilon$

TABLE 8

Cylinder	Major Axis	Minor Axis	ε	$2a\varepsilon$
1	3.97"	3.67"	0.380	1.51"
2	3.96"	3.68"	0.370	1.48"
3	3.98"	3.68"	0.384	1.52"

(ii) By measurement of the diameters (2r) at 45° to the major and minor axis. From the geometric properties of the ellipse it is easy to show that

$$2r = \frac{\sqrt{2}\ (2a)\,.\,(2b)}{\sqrt{(2a)^2 + (2b)^2}}$$

The measured and calculated values of 2r are given in Table 9 and they are in agreement to within 0.02".

TABLE 9

Cylinder	(2r) measured		(2r) calculated	
1	3.85"	3.84"	3.82"	3.82"
2	3.83"	3.84"	3.83"	3.83"
3	3.83"	3.86"	3.84"	3.84"

(iii) By placing the polished cylinder on a ground glass plate under which was placed an illuminating source. It was then possible to see the image of a line object such as a pencil, the quality and position of which suggested that an accurate ellipse had been formed.

The cylinders were then hand polished. First, grade 150 and 450 emery paper was used to remove the deep scratches in the surface, and this was followed by emery down to the 6/0 grade. The final polish was obtained with metal polish which was followed by 5μ, 1μ, and 1/4μ diamond paste using paraffin as solvent.

Plane samples of 2" x 2" dimensions were also prepared by the same method and their spectral reflectivity in the wavelength range 0.3μ to 0.8μ was determined by using an optica reflecting spectrometer. The results and implications of this work are discussed in detail in Chapter 6.

Using these polished cylinders it was decided to measure the difference in coupling efficiency between a single, and a 2-section partial ellipse, coupling systems, both of the same eccentricity of $\varepsilon = 0.38$. One cylinder was mounted between two highly reflecting end plates polished in the manner described above. The whole assembly was held rigid by 4BA tapped rods, and it is shown in Figure 11. The 2-partial section ellipse was then constructed by first sectioning each ellipse, the section being defined by the line parallel to the minor axis and passing through one of the calculated foci positions. These sections were carefully cut with a hacksaw, and the edges were hand polished so that both sections accurately fitted together. The two sections were mounted between two highly polished end plates and the complete assembly was held rigid by tie rods made from 4BA rod. The complete cavity is shown in Figure 23.

Two 10 kilojoule flashtubes and the $6^{1}/_{2"} \times 5/_{8"}$ wedge end ruby were then mounted in this double cavity. Two capacitor banks and drive units were used, as shown in Figure 9, but only one trigger was used for both flashtubes to ensure that they both discharged at the same time. Two series inductances were used, one for each flashtube. As only one low resistance spiral inductance was available, two of the solenoid inductances of L = 345uH were used instead. The

laser output energy was measured for total energy inputs to the two flashtubes of up to 20 kilojoules.

The 10 kilojoule flashtube was then mounted in the single elliptical cavity. A capacitor bank and a solenoid inductance of L = 345u H WERE used so that measurements of laser output energy could be compared with the results for the double cavity. The $6^{1}/_{2}$" x $^{5}/_{8}$" wedge ended ruby was again used and output energy was measured for energy inputs to the flashtube of up to 10 kilojoules.

5.3 RESULTS AND DISCUSSION.

The laser output energy for varying flashtube input energies for both the single and double cavity is shown in Table 10, and they are represented graphically in Figure 24.

TABLE 10.

SINGLE CAVITY		DOUBLE CAVITY	
ENERGY IN	ENERGY OUT	ENERGY IN	ENERGY OUT
KILOJOULES	JOULES	KILOJOULES	JOULES
4	-	6	-
5	3.0	8	2.5
6	5.6	10	7.1
7	8.0	12	9.0
8	10.4	14	12.1
9	13.1	16	16.2
10	15.9	18	21.0
		20	25.2

These results are in good agreement with the theory described in section 5.1. If the threshold energies are used as an indication of the relative efficiencies of the two systems, the ratio of the efficiencies for the single to double cavities is approximately 6 : 4 which is in reasonable agreement to the ratio 1.6 : 1 calculated from the data in Figures 17 and 19. A more accurate estimate of efficiency is given by slopes of the output energy versus input energy curves of Figure 24 from which an efficiency ratio of about 1.45 : 1 is calculated.

The ultimate advantage of using a multiple cavity arrangement is also demonstrated. For the single cavity the maximum output energy was about 16 joules at 10 kilojoules input, while for the same total input to the double cavity the output energy was only 7 joules. However, for the double cavity a total of 25 joules output was ultimately obtained from a total energy input of 20 kilojoules. By extrapolating the graph on Figure 24 it is seen that this energy could have been extracted from the single cavity for only 13 kilojoules input.

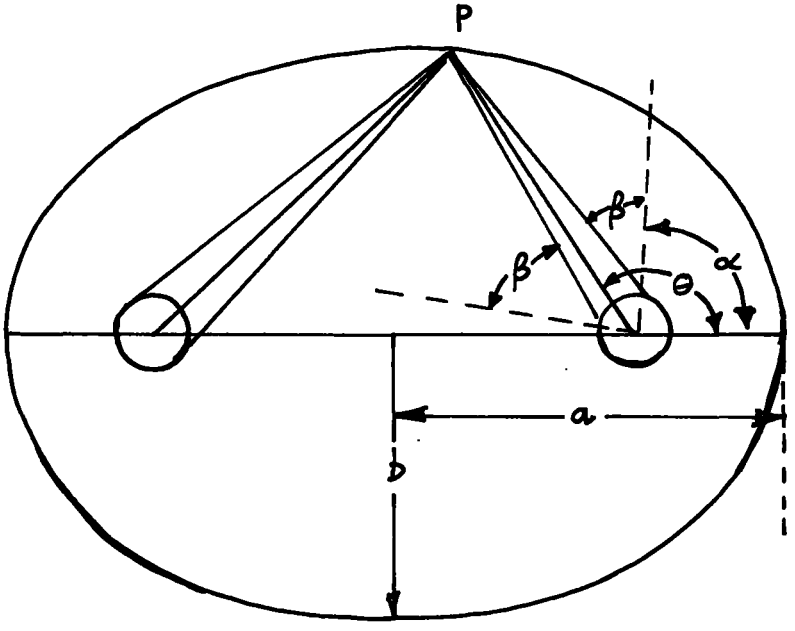

FIG 16. SINGLE ELLIPTICAL CAVITY

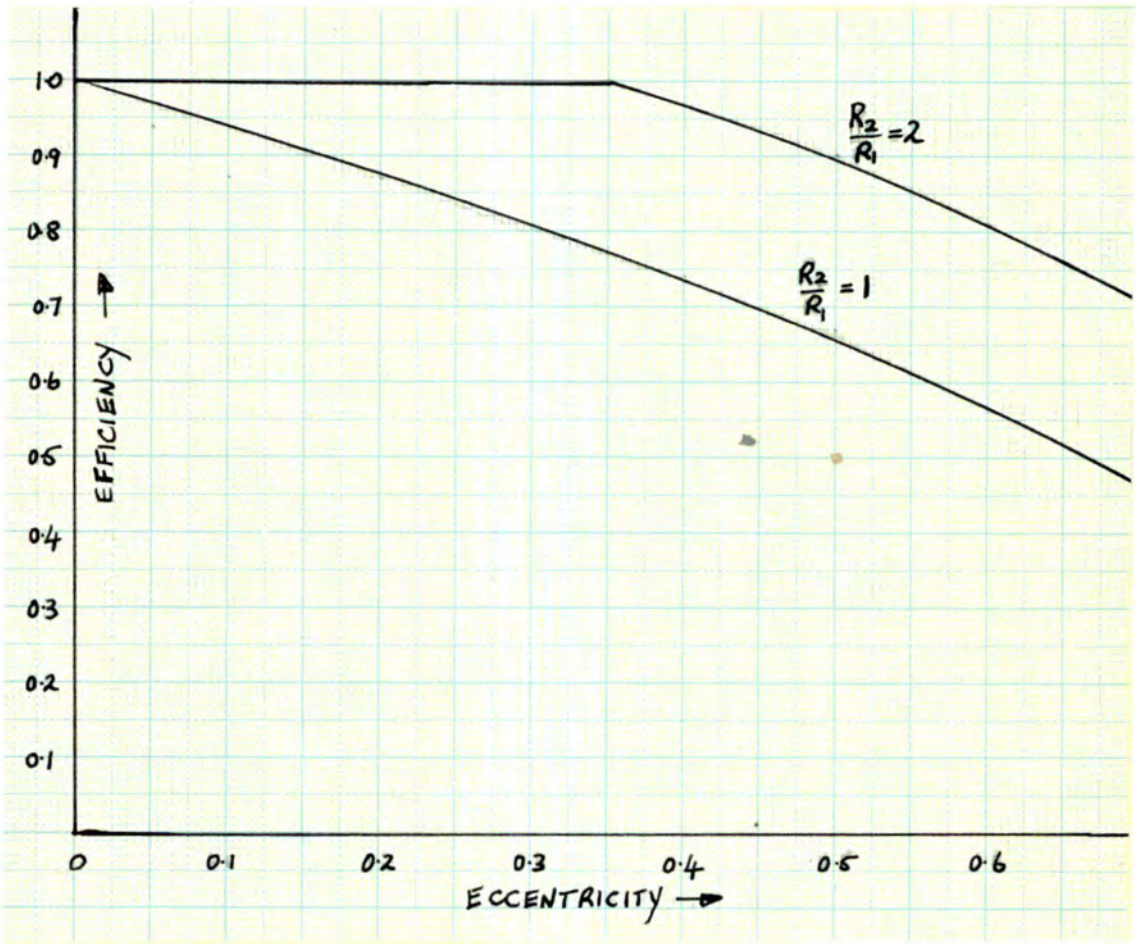

FIG 17 PUMPING EFFICIENCY OF A SINGLE ELLIPTICAL CAVITY

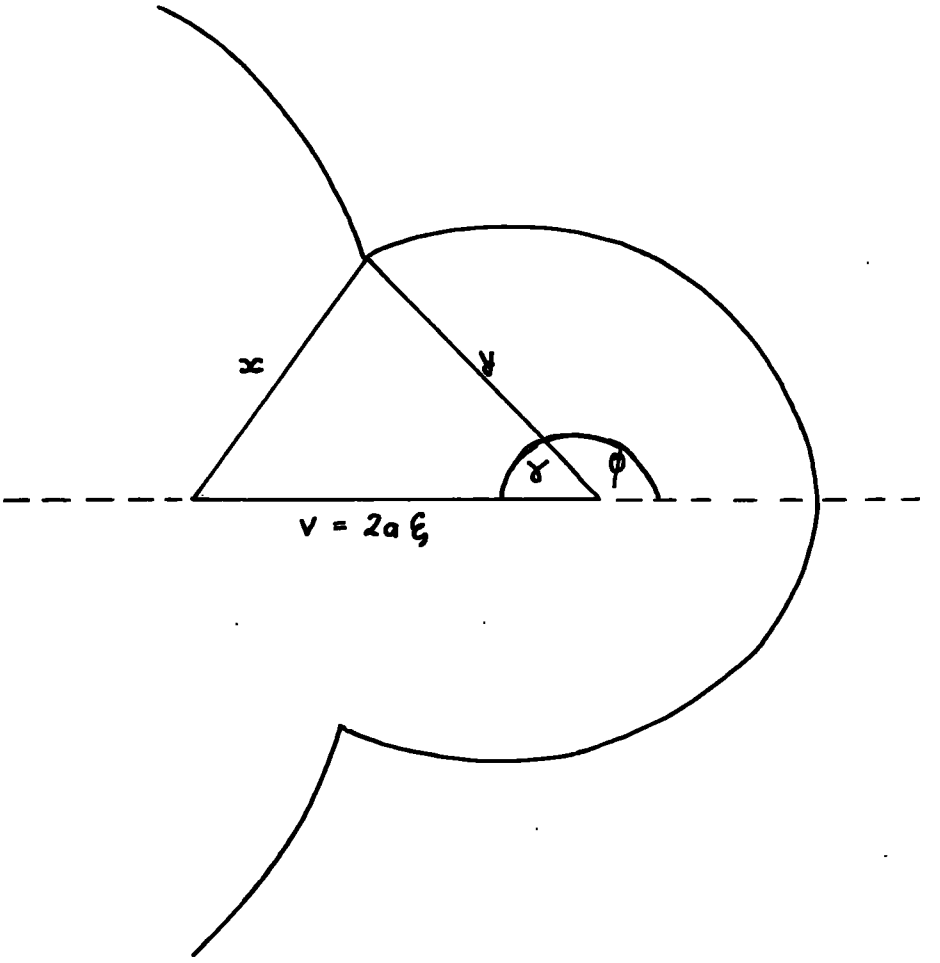

FIG 18 MULTISECTION ELLIPTICAL CAVITY.

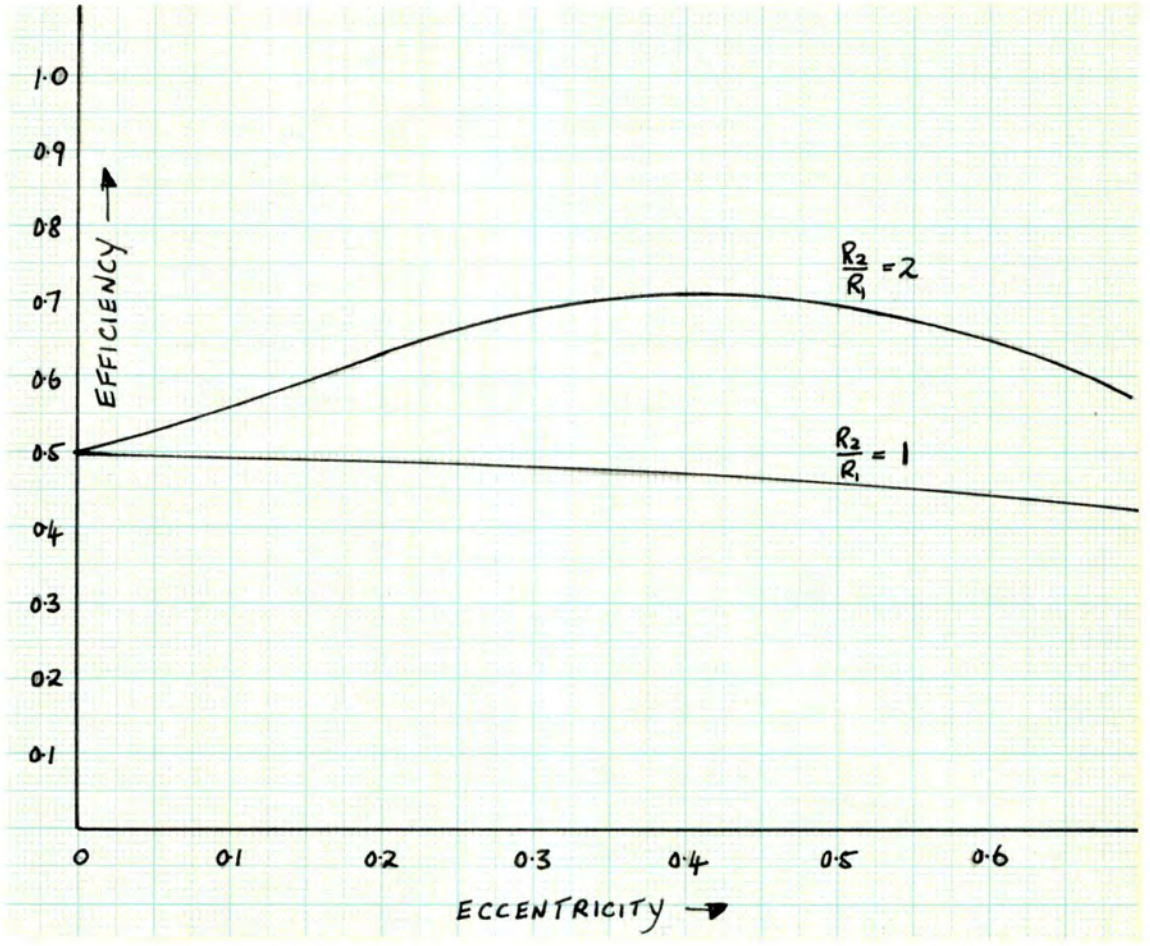

FIG 19. PUMPING EFFICIENCY OF A TWO-
- SECTION ELLIPTICAL CAVITY

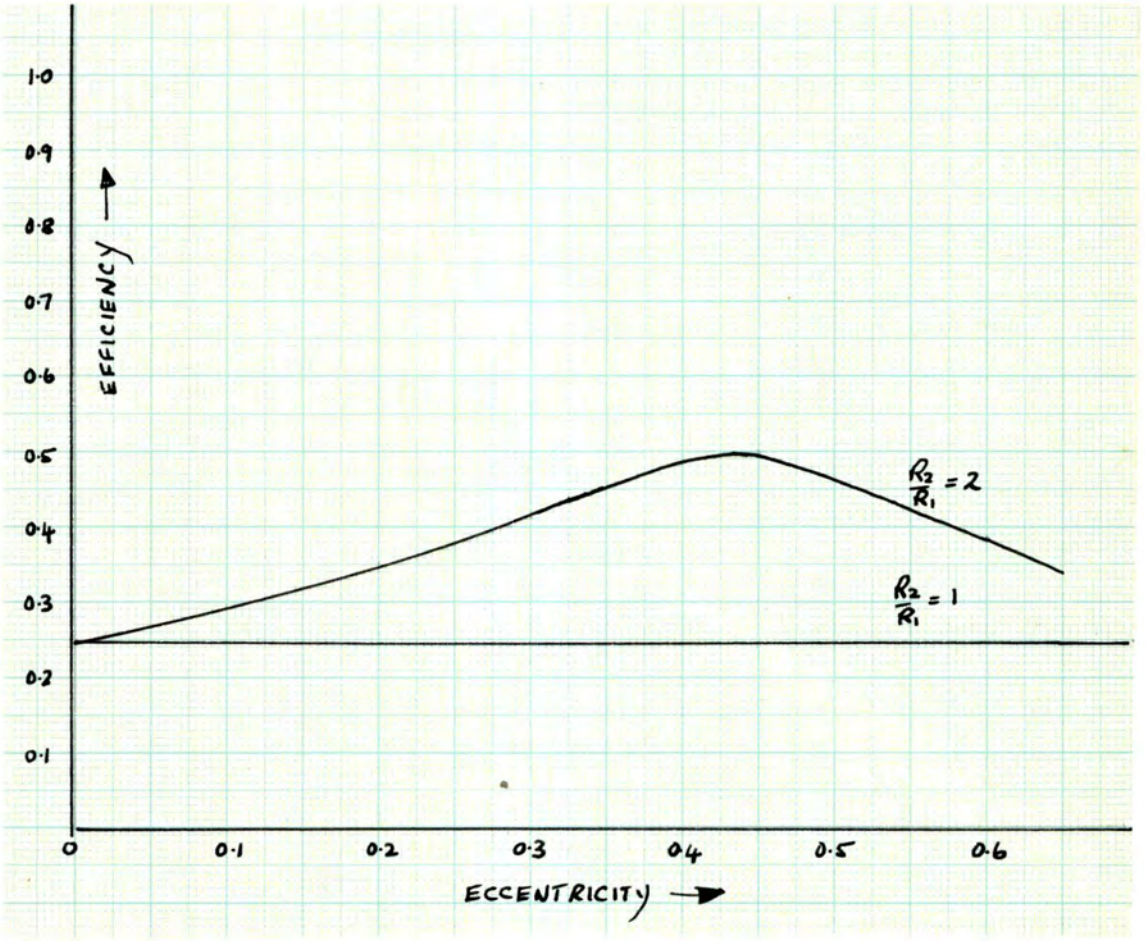

FIG 20 PUMPING EFFICIENCY OF A FOUR—
— SECTION ELLIPTICAL CAVITY

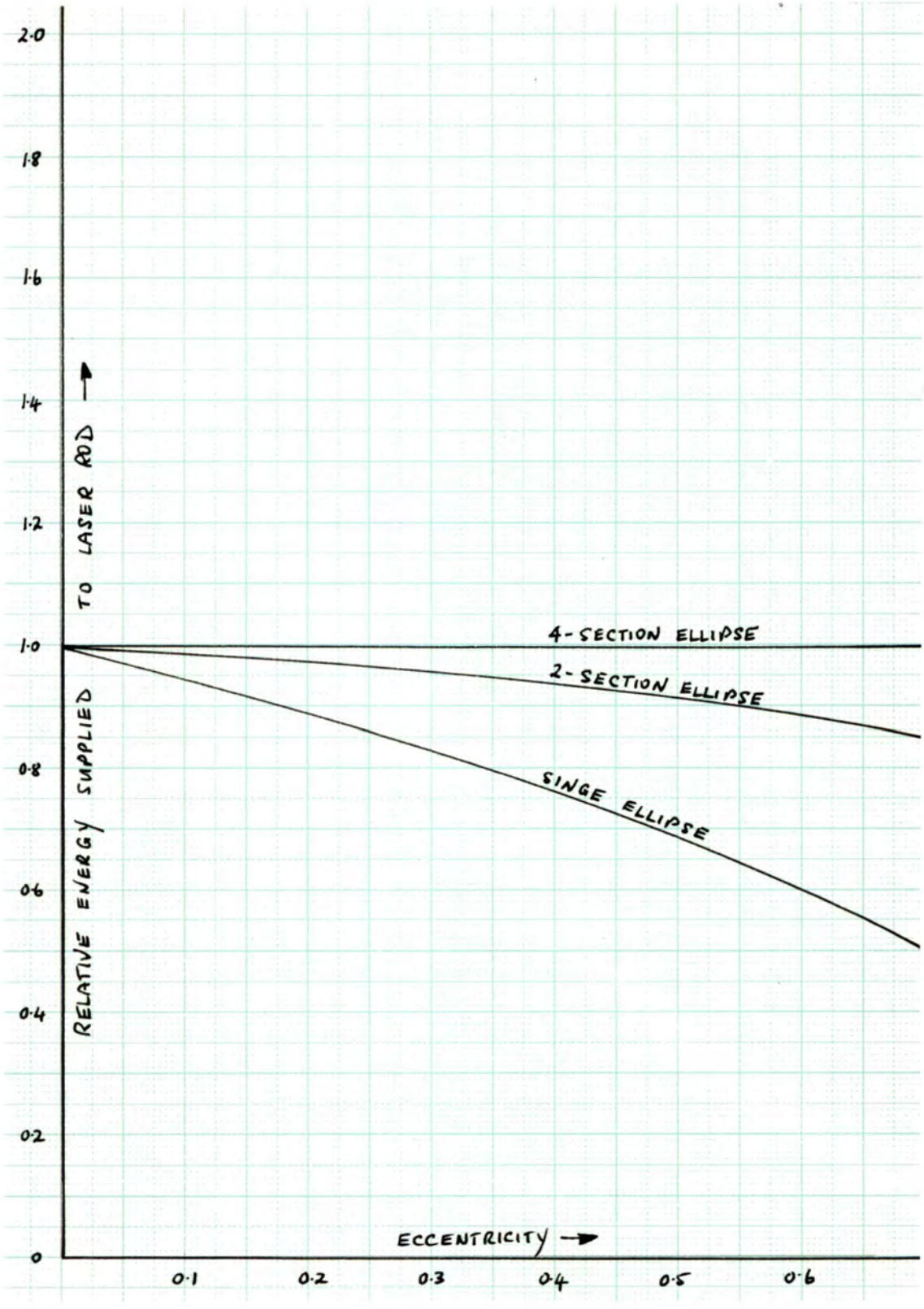

FIG 21. RELATIVE ENERGY SUPPLIED TO THE LASER ROD FOR $R_2/R_1 = 1$

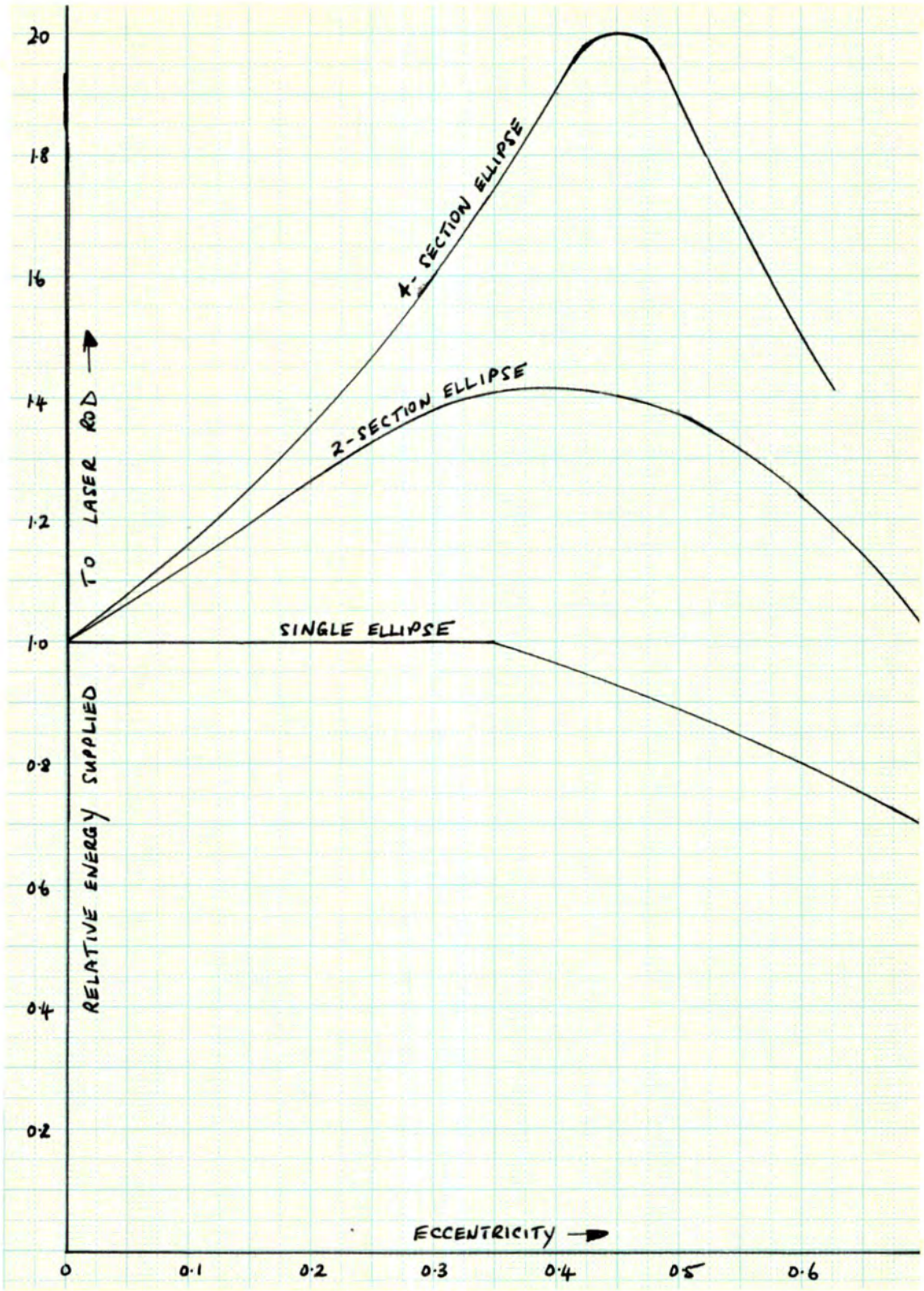

FIG 22. RELATIVE ENERGY SUPPLIED TO THE LASER ROD FOR $R_2/R_1 = 2$

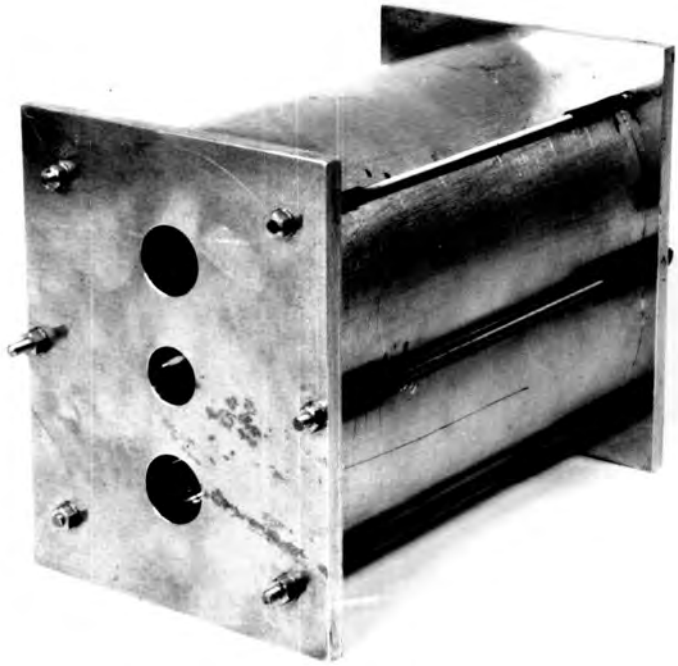

FIG 23. TWO-SECTION ELLIPTICAL CAVITY

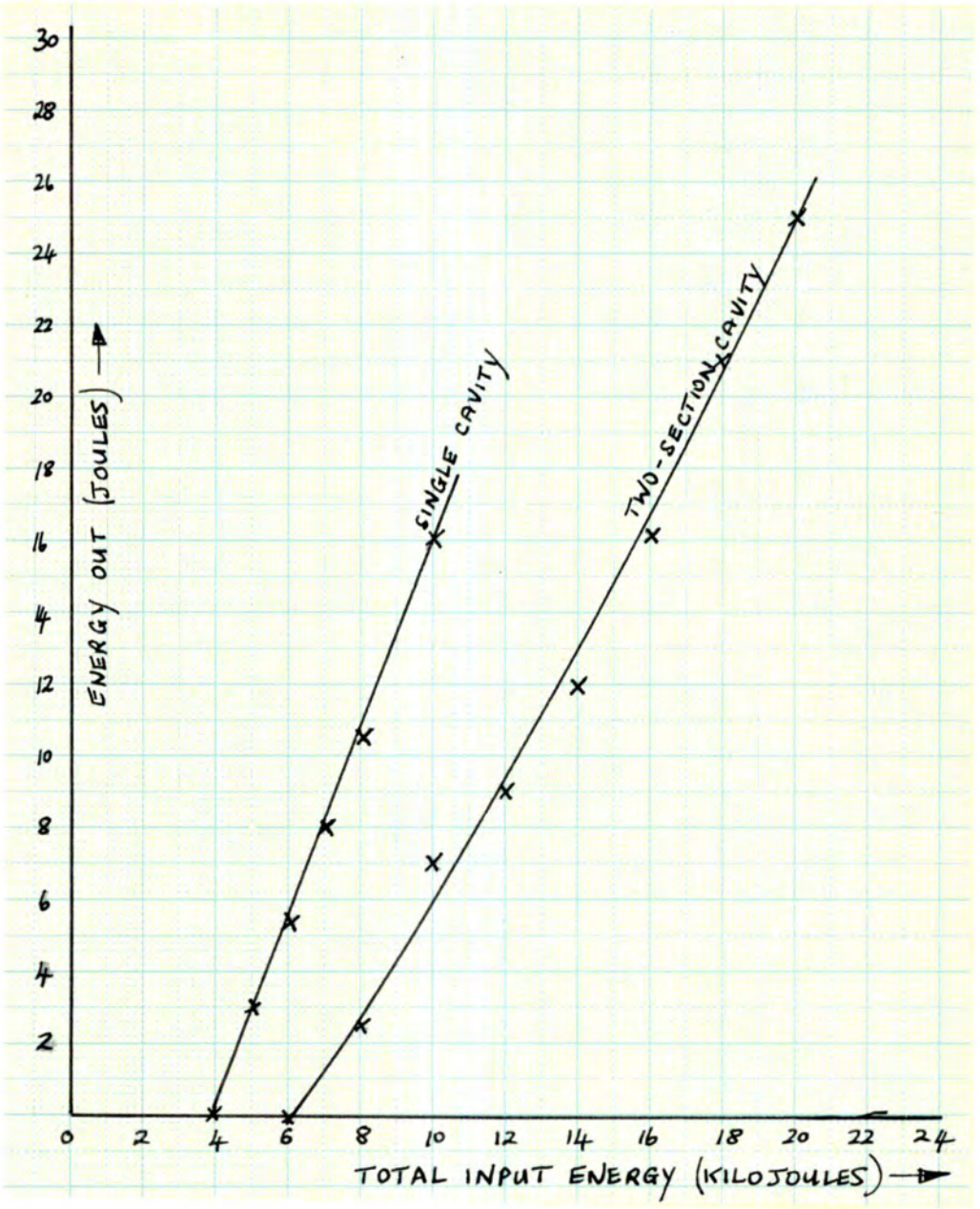

FIG 24. ENERGY OUTPUT VERSUS ENERGY INPUT FOR SINGLE AND TWO — -SECTION ELLIPTICAL CAVITIES

CHAPTER 6. Coupling System II.

Reflectance of Focussing Ellipse.

6.1 Theoretical Considerations.

In the theory of section 5.1, it was assumed that the reflection coefficient at the walls of the cavity was equal to one. In practice this is not the case, and as most of the light suffers at least one reflection between leaving the flashlamp and arriving at the ruby, the effect of the surface wall reflection coefficient must be considered as affecting the overall efficiency of the laser system. This, however, does not invalidate the comparative efficiencies calculated in section 5.1 as a similar surface preparation was used for each cavity arrangement.

The overall coupling efficiency is given by $F.R_c$, when R_c is the surface spectral reflection coefficient of the cavity wall, and F is the efficiency as defined by equations (5.3) or (5.4). If the effect of reflection at the surface of the ruby rod R_L, is also considered, then the coupling efficiency is given by $F.R_c.R._L$, WENZEL (1963), and the maximum efficiency is obtained at normal incidence for which R_c and R_L are a maximum. In this work only ruby was used, thus R_L was constant for all the systems considered and was neglected.

6.2 Experimental Arrangement.

The aluminium reflecting cavities were polished by the method described in section 5.2. In addition 2" x 2" square sample of the same material were prepared by the same method, and the spectral

reflectivity coefficients of these were measured at 3° incidence with an Optica Reflecting Spectrometer. The results are given in Table II, and are also shown graphically in Figure 5.

TABLE 11.

Spectral Reflection Coefficients of Polished Aluminium

Wavelength A°	Piece 1 %	Piece 2 %	Piece 3 %	Mean %
4000	68	66	69	68
5000	73	76	77	75
6000	77	76	75	76
7000	72	74	73	74
8000	68	71	71	70

Another method of surface preparation was attempted. i.e. 'Brightalising', a hot dip process by which the aluminium is polished by chemical reaction; a standard solution was used, Phosbrite 159, Manufactured by Albright and Wilson Ltd.,

The results of this work were comparable with the hand polished samples, but the process was not used since considerable precautions had to be taken to avoid the copious amounts of poisonous fumes given off by the hot solution. High reflection coefficients in excess of 90% were obtained by evaporating pure aluminium on to the polished samples. The adherance of the coating was not strong and under test

they rapidly pealed when high energy density radiation from the xenon flashlamps was incident upon them. Electrolytic polishing was also considered, but equipment capable of generating up to several hundred amperes, which would have been required for the polishing of the large area of the cavity walls, was not available.

Another type of cavity used was a dielectric coated glass cavity. This was purchased from Schott and Genossen Jenaer Glassworksm Mainz, Germany and consisted of an elliptically formed glass cylinder of major axis 11.8 cms (4.65"), minor axis 11.4 cms (4.49"), giving a separation of line foci of 3.05 cms (1.20"). This glass cavity was supplied with a hard dielectric coating on the inner and outer walls, which it was claimed was specially developed to give a high spectral reflection coefficient corresponding to the pump bands of ruby. Flat pieces of the coated glass were also supplied, the spectral reflectivity coefficient of which were measured by the same method as for the aluminium samples. These results are also shown on Figure 25.

It is seen that, in the two ruby pump bands, the glass cavity has a considerably greater reflection coefficient, as compared to aluminium cavity. An additional advantage is that the reflection coefficient drops rapidly to about 20% after 7500A°, and thus the large amount of red and infra-red radiation emitted by the flashtube, which only serve to heat up the ruby and thus lower the efficiency, is transmitted through the cavity walls.

It was therefore apparent that the glass cavity should have two principal advantages over the aluminium cavity.

(1) Because of the higher reflectance in the pump bands, a higher efficiency and thus higher energy output should be obtained from the laser system.

(2) Because the infra-red radiation flux on the ruby is reduced, the ruby should remain cooler, and thus the output energy under repetive firing conditions should be easier to maintain at a constant level than for systems incorporating metal cavities.

In order to make comparative measurements with the coated glass cavity, a metal cavity of nearly similar dimensions was constructed. This was made from 4.5" internal diameter aluminium tube which was formed and polished as described in section 5.2. The measured dimensions were, major axis 4.57", minor axis 4.42", and calculated eccentricity and foci separation were 0.26 and 1.23" respectively.

Two 5" x 5" polished aluminium end plates were made to contain either the glass or metal cavities. The previous method of assembling the cylinders and end plates as described in section 5.2 was tried, but the necessary requirement for the glass cavity of applying equal pressure on the metal tie rods during assembly proved difficult to achieve and the edges of the glass cylinder started to chip and crack.

A new method of assembly was used. This is shown in Figure 26, which also shows the coated glass cavity assembled with a flashtube and ruby. The pressure required to hold the glass cavity between the end plates was obtained with spring loaded tie rods and the pressure on each rod was easily controlled by either tightening

or loosening a screw; this proved to be a simple and effective method of assembly.

Both the glass and metal cylinders were assembled in turn and the output laser energy as a function of the flashtube input energy was measured for each. For both systems, a 10 kilojoule flashtube and the $6\frac{1}{2}$ x $5/8$" wedge ended ruby were used, the ruby was operated with only the 7% ruby/air interface to complete the laser resonator.

Finally, repetitive laser energy measurements for both systems, for 6 kilojoules input, were made at 1 minute intervals.

All measurements were made at 15 minute intervals to ensure that the ruby was at a uniform initial temperature. Each measurement was repeated three times and results given show the mean of these readings.

6.3 Results and Discussion.

The results of laser energy output as a function of the energy input to the flashtube is given in Table 12 and ~~is~~ are plotted graphically in Figure 27.

TABLE 12

ENERGY INPUT	ENERGY OUTPUT JOULES	
Kilojoules	Glass Cavity	Metal Cavity
4.5	5.0	1.0
5.25	9.6	2.5
6	14.5	4.6
7	24.0	8.1
8	35.2	14.0
9	47.0	19.8
10	54.5	24.9

It is apparent that the effect of the high reflectance properties of the glass cavity upon the energy threshold and energy output of the laser system has been shown to be most marked. The relative threshold energies of the glass and aluminium cavities should give an indication of the conversion efficiency in the pump band of ruby for the two systems. On the basis, the results show that the conversion efficiency of the glass cavity is 1.33 times that of the aluminium cavity. This figure agrees with that obtained by comparing the spectral reflectance in the ruby pump bands of the glass and aluminium cavities i.e. aluminium 70% and glass cavity 95%.

The efficiency at high input energies can be obtained by comparing the slopes of the curves in Figure 27. This gives an efficiency ratio of 2 : 1 for the glass and aluminium cavities respectively, which is larger than expected from the reflectance measurements. This is probably due to two factors. The glass cavity is probably the more accurate ellipse and the coupling efficiency would be greater than for the aluminium cavity; also, the infra-red radiation is transmitted away from the ruby and probably causes a reduction in temperature rise of the ruby during the flashtube discharge duration.

The results for the repetitive discharge measurements are given in Figure 28, for a constant 6 kilojoules input to the flashtube. They are normalised to 100% for the first discharge in each case, where this corresponds to about 15 joules and 5 joules energy output for the glass and aluminium cavities respectively. It is seen that in the case of the glass cavity, the fall off in output with an increasing number of shots is not as great as for the aluminium cavity. This illustrates the detrimental effect of the large amount of unwanted infra-red radiation which is emitted by the flashtube.

After an estimated 100 to 150 flashtube discharges with an average energy input of 5 kilojoules, no visible surface damage was observed on the walls of the glass cavity. However, it is relevant to point out that extreme care was taken to ensure that the inside of the glass was clean and free from grease and dust.

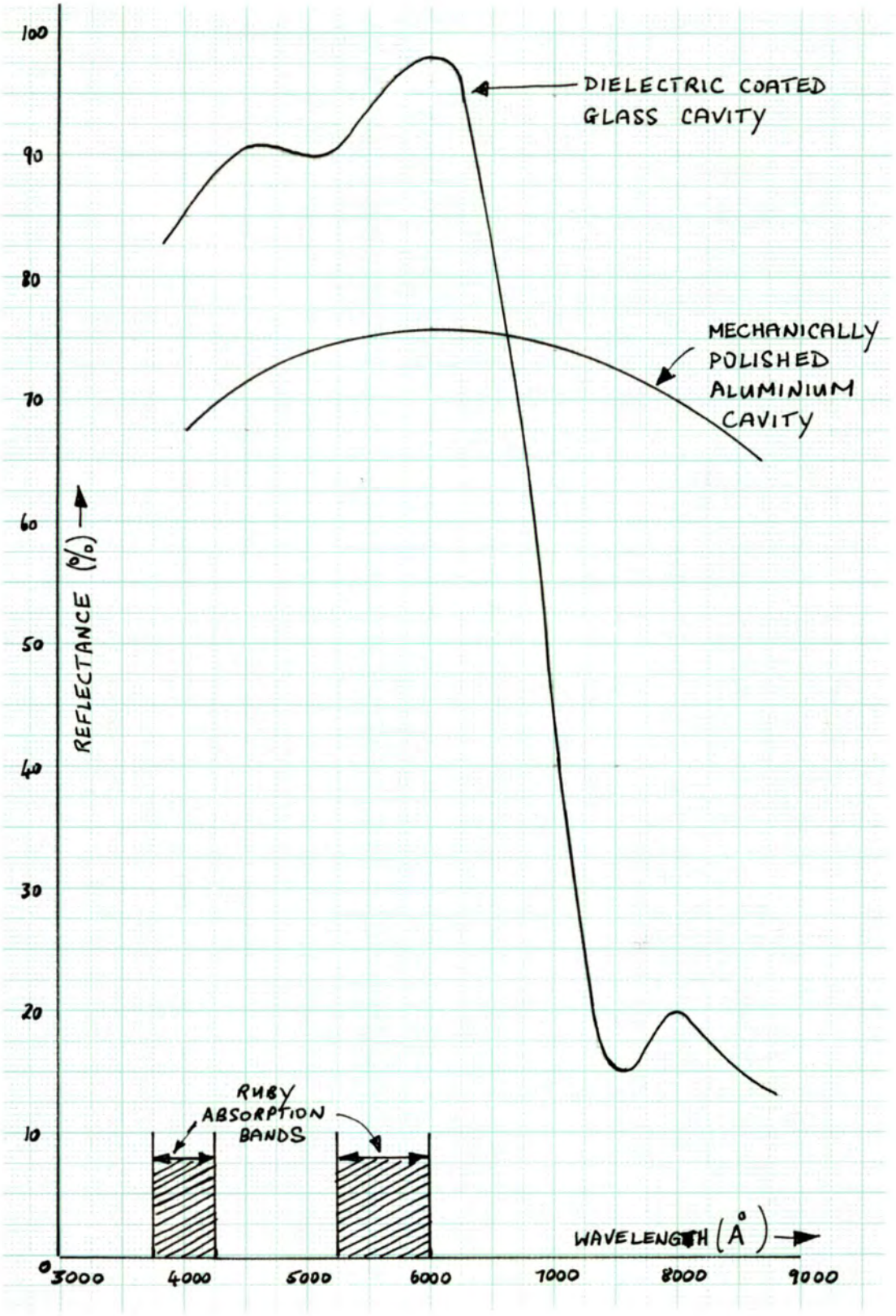

FIG 25. REFLECTANCE CHARACTERISTICS OF ALUMINIUM AND GLASS CAVITIES.

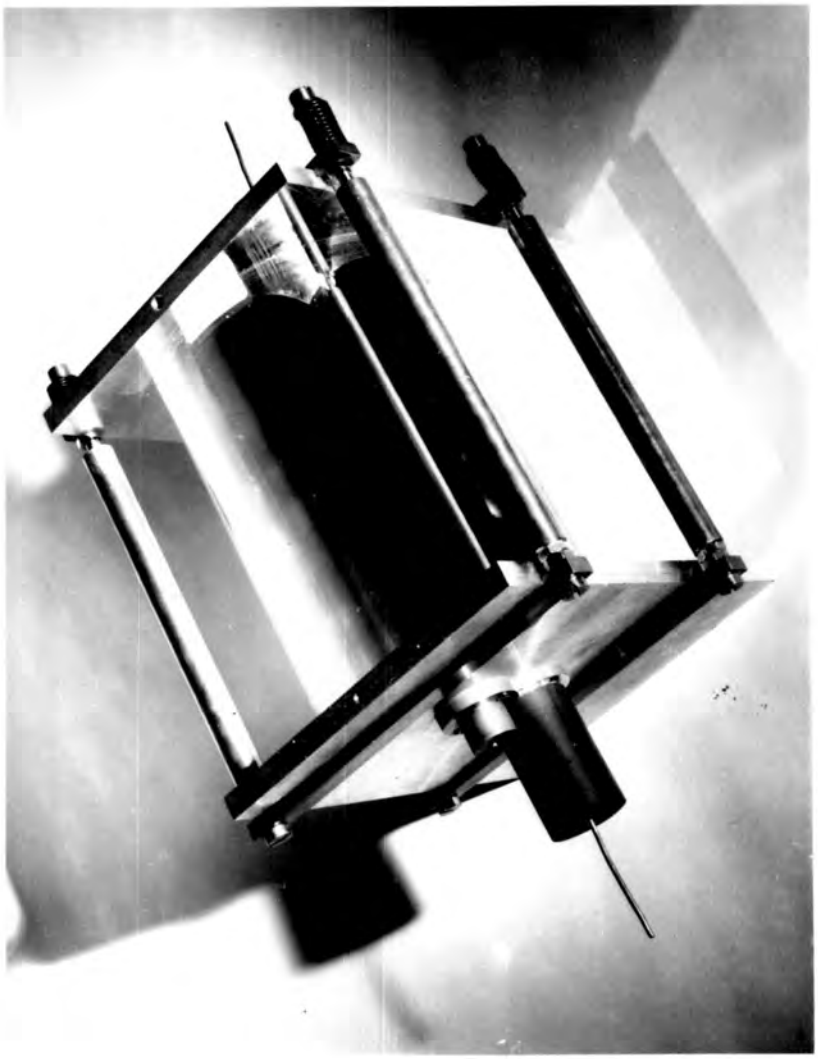

FIG 26 GLASS CAVITY

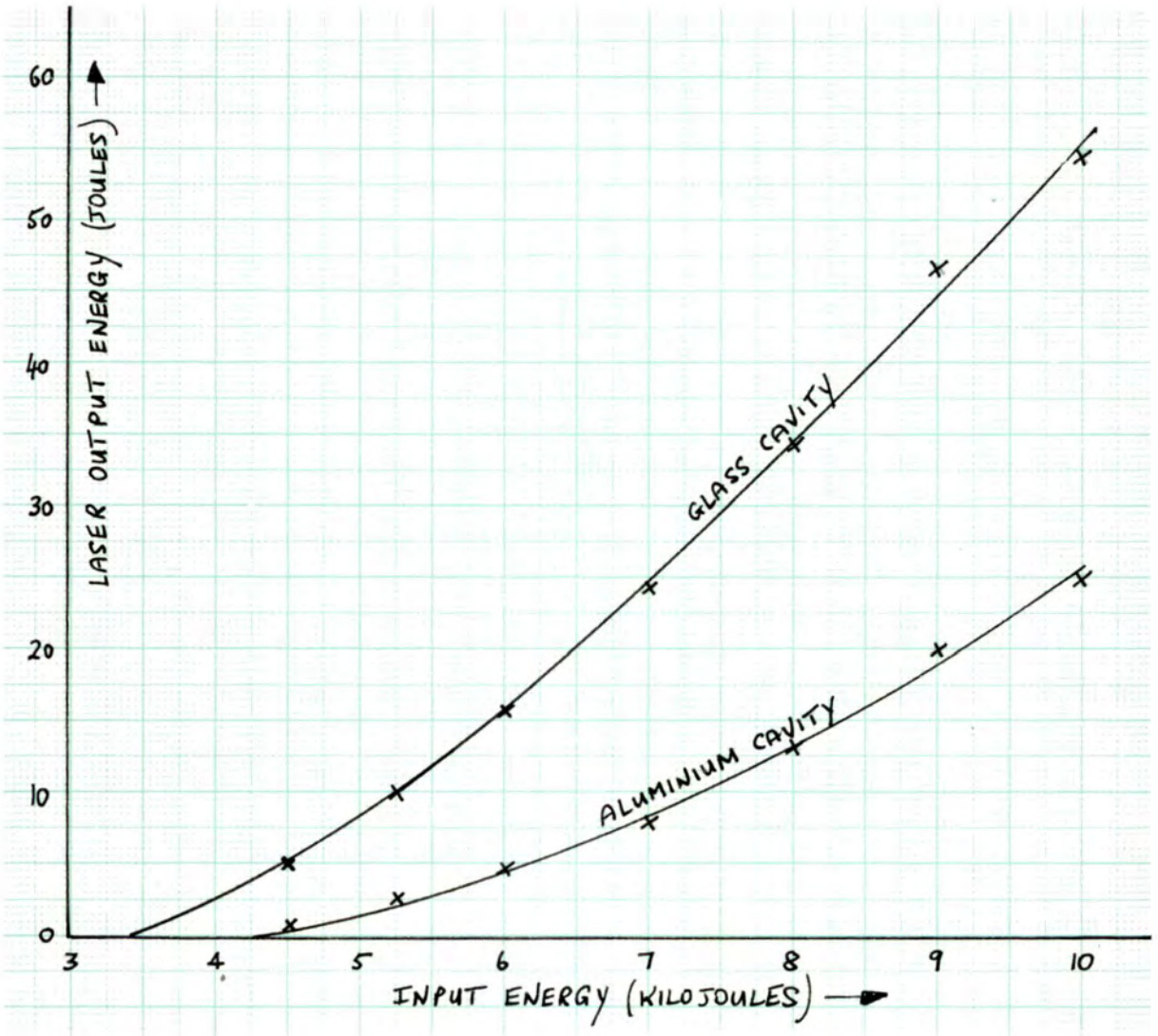

FIG 27. LASER OUTPUT ENERGY FOR THE GLASS AND ALUMINIUM CAVITIES

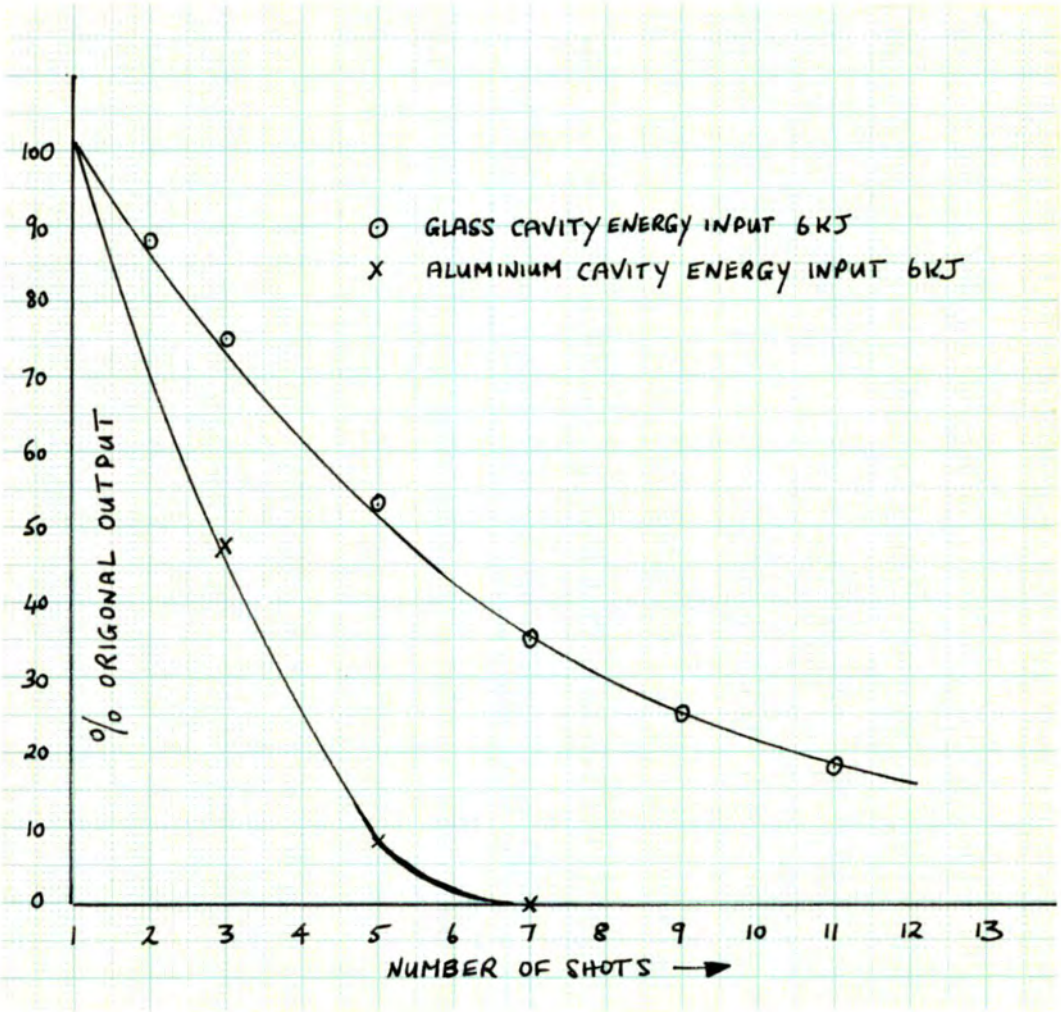

FIG 28. NORMALISED LASER OUTPUT ENERGY AT A ONE MINUTE PULSE REPETITION RATE.

CHAPTER 7. EXTERNAL REFLECTORS.

7.1 Theory

The essential part of the ruby laser system is the amplifying medium which resonates at the output frequency. This consists the ruby laser rod and two mirrors or prisms which are accurately positioned at either end. One reflector is usually considered as 100% and the other reflector has a reflectivity coefficient of $R < 100\%$, so that some radiation is emitted out of the system.

Laser oscillations occur when the gain is sufficient to overcome the loses in the laser amplifier. This has been previously considered in section 2.2 and the laser threshold condition derived was

$$N_2 = \frac{N_0}{2} - \frac{\log R}{4\sigma_0 L}$$

$$\text{or} \quad N_2 = \frac{N_0}{2} + \frac{\gamma}{2\sigma_0 L} \qquad (7.1)$$

where $$\gamma = -\log R^{1/2} \qquad (7.2)$$

is termed the loss coefficient per double pass through the ruby, and which is due to the external mirror.

If R = 100%, none of the laser energy generated in the amplifier can emerge and thus the output will be zero. Also if $R < 100\%$, then the output will also be zero when R is defined by equation (7.1), since the system will only be at its threshold condition. Between these two extremes there must be a value of R for which the system output and efficiency is a maximum.

Equation (7.1) is in reality a description of an idealised laser, since only the losses due to the transmission of the external mirror have been considered and the internal losses of the laser material have not. If the total internal losses are denoted by γ', equation (7.1) becomes

$$N_2 = \frac{N_0}{2} + \frac{(\gamma+\gamma')}{2\sigma_0 L} \qquad (7.3)$$

and thus for any system optimisation both γ and γ' have to be considered.

Apart from system optimisation, it is also useful to know the total internal losses since this gives a method of comparing and evaluating different ruby materials. The usual method of grading ruby rods which has been adopted by most manufacturers is by the number of fringes per inch length, per inch diameter of ruby. This, in most cases, gives a misleading standard of ruby performance, since apart from the optical homogeneity, impurity absorption and scattering by line and point defects also contribute to the total internal losses.

The relation between the optimum external mirror reflectivity, the internal losses and the other system parameters has been determined as follows.

The maximum energy output per unit volume of ruby is

$$U_{out} = U_{in} - N_2 h\nu \qquad (7.4)$$

where U_{in} is the net energy absorbed per unit volume of ruby, N_2 is the threshold atom density in the upper laser level defined by equation 7.3, h is Planek's constant and ν the laser frequency, YARIV (1963).

The degree of coupling between the inside and outside of the laser amplifier must also be considered in respect to the energy out which is available externally. This is given by U_{EXT} per unit volume of crystal and is defined by:-

$$U_{EXT} = \frac{\gamma}{\gamma+\gamma'} U_{OUT} \qquad (7.5)$$

If equations (7.3) and (7.4) are substituted into equation (7.4) then

$$U_{EXT} = \frac{\gamma}{\gamma+\gamma'} \left[U_{IN} - \frac{N_0}{2} h\nu - \frac{(\gamma+\gamma')}{2G_0 L} \right]$$

The total energy output is given by U_{EXT} V where V is the volume of the laser crystal, this is denoted by E_{EXT} and

$$E_{EXT} = \left[\frac{\gamma}{\gamma+\gamma'} E_{IN} - \gamma B \right] \qquad (7.6)$$

where

$$E_{IN} = \left[U_{IN} - \frac{N_0}{2} h\nu \right] V$$

and $$B = \frac{hJV}{2G_0L}$$

The optimum value of γ is then found from equation 7.6

by equating $\frac{d(E_{EXT})}{d\gamma} = 0$ and

$$\gamma_{OPT} = \gamma' \left[\left(\frac{E_{IN}}{\gamma' B} \right)^{1/2} - 1 \right] \qquad (7.7)$$

From equation 7.7, E_{in} can be written

$$E_{IN} = B \frac{[\gamma_{OPT} + \gamma']^2}{\gamma'} \qquad (7.8)$$

If equation (7.8) is now substituted in (7.6) then the optimum energy output is found to be:-

$$(E_{EXT})_{MAX} = \frac{(\gamma_{OPT})^2}{\gamma'} B \qquad (7.9)$$

Therefore if an experimental curve of E_{EXT} as a function of R and hence γ is measured, then $(E_{EXT})_{MAX}$ and γ_{OPT} are determined. Thus γ' can be calculated from equation (7.9) and also E_{IN} can be calculated from equation (7.8) These

calculated values of E_{IN} and γ' can be substituted into equation (7.6) and thus E_{EXT} can be calculated over a range of γ. By this method the calculated curve will fit the experimental points at the point defined by $\left[(E_{EXT})_{MAX}, \gamma_{OPT}\right]$.

7.2 Experimental Arrangement.

Two complete laser systems were constructed for this work, one capable of accommodating ruby rods 6" or 6½" in length, the other capable of accommodating ruby rods of 2" to 3" in length.

The first system is shown in figure 29. It consisted of the elliptical focussing reflector shown in figure 11, of $\mathcal{E} = 0.38$ and with a foci separation $2a\mathcal{E}$ of 1.5"; this was mounted on an aluminium base plate. As it was required to use other than wedge end ruby rods, an external 90° roof prism was provided to act as an external 100% reflector for use with flat ended rods. At the start of this work it was indicated by IRD Co. Ltd., that this laser would be later required for Q- spoiling studies. To this end the 90° prism was mounted on the spindle of 115 volt 3-phase, 400 cycle per second electric motor, so to act as a spinning prism Q-switch when a future requirement so desired it. To drive the motor a 115 volt 3-phase power supply was constructed by IRD Electronics Group, this is also shown in figure 29. For normal laser operation the prism was locked in a position normal to end of ruby, this was done by the use of an auto-collimator. Provision was also made for the attachment of external reflecting mirrors, and the holder can be seen attached to one of the end plates of the cavity assembly.

The other laser system was constructed to a new design and consisted of a split-elliptical focussing cavity shown in figure 30. This was made from 1.85" inside diameter aluminium tube. Two end plates with centre holes of the same diameter as the outer diameter of the aluminium tube, were made. These were welded to the tube so that they were normal to the cylinder axis. The assembly was then cut down the middle, and the inner edges of the cylinder and end plates were accurately milled so that a total cut thickness of 0.15" was taken off the two portions of the split cylinder. This produced an approximate elliptical section of $\mathcal{E} = 0.4$ and with a line foci separation of 0.75". Screw thread attachments were fitted to both halves of the cylinder as shown in figure 29.

The complete laser system is shown in figure 31. The two halves of the split cylindrical reflector were held in position by using wing nuts, these bore against two end plates which also served to hold the flashtube and ruby elements. Provision was also made for an external 90° prism and mirror holders which are also shown in Figure 31.

This split cavity arrangement possessed several advantages over the original cavity design. It was possible to remove the two halves without disturbing the alignment of the system; it also facilited easier assembly of the flashtube and ruby. The focussing properties of the ellipse was also excellent.

When the flashtube and ruby were assembled with only one portion of the focussing cylinder in position, see figure 30, it was possible to see sharp images in their complementary positions.

Two kinds of external reflector were used, multidielectric coatings in the range 40% to 90%, below this value optically polished quartz and D.E.D.F. glass flats were used. These were lined up to end faces of the rubies with an autocollimator and the reflectivity coefficient was corrected for the contribution of the 7% ruby/air interface. The reflectivity values are given in Table 13.

TABLE 13.

Type	Measured Reflectance	Ruby Reflectance	Total Reflectance
	%	%	%
Dielectric	89	7	90
"	79	7	80
"	63	7	65
"	39	7	41
Quartz	7*	7	13
D.E.D.F.	18*	7	23
NONE	-	7	7

*Calculated from refractive index.

The two laser systems shown in figures 29 and 31, were then used for the determination of the output energy as a function of the external mirror reflectivity, for a number of ruby rods.

The following rods were used:-

A $6\frac{1}{2}$" x $^{5}/_{8}$" wedge ended ruby and 6" x $\frac{1}{2}$" flat ended ruby. These were used with the laser shown in figure 29, with a 10 kilojoule flashtube and measurements for 10 kilojoules input were made in each case.

A 3" x $^{1}/_{4}$" and a 2" x $^{1}/_{4}$" ruby, both with flat ends. These values were used with the laser shown in figure 31, the power pack used was a standard NELAS R1 1050 joule power pack with a built-in inductance of 100uH. The 3" ruby was used with a 3" arc length type T/E6/60/A2 Thermal Syndicate flashtube and measurements were made at 1050 joules input. The 2" ruby was used with a 2" arc length type T/E6/59/A Thermal Syndicate flashtube and measurements were made at 875 and 500 joules input.

Finally, to determine the effect of mirror misalignment, energy output measurements were made with the 3" ruby system described above, with a 40% reflecting mirror which was misaligned with respect to the end face of the ruby by up to 20 minutes of arc.

7.3 Results and Discussion

For the easier presentation and discussion of results, the different systems used for the energy input versus external reflectivity measurements are numerated as below:-

1 - 2" ruby 500 joules input

2 - 2" ruby 875 " "

3 - 3" ruby 1,050 " "

4 - 6" ruby 10,000 " "

5 - $6\frac{1}{2}$" ruby 10,000 " "

The energy output measurements are given in Table 14 below:-

TABLE 14

ENERGY OUTPUT (JOULES) AS A FUNCTION OF MIRROR REFLECTIVITY (R%)

System	R						
	7	13	23	41	65	80	90
1	-	-	-	-	0.15	0.19	0.14
2	-	-	0.12	0.37	0.55	0.45	0.23
3	0.62	-	1.45	1.60	1.20	0.86	0.50
5	20.9	23.0	24.0	21.0	15.9	10.1	5.6
4	31.0	33.0	32.6	30.4	22.5	16.0	8.2

From these results the maximum energy output $(E_{EXT})_{MAX}$, at the optimum values of R_{OPT} or γ_{OPT} were found. The value of β was calculated for each system, and then the constants $\gamma 1$ and E_{IN} were calculated from equations 7.9 & 7.8 These are shown in Table 15.

TABLE 15

System	E_{EXT} max Joules	(R) opt %	γ opt	β	γ'	E_{IN} Joules
1	0.20	78	0.124	1.6	0.124	0.80
2	0.55	65	0.125	1.6	0.135	1.45
3	1.6	40	0.458	1.6	0.210	3.4
4	33	15	0.940	7.2	0.190	48
5	24	20	0.804	11.5	0.310	45

These values of γ' and E_{IN} were then substituted in equation (7.6) and E_{EXT} calculated as a function of R and γ. These calculated values are given in Table 16.

TABLE 16

CALCULATED ENERGY OUTPUT (Joules) AS A FUNCTION OF MIRROR REFLECTIVITY (R%)

System	R								
	10%	20%	30%	40%	50%	60%	70%	80%	90%
1	-	-	-	-	0.03	0.12	0.18	0.20	0.15
2	-	-	0.22	0.39	0.49	0.54	0.54	0.48	0.33
3	1.03	1.40	1.56	1.60	1.56	1.46	1.30	1.00	0.60
4	33.3	33.4	32.3	30.9	28.8	25.9	22.7	17.2	10.2
5	22.9	24.0	23.3	22.0	20.2	17.7	15.1	11.0	6.1

The measured and calculated characteristics of systems 1 and 2 are shown graphically in figure 32. The measured and calculated

characteristics of system 3, 4 and 5 are shown graphically in figures 33, 34 and 35 respectively.

It is seen, that apart from the coincidence at the maximum energy output and optimum reflectance ordinate, excellent agreement was obtained between the theory and experiment. It is interesting to note that apart from the maximum the experimental points fall slightly below the calculated curves. This could not be due to experimental error since the effect was the same for all the measurements for all the five systems investigated.

The internal loss coefficient γ^1 should be a constant for any one ruby, and thus the measurements of γ^1 = 0.124 and 0.135 for systems 1 and 2 with the same ruby are in good agreement. The loss coefficient of the 3" ruby was measured as 0.21. The 6" ruby (system 4) appeared to be of superior quality than the $6\frac{1}{2}$" ruby (system 5) since their internal loss coefficients were calculated as 0.19 and 0.31 respectively.

These internal loss measurements are in reasonable agreement with other reported results. OHTSUKA (1966) measured the loss coefficient of 0.28 for a 2" ruby rod with 23 cms separation between reflecting mirrors. This value was calculated by a similar analysis as described in section 7.1, except the value of R was kept fixed, and the variable was made to be γ^1 which was altered by additional losses induced between the reflecting mirrors. HANNA (1966), measured the internal loss of a 2" ruby as $T^1 = (1-R^1) = 25\%$, which is equivalent to a γ^1 of 0.15. The value was determined by comparison of thresholds of the R_1 and R_2 laser lines (defined in

section 2.3).

The importance of selecting the optimum value of mirror reflectivity is also demonstrated. The optimum reflectance is a function of the energy input to the system, for example the values are 80% and 65% for the 2" rod at 500 joules and 850 joules input respectively. It is also a function of the length of the ruby rod, the greater the length then the smaller the value required. Also the effect of Ruby internal losses have to be considered, the higher the internal losses the higher the reflectance value required.

The results of the misalignment experiment is shown in figure 36, they are normalised to one for a misalignment angle of zero. It is seen that alignment accuracy for the 3" ruby system considered was not very critical, the requirement being about $\pm$5 minutes arc for a 95% value of theoretical maximum output.

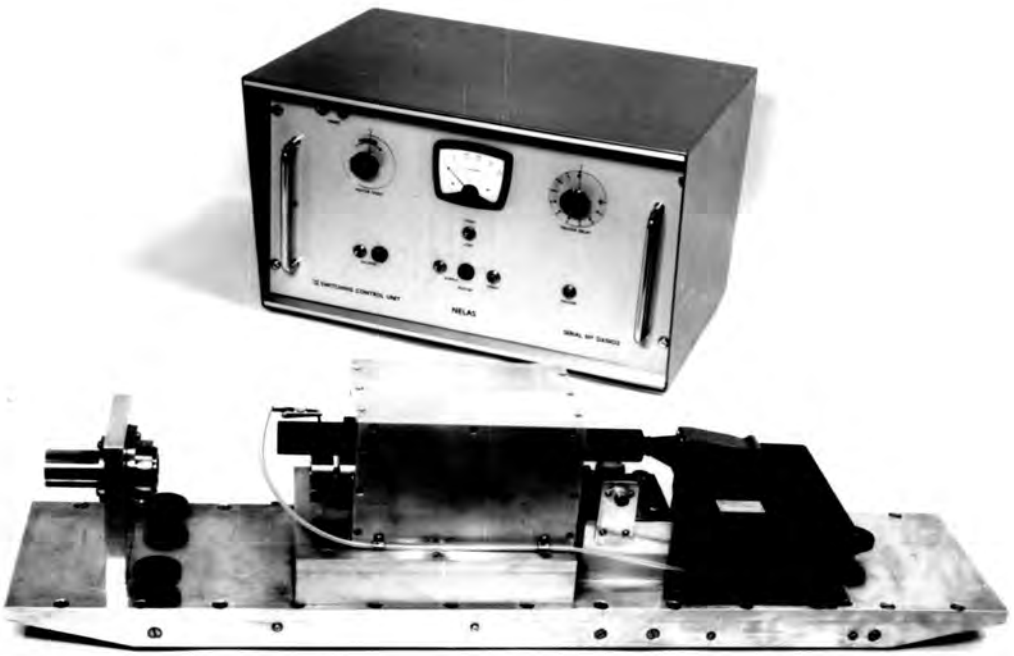

FIG 29 LASER SYSTEM

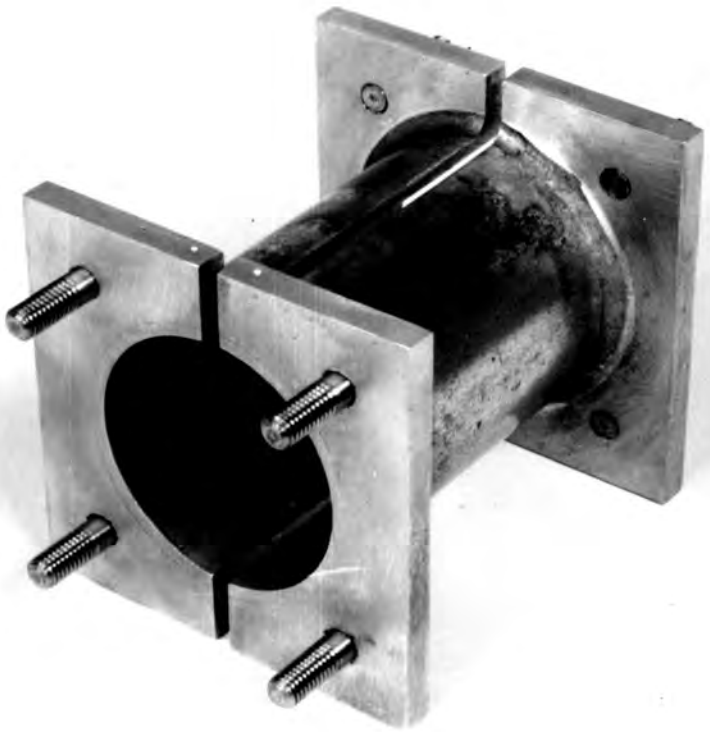

FIG 30 SPLIT ELLIPTICAL CAVITY

FIG 31 LASER SYSTEM

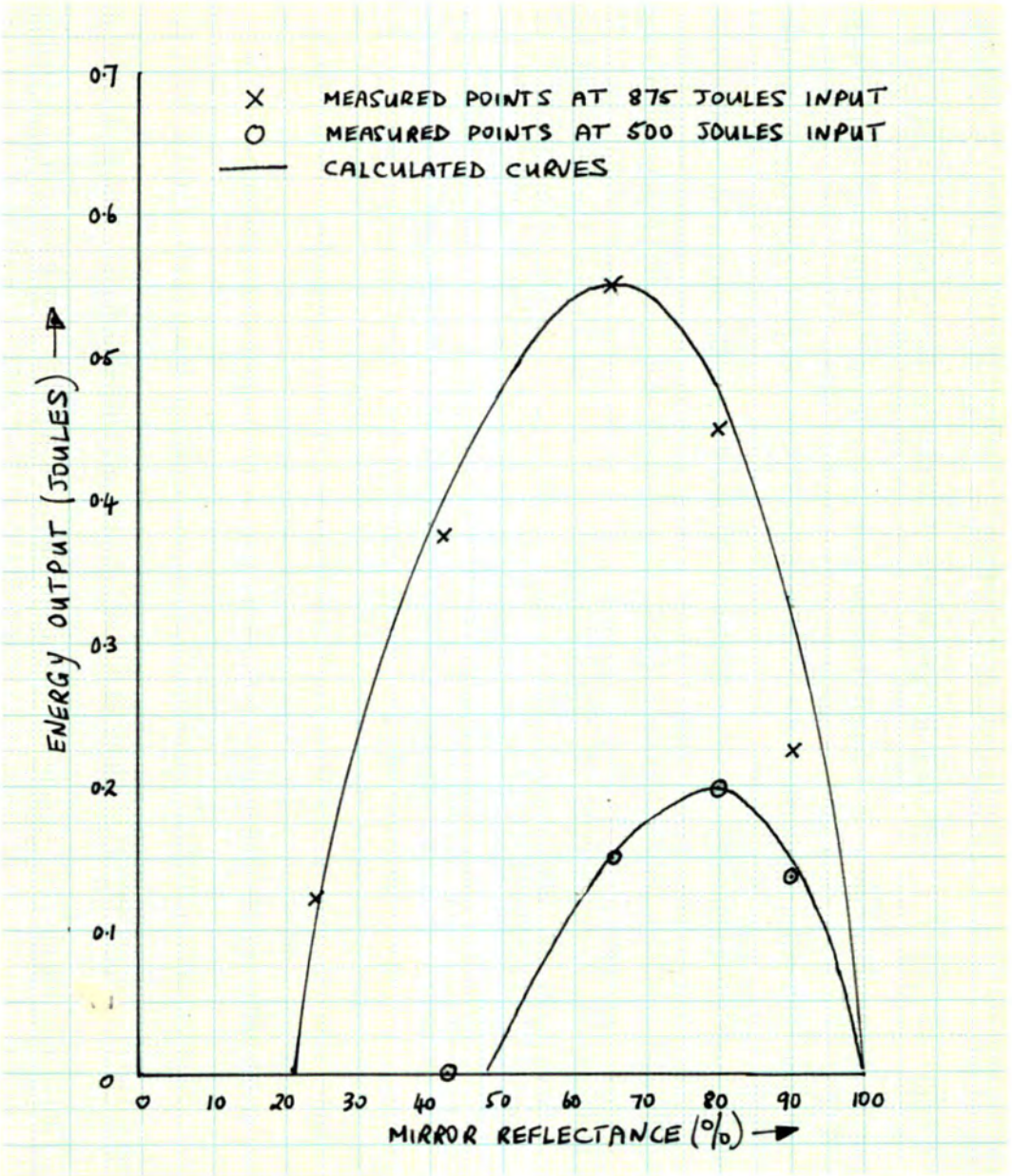

FIG 32. ENERGY OUTPUT OF 2" RUBY AS A FUNCTION OF EXTERNAL MIRROR REFLECTANCE.

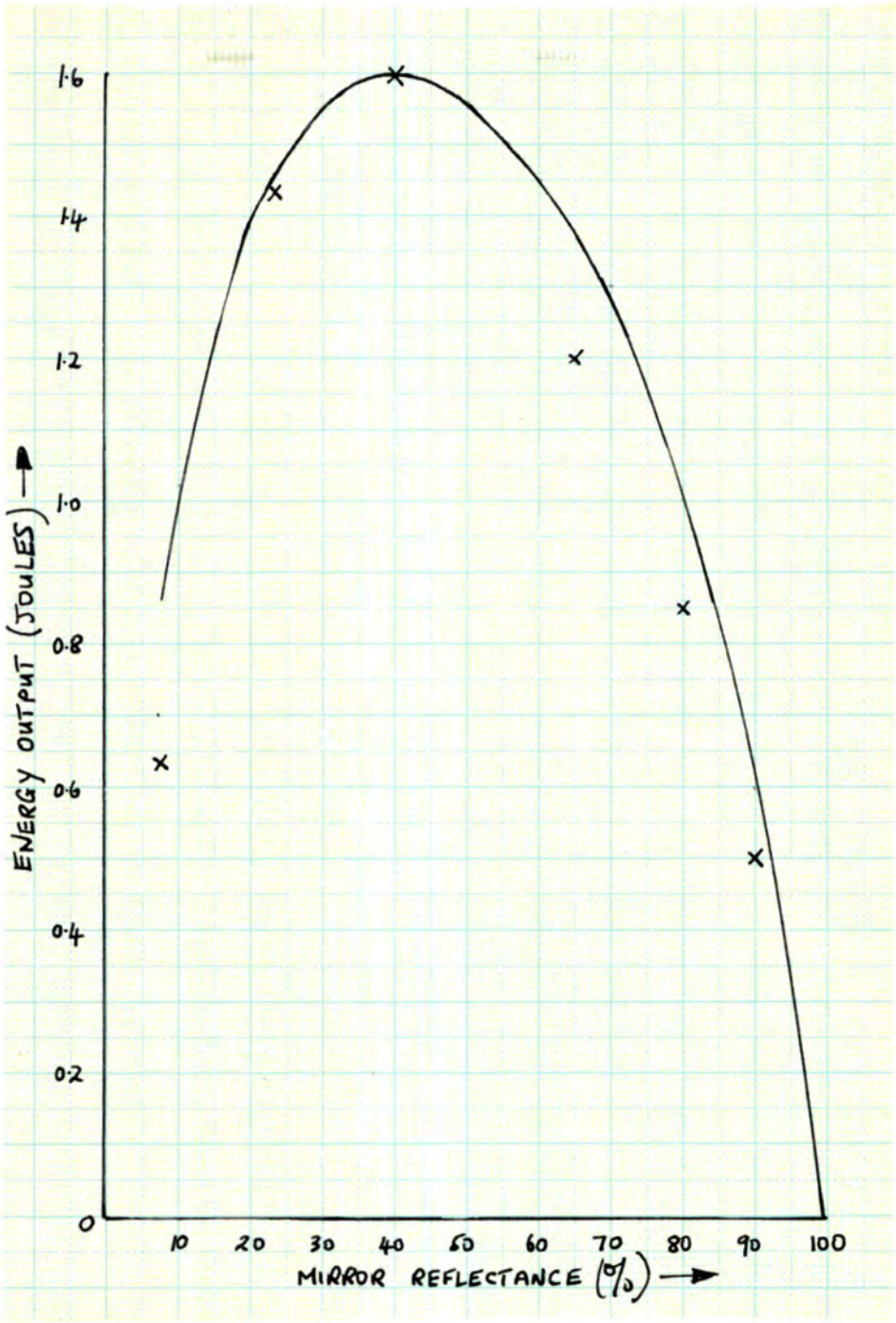

FIG 33 ENERGY OUTPUT OF 3" RUBY AS A FUNCTION OF EXTERNAL MIRROR REFLECTANCE

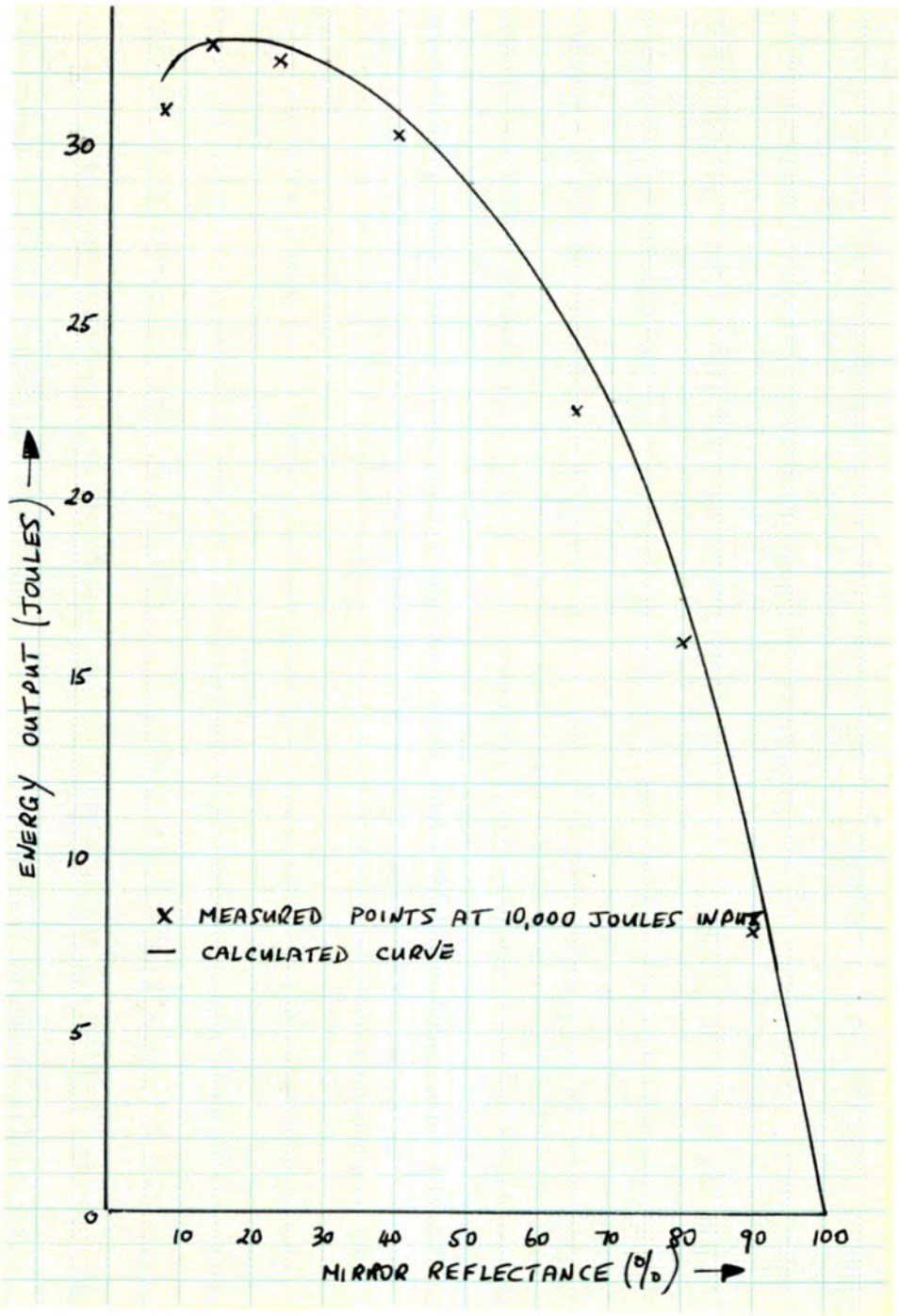

FIG 34. ENERGY OUTPUT OF 6" RUBY AS A FUNCTION OF EXTERNAL MIRROR REFLECTANCE

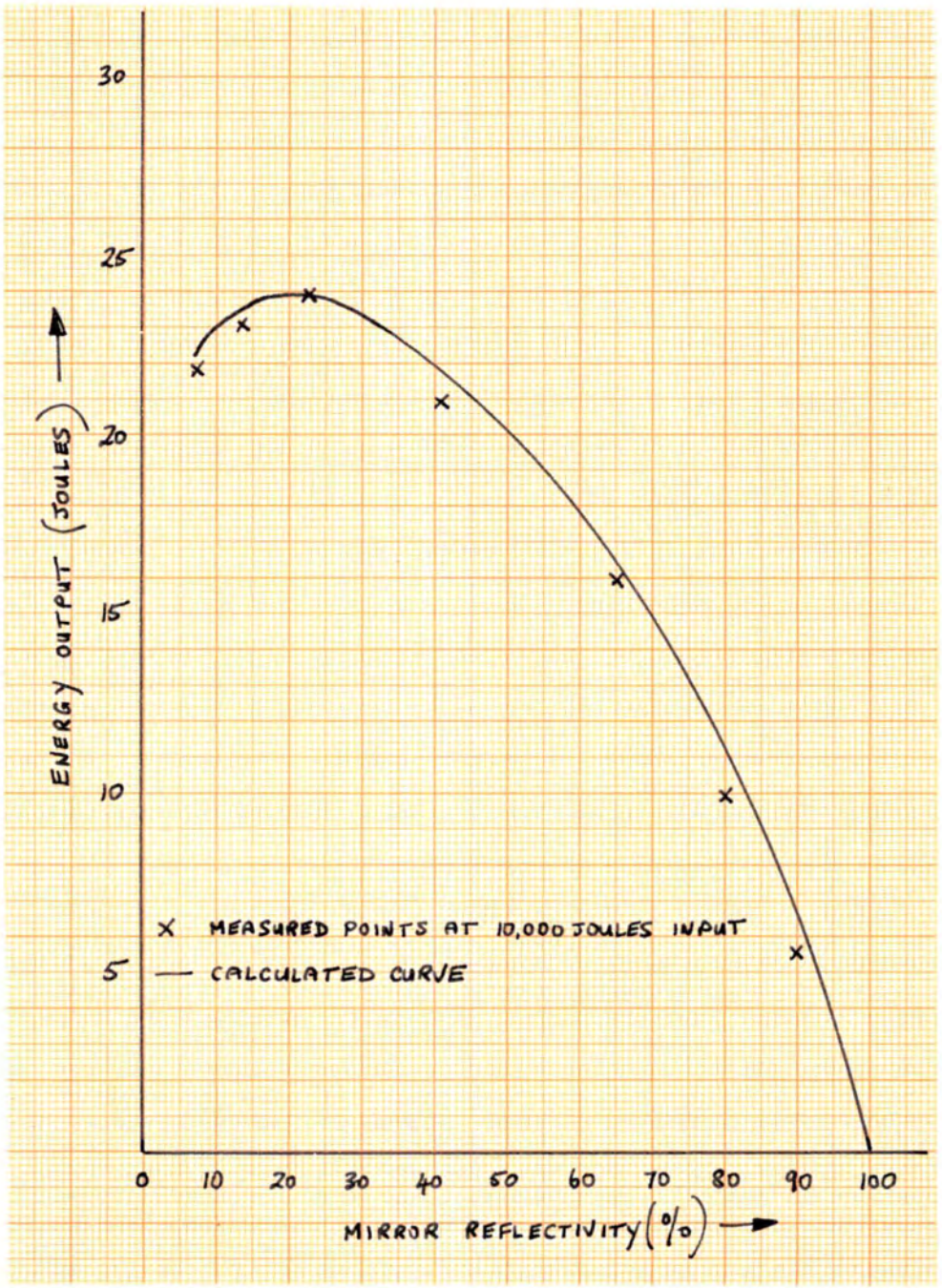

FIG 35. ENERGY OUTPUT OF 6½" RUBY AS A FUNCTION OF EXTERNAL MIRROR REFLECTANCE

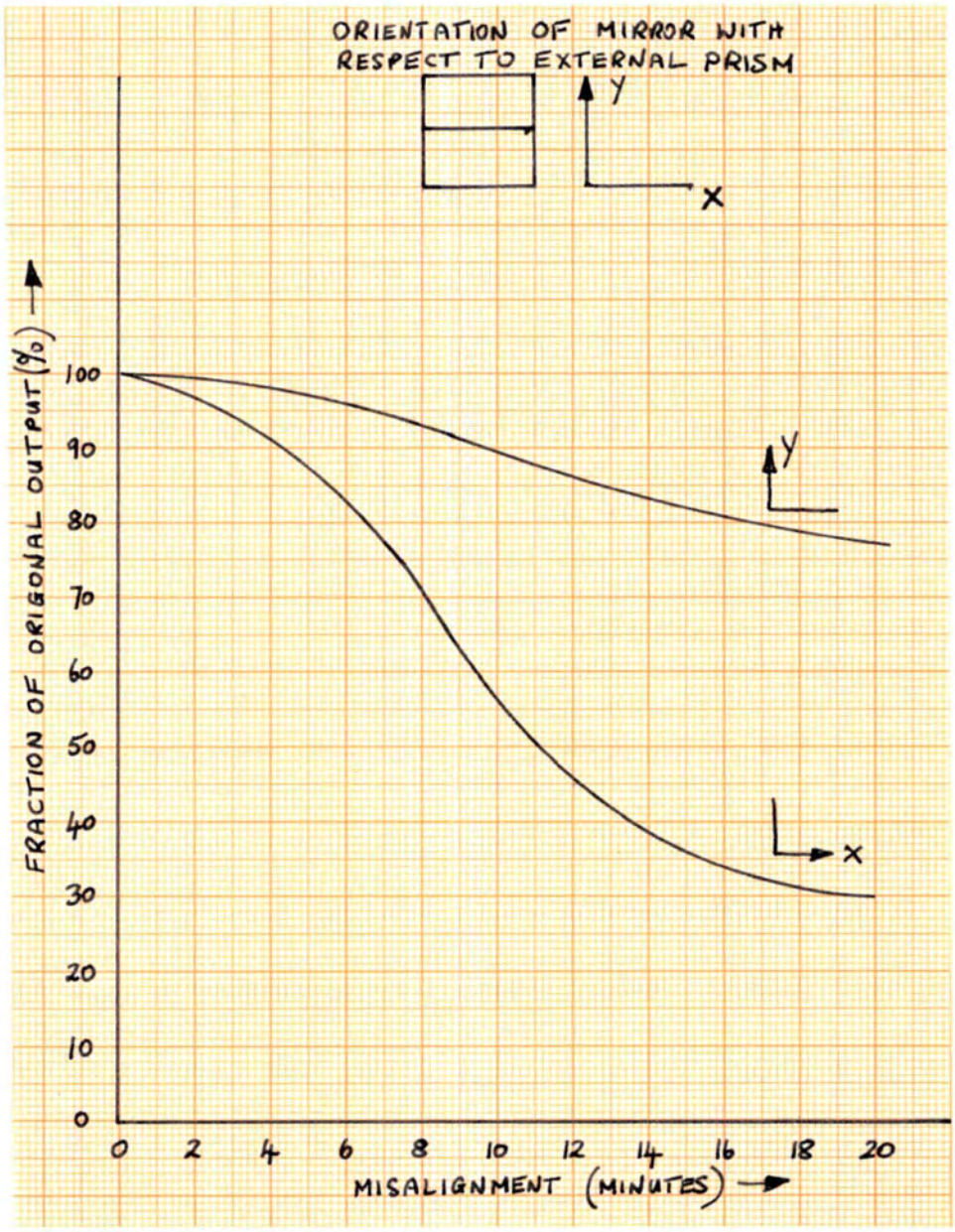

FIG 36 LASER OUTPUT ENERGY AS A FUNCTION OF EXTERNAL MIRROR MISALIGNMENT

CHAPTER 8. EFFECT OF TEMPERATURE ON OUTPUT ENERGY

8.1 Theoretical Considerations.

The fact that the energy output from the ruby laser is dependent upon crystal temperature has been well known since ruby laser systems first came into usage. The temperature of the ruby crystal rises considerably upon irradiation by the flashtube and this means that a constant output is difficult to maintain when the laser is fired at a fast repetition rate. For this reason artificial cooling has been introduced into many laser systems.

The variables which primarily effect the energy output of the ruby laser, and which are critically dependent on temperature are:-

(i) The lifetime T of the metastable ^2E state

(ii) The linewidth $\Delta\nu$ of the $^2E - {}^4A_2$ transition.

Measurements of the fluorescent quantum efficiency and lifetime of ruby were made by MAIMAN (1961). At 77°K and 300°K the measured fluorescent quantum efficiency was 100% and 70% respectively and the lifetime was 4.3 and 3.0 milliseconds respectively. These measurements were extended to 400°K by WITTKE (1962), and at 400°K a quantum efficiency of 20% was determined from which a lifetime of 1.3 milliseconds is inferred.

The manner in which the reduction of T with increasing temperature effects the pumping efficiency of the laser system has been considered by SOOY (1964) by approximating the ruby to a 3-level system and assuming the relaxation time between states 3 and 2 was much shorter than the relaxation time between states 2 and 1,

see Figure 1b; the following equation relating ground state population density, N_1, to the pumping energy was obtained.

$$\frac{N_1}{N_o} = \frac{1 + \frac{T}{t} fE \exp -(fE) \exp -(t/T)}{1 + T/t\, f E}$$

where E is proportional to the pumping energy which is assumed to be of rectangular shape and of duration t, and where f is some efficiency factor relating to the system in use.

This equation may be written in terms of the upper laser level population inversion N_2/N_o :-

$$\frac{N_2}{N_o} = \frac{T/t\, f E \left\{1 - \exp -(fE + t/T)\right\}}{1 + T/t\, f E}$$

As T is reduced, then the value of energy output function fE has to be increased to maintain a given population inverstion, and thus the overall efficiency of the system is reduced.

Studies of the fluorescent linewidth changes with crystal temperature have been made by SCHAWLOW (1961) and WITTKE (1962). Both the R lines of ruby become much sharper as the temperature is reduced, and for the R_1 line the measured values of linewidth are 21 cm^{-1} at 380°K, 0.3 cm^{-1} at 77°K and 0.07 cm^{-1} at 2°K.

The linewidth $\Delta\nu$ is related to the peak absorption cross section per atom, σ_o, by equation (2.13)

$$\sigma_o = \frac{2C}{\pi \Delta\nu N_o}$$

thus with increasing temperature $\Delta\nu$ increases and σ_o decreases. As σ_o decreases the threshold value of $\frac{N2}{N_o}$ (equation (2.17) increases and thus the overall system efficiency decreases.

It is therefore of interest and importance to determine the effect of temperature on ruby laser energy output and the following experiment was designed to determine this information.

8.2 Experimental Arrangement.

This work was done by the laser system shown in Figure 29 which was modified to enable the laser rod to be enclosed in a water sheath.

The water sheath assembly is shown in figure 37. The laser rod (7) was supported between concealed neoprene 'O' - rings in the end seals (2) and (9). These were made of brass and they were sealed into a quartz tube (3) of 28.3 mm bore by means of neoprene 'O' rings. Water passed into the system through a tube (5) and out of tube (1). Also a bleachable 'Q' spoiling dye could be passed into the cell provided in the centre of (9) through the tubes (4) and (6). This cell is bounded by walls of the brass and seal, the end of the laser rod and a transparent glass window. Under normal laser operation this cell was empty. A hole (8) was provided in the end seal (2) at the emitting end of the rod.

The two end plates of the focussing ellipse were modified so that the outer diameter of the quartz tube was a push fit into it.

The laser was assembled with the 6" x $\frac{1}{2}$" diameter ruby previously described in Chapter 7, and one quartz flat lined up with end face of the ruby gave a total output reflectance of 13%

which was near optimum for this ruby. The other reflector was a wedge ended 90° prism. A 10 kilojoule flashtube was used and all measurements were made at 10 kilojoules input energy.

The water sheath was connected to a combined hot and cold water tap, so that, by adjustment of the hot and cold water flow rates, any water temperature in the range of about 15°C to 75°C could be obtained. At each temperature, sufficient time (about 30 mins) was allowed to enable the ruby to attain thermal equilibrium with its surroundings, and the measurement of the laser output energy was made by previously described method.

8.3 Results and Discussions.

This water cooling arrangement was very effective in maintaining constant laser energy output under repetitive firing conditions, and no significant change occurred after firing 20 successive shots at 15 second intervals.

The measurements of laser output energy as a function of operating temperature are given in Table 17 below.

TABLE 17

Temp °K	Energy out (Joules)
290	48
305	31
317	20
330	10
340	0

It is seen that there is a marked dependence of output energy on the crystal temperature, and for this particular system the output fell to zero at only about 45°C above ambient temperature. This emphasises the importance of adequate cooling for the maintainence of both high system efficiency and constant energy output.

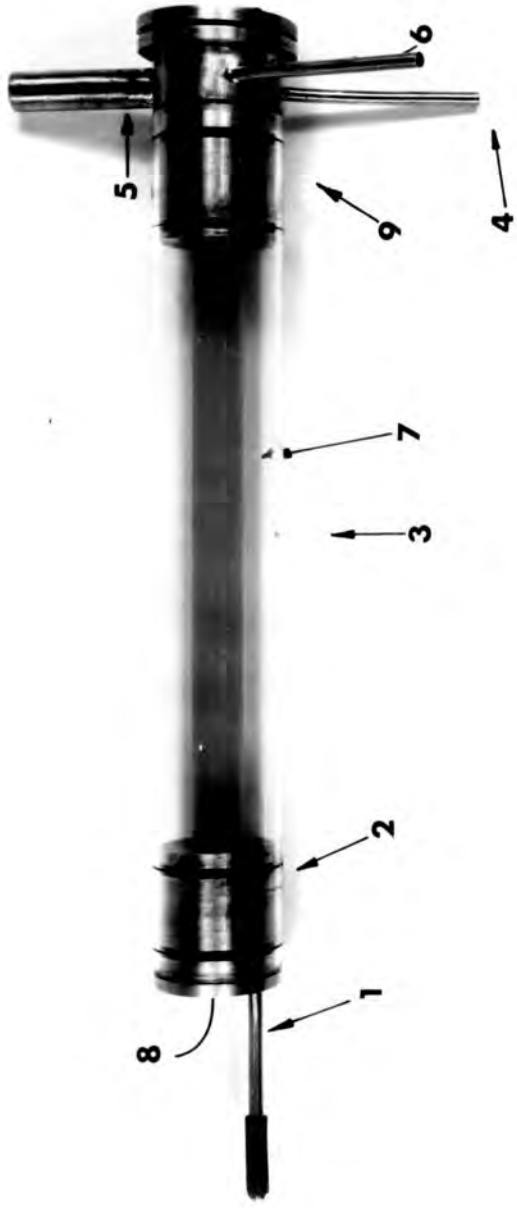

FIG 37 WATER SHEATH

CHAPTER 9. THE APPLICATION OF THE RUBY LASER FOR METALWORKING.

9.1 Introduction.

Laser research now falls into two fields; the development of basic laser equipment and the use of lasers for specific applications. Before a laser application can be considered, two questions must be asked. Can it be done only with the laser ? and, if not, can it be done more easily or economically by other methods ? From such considerations it is evident that the laser will probably find an immediate commercial application in the field of machining and welding.

Laser radiation is unique in several respects. It is virtually monochromatic and coherent, under suitable conditions it has a high degree of parallelism and compared to conventional light sources it can have a high energy density. For metal working two types of laser are available; gas and solid state. Depending on the method of pumping, gas lasers can emit either continuous or pulsed radiation; with the former continuous powers of several watts and with the latter method peak powers of about a hundred watts and mean power of about a watt, are commercially available. Solid state lasers, such as ruby, emit a single pulse of about a millisecond duration. Mean unfocussed powers of fifty kilowatts for pulse energies of up to a hundred joules, are readily available, while the technique of 'Q'-switching has resulted in pulses as short as twenty nanoseconds and with peak powers of several hundred megawatts. Solid state lasers have been made to operate continuously, but the power outputs are low, and much development work is required before they will be used for any commercial machining or welding application.

The use of the pulsed solid state ruby laser for both machining and welding has certain advantages over conventional fabrication techniques:-

1. The laser radiation is easily focussed and directed
2. No vacuum is required.
3. There is no beam momentum and thus no pressure on the workpiece.
4. The short pulse duration limits grain growth

The disadvantes are :-

1. The worked areas can be irregular due to off axis modes that may be generated.
2. The beam divergence, and thus the focussed beam diameter, are functions of the quality of the laser crystal and the degree of pumping above threshold.
3. Accurate control of output energy is difficult
4. The low pulse repetition rate
5. Comparatively high cost of capital equipment.

At the moment both laser machining and welding are in the experimental stage, but there seems every possibility that the technique will be developed for the fabrication of small components, particularly those made from materials which are difficult to work by conventional methods. For its successful development and utilisation it will be necessary to understand the mechanism of the processes involved, which are now discussed.

9.2 Control of the Laser Beam

For metalworking applications coherent radiation in the form

of a plane wave is an advantage because it can be directed at objects with only small diffraction losses, whereas only a small proportion of the radiation from a non-coherent source can be converted into an approximate plane wave.

It is possible, in theory, to focus the coherent light down to an area of very small dimensions, of the order of a few wavelengths in diameter. In practice the focal spot size is limited by the beam divergence. Zero beam divergence can only be obtained from a source of infinite aperture. For an aperture of d cms, taken as the diameter of the ruby rod, and for radiation of wavelength λ , the diffraction limited beam divergence is:-

$$\theta = \frac{1.22\lambda}{d} \text{ radians} \qquad (9.1)$$

For ruby it is known that the beam divergence can be a factor of a hundred greater than this, due to off-axis modes which are generated when $d \gg \lambda$, and scattering. For a given ruby rod length L cms, the maximum beam angle that could be expected is :-

$$\phi \approx d/L \text{ radians} \qquad (9.2)$$

By equating equations (9.2) and (9.1) it is possible to estimate the length of ruby (or the distance between external reflecting mirrors) which would be required for a diffraction limited beam to be produced. Taking d as 1 cm then this length is about 100 meters which is of course impracticable. In practice, to obtain a low beam divergence, certain mode selection techniques are now used; GIORDMAINE and KAISER (1964), and COLLINS and WHITE (1963).

The diameter, S cms, of the focussed laser beam is

$$S = f\theta \text{ radians} \qquad (9.3)$$

where, f cms, is the focal length of the focussing lens; for a typical value of θ of 10 milliradians then equation (9.3) gives S = 0.05 cm for a 5 cm focussing lens.

When θ is defined by equation (9.1) then,

$$S = f \frac{1.22\lambda}{d} \text{ cms} \qquad (9.4)$$

and if the laser energy is E joules, the thermal flux, T joules per cm^2, incident on the workpiece is

$$T = \frac{E}{\pi} \left[\frac{2d}{f\ 1.22\lambda} \right]^2 \qquad (9.5)$$

Figure 38 gives values of T defined by equation (9.5) above.

The average power density incident upon the workpiece, P watts per cm^2, is given by $T/_t$ where, t seconds is the laser pulse duration, which is usually of a millisecond duration, can be effected by 'Q'-switching for producing shorter than normal pulses. However, as will be shown for welding, it is very advantageous to have longer pulses and two methods have been used: multiple pumping and a pulse forming network for the flashtube supply circuit. The latter system is more efficient and more flexible than the ~~latter~~ FORMER. For a pulse forming network containing n sections, the line impedence is

$$R = \left(\frac{L}{C}\right)^{\frac{1}{2}} \Omega \qquad (9.6)$$

where L and C are the values of the inductance and capitance of each section. R should equal the flashtube arc resistance, R_o, for maximum power transfer to the flashtube. The pulse duration, t seconds, of the system is:-

$$t = 2n R_o C \qquad 9.7$$

Since Ro is typically 0.5 Ω, long pulse times can only be obtained

by having either large values of C or large numbers of sections. Using large capitances, t has been extended to 10 milliseconds for ruby lasers, BAHUN and ENGQUIST (1964)a.

9.3 Efficiency Considerations

Metal surface reflectivity is one loss mechanism which is common to both laser machining and welding processes. For normal light intensities at 6943A°, reflectivity losses can be large as 90% for metals such as copper. For high intensity laser light the true metal reflectivity is difficult to estimate since the nature of the surface is altered by the incident light beam. Measurements made by BAHUN and ENQUIST (1964)b, indicate that the true metal reflectivity losses for laser light are much less than expected from measurements made at normal light intensities. The probable explanation is that there is a small loss at the beginning of the laser pulse which is also associated with the melting of the metal surface, the remaining portion of the pulse is then absorbed by what could be a black body absorber.

Apart from the reflectivity losses (which for the purpose of future analysis are neglected), the machining and welding applications have conflicting requirements for high efficiency. For machining the efficiency M can be written as:-

$$M = \frac{\text{Energy used in vaporising metal}}{\text{Total energy supplied}}$$

For welding, the efficiency, W, can be written as:-

$$W = \frac{\text{Energy used in melting metal}}{\text{Total energy supplied}}$$

and the relationship between these factors is M+W = 1.

Estimates of M and W can be made by considering the idealised model of the laser energy flux incident on a point on the surface of a semi-infinite metal block. If heat losses due to changes in state are neglected, then at the end of the laser pulse at $t = t_m$, the temperature $T^{o}C$ above ambient, at a distance r cms from the surface is:-

$$T = \frac{q}{2\pi Kr} \quad \text{erfc} \left\{ \frac{r}{(4\alpha t_m)^{\frac{1}{2}}} \right\} \qquad (9.8)$$

where α is the thermal diffusivity $cm^2 sec^{-1}$, K the thermal conductivity cal $cm^{-1} {}^{o}C^{-1} sec^{-1}$ and q the mean laser power density equal to E/t_m. The radius r_B of the boiling point isotherm T_B can be found from equation 9.8, and an estimate of the fraction of the incident energy used in vaporising metal can be found from the total energy in the region $0 < r < r_B$ for which $T > T_B$. This fraction, M, is given by :-

$$M = \frac{1}{E} \int_0^{r_B} 2\pi r^2 T \rho c \cdot dr \qquad (9.9)$$

where ρ is the density gm cm^{-3} and c the specific heat cal $gm^{-1} {}^{o}C^{-1}$

Equation (9.9) was evaluated for copper and iron, high and low thermal diffusivity metals respectively with almost identical boiling points. The results are shown in figures 39 and 40 respectively, for various values of laser energy and pulse duration. From the figures can be seen the importance of a short pulse duration and low metal thermal diffusivity for high values of machining efficiency M. Conversely long pulse durations and high metal thermal diffusivities are important for high values of melting or welding efficiency W.

9.4 Laser Welding

To ensure a good weld, it is necessary for the heat which is absorbed at the surface of the metal to be conducted through the parts to be joined without causing excessive vaporisation from the incident surface. The laser pulse must be long enough to allow the process to occur.

The optimum conditions for laser welding, can be found from thermal conductivity models, which have been set up to describe the process. The point source model discussed in section 9.3 is obviously an over simplification. The more realistic model is the temperature distribution in a metal thickness Z cms due to laser energy incident upon an area of diameter $r = 2a$ cms, on one surface. For this case the temperature distributions at the front and back surfaces at the points ($r = 0$, $Z = 0$) and $r = 0$ $Z = Z$) are given by CARSLOW and JAEGER (1959).

These solutions have been used by FAIRBANKS and ADAMS (1964) to obtain optimum laser welding conditions. If the temperature at the front at the point ($r = 0$ $Z = 0$) is T_F', and the temperature at the back at the point ($r = 0$ $Z = Z$) is T_B', then it was shown that there is an optimum value of laser pulse duration t_m, for any given total laser energy, for which T_B' is a maximum. If the time is longer, then T_B' is reduced since more heat is conducted away by the surrounding metal. If the time is shorter then there is a greater potential for lateral heat conduction because of the higher front surface temperature, and thus T_B' is again reduced.

As a result of this analysis the following results were obtained. For a spot diameter to material thickness ratio of 1 : 1, the optimum time to weld penetration is

$$tm = \frac{1.5\ Z^2}{\alpha} \qquad (9.10)$$

For a ratio of 2: 1 then

$$tm = \frac{0.5Z^2}{\alpha} \qquad (9.11)$$

The total energy requirement being about equal in each case.

The effect of making the ratio $>$ 2 : 1, produces very little decrease in t_m, but there is a considerable increase in the total energy requirement. It was thus concluded that for laser welding the optimum spot diameter to thickness ratio is 2 : 1 and the minimum laser pulse duration is then given by equation (9.11) Using this it is possible to calculate maximum thickness of metal that may be welded for a normal laser pulse of about 2 milliseconds duration. Typical values for copper and mild steel are 0.030" and 0.005" respectively.

The possibility of using continuously, operating lasers for welding operations has been considered by the author WHITEMAN (1965)a; and generally the low powers available make them unsuitable for this work. This can be demonstrated by considering the problem of maintaining a molten area of radius r_1, in a copper film of radius r_2, and of thickness Z. If it is assumed that the metal inside the cylinder of radius r_1, is at the melting point T_m, then the heat

leaving the cylinder, U watts, due to thermal conduction is:-

$$U = \frac{2\pi Z K T_m}{\log_e (r_1 / r_2)} \qquad (9.12)$$

For copper K = 0.94 cal cm^{-1} $^oC^{-1}$ sec^{-1}; and if r_1 = Z = 0.001 cm and r_2 = 1 cm then U is approximately 0.1 watt. If the heat losses due to reflection and radiation are also considered then a more reasonable estimate of the power required to maintain the molten film is about 1 watt; which is a reasonable figure for present day continuous lasers.

The seam welding of metal of any appreciable thickness has to be done with a series of spot welds. If the spot welding of 0.03" copper is required, then assuming a weld diameter of 0.06", about 30 welds to the inch would be required for the individual welds to overlap and produce a continuous weld. If a repetition rate of 1 pulse every 10 seconds were available, then a welding rate of about 1" per 5 minute would be achieved.

9.5 Laser Machining

One of the problems associated with laser machining is the prediction, from the laser pulse and material properties, of the penetration depth of the damage in the material under irradiation. With the heat transfer models, the maximum depth of the boiling point isotherm is used to calculate the penetration depth. Good agreement is obtained between theory and experiment for low beam energies of up to a few joules, BAHUN and ENQUIST (1964)a. For higher beam

energies large discrepancies occur and measured penetration depths are considerably greater than the calculated values. Also, the shape of the pit is conical and at high beam energies depth to diameter ratios as high as 10 : 1 have been measured, MISSIO (1964), whereas the heat transfer models discussed predict an approximately hemispherical pit. Other objections to the heat transfer models are that the back pressure resulting from the evaporating atoms would cause a considerable rise in the boiling point, which would make it more difficult in theory to vaporise any material at all; also for the short pulse durations of less than a microsecond generated by "Q" switched lasers, it is difficult to visualise any heat transfer process that could account for the considerable damage produced in this short time.

Because of these inadequacies, the author, WHITEMAN (1965)b, developed an electromagnetic wave model. When laser light, an electromagnetic wave, is incident upon a metal SURFACE, the energy density of the absorbed wave decays exponetially with distance from the metal surface, and most of the energy is absorbed in the skin depth. For metals, at optical frequencies the skin depth is of the order of 10 - 100Å. To explain how the energy wave can penetrate a distance much greater than the skin depth, it is assumed that metal is evaporated off the surface as soon as the energy density of the absorbed wave equals the binding energy of metal. This is a similar mechanism to that proposed for the penetration of metals by electron beams, SCHWARTZ (1964), for which the observed penetration is of the order of a 1000 times greater than the theoretical penetration depth.

This electromagnetic wave model differs from the thermal conduction models in that the binding energy of the metal is used to calculate the penetration depth. As the binding energy is the same as the latent heat of sublimation at room temperature (which is approximately equal to latent heat of fusion plus the latent heat of vaporisation), it would appear that the former model is more satisfactory since the binding energy of all metals is considerably greater than the thermal capacity cT_B, where c is the special heat. For copper the binding energy is approximately 80,000 cal per mole, while the product cT_B is approximately 15,000 cal per mole; for lead the figures are 48,000 and 10,000 cal per mole respectively. With the latter model the binding energy and thus the latent heats are neglected and only the product cT is used for determining the total thermal capacity of the metal.

In most cases, for high energy densities and short pulse times, it is reasonable to neglect thermal conduction losses, see figures 38 and 39; then for a parallel beam of light of diameter S cms and of energy E joules, incident on a metal surface, which has a binding energy of B joules per cm^3, the penetration depth is

$$x = \frac{4E}{\pi S^2 B} \quad \text{cms} \qquad (9.13)$$

In practice, to obtain high local power densities, the laser beam is focussed on to the metal surface with an optical lens, and, therefore as the metal surface 'evaporates', the energy density decreases because of the defocussing effect. If it is assumed that the surface

of the metal is initially at the position x = 0 and at the focal point of the lens of focal length f cms; the beam diameter at x = 0 is S cm and is defined by equation (9.3). For x > o the beam diameter is

$$S' = S + b\,x \qquad \text{cms} \tag{9.14}$$

where b is a constant given by approximately d/f, where d is the beam aperture which can be taken as the ruby rod diameter. The penetration depth x is found from:

$$\int_0^x (S')^2\,dx = \frac{4}{\pi B}\int_0^E dE .$$

from which:

$$x + \frac{b}{S}x^2 + \frac{b^2x^3}{3S^2} = \frac{4E}{\pi S^2 B} \tag{9.15}$$

For parallel beams for which b = 0, or for large values of S then equation (9.15) reduces to equation (9.13) and $x \propto E$. As $S \to 0$ then $x \propto E^{\frac{1}{3}}$, and for this case the penetration depth x is given by

$$x = \left(\frac{12E}{\pi B b^2}\right)^{\frac{1}{3}} = A_1 E^{\frac{1}{3}} \tag{9.16}$$

This can be compared with the value of x calculated from equation (9.8) for the condition $t_m \to 0$ which is

$$x = \left\{\frac{E}{T_B}\cdot\frac{1}{4\rho c}\right\}^{\frac{1}{3}}\left\{\frac{6}{\pi e}\right\}^{\frac{1}{2}} = A_2 E^{\frac{1}{3}} \tag{9.17}$$

For copper, taking typical values of $\rho = 9$ grms cm^{-3}

c = 0.1 cal gm^{-1} $^{o}C^{-1}$, T_B = 2700°C, B = 48,500 joules cm^{-3}, and taking b as 0.2 which is typical for a ruby system with a 5 cms focussing lens; then A_1 = 0.13 and A_2 = 0.04, this demonstrates the greater penetration depth which is predicted by the electromagnetic wave model which is more in line with experiment observations.

Figure 41 shows the calculated penetration depth, x, as a function of laser energy E, for S in the range 0 to 2000u and for b = 0.2 for copper. The experimental points are taken from a paper by MISSIO (1964). The high penetration points are for an unspecified small focussed beam diameter produced by a low beam divergence long cavity length ruby laser. The two low penetration points are for the same ruby but with the mirrors on the ruby, thus producing a much higher beam divergence and ~~smaller~~ LARGER focal area.

Further experiments were carried out with lead targets. The beam divergence of the ruby was measured as 10 milliradians. Two focussing lens of 50 mm and 100 mm focal lengths were used giving focal spot diameters 500u and 1000u respectively, for values of b of 0.2 and 0.1 respectively. The focussed beams were incident upon lead targets of about 1 cm total thickness. The penetration depth was determined by simply filing away the edge of the sample until the hole was exposed. The results of this work are shown in figure 42 which also shows the theoretical curves calculated from equation (9.15).

The results shown on figures 41 and 42 indicate that the relationship between x and E as defined by equation (9.15) may be correct.

9.6 Applications

It has been shown that, for both machining and welding applications, such parameters as pulse duration, total energy, power density and focal spot dimensions have to be carefully controlled. The simplest laser tool that could be made is a laser head with a simple focussing lens. This system would have several disadvantages in that the pulse duration would be fixed if a conventional flashtube pumping system were used, and the focal spot size would be dependant on the beam divergence and could only be altered to any appreciable extent by changing the focal length of the focussing lens.

For research work, laser metalworking tools must be a high degree of versatility. This could be obtained by having available pulse forming techniques to vary the pulse duration, the ability to vary the beam divergence and focal spot size by optical systems either inside or outside the laser cavity, a wide range of output energy and an efficient cooling system to ensure a rapid firing rate. Such tools will be expensive and the probable trend for production purposes will be the development of laser tools for specific applications, where the laser parameters required are previously determined from one of the more versatile tools which may exist in the larger research establishments. The reason for this is twofold: a tool designed for a specific application will be cheaper; and from an engineering standpoint, the tool would probably have to fit into some kind of production line, and its detailed design would depend upon the type and size of the component and its rate of arrival at the toolhead.

The laser is an excellent source of welding energy and, if used in the correct way, it should be possible to attain the fusion temperature of all metals. From the consideration of the characteristics of pulsed ruby lasers and of the thermal properties of the metals used, high diffusivity metals such as copper and aluminium are the most suitable for laser welding applications. To date the most successful welds that have been made are small spot welds in wire and sheet. Examples of some of these made with a small 1 Joule ruby laser with a manual focussing arrangement are shown in figures 43, 44 and 45. Figure 43 shows a thermocouple type weld of 0.002" copper wire, a wide range of similar welds were also made for a variety of other metals. Figure 44 shows the application of the welding of a fine tapping wire on to a selected turn of a potentiometer winding. Figure 45 shows the connection of a silicon chip transistor to its base with three gold plated kovar wires; a total of six welds were made.

For machining, the amount of metal removed is proportional to the incident energy, and the geometry of the machined area is dependent on the dimensions of the focal point. Thus, for accurate machining, it is essential that these two parameters are closely controlled. Also, the state of the metal surface governs, to some extent, the proportion of the incident energy that is absorbed. Rough blackened surfaces absorbed more energy than polished bright surfaces and, thus by the method of surface preparation, it may be possible to machine (or weld) difficult geometries without the use of special optical systems and beam stops.

The laser will probably find a more immediate application for machining rather than welding, as the short pulses required for efficient metal removal are more easily produced than the longer pulses which are required for welding. With the high energy densities now available, it is possible to vaporise all materials and even diamond can be accommodated, WHITEMAN and WILSON (1965). To date, the most successful application has been the drilling of small holes in difficult materials. Other suggestions have been the dynamic balancing of rotating devices, and the adjustment of the frequency of tuning fork controlled clocks, in situ. Two further applications are shown in figures 46 and 47. Figure 46 shows the application of a small Q switched laser for the etching of thin film microcircuits which were made by firing the laser through a tantalum mask. Figure 47 shows a thin film, mechanically spiralled, resistor. These initially spiralled to about 1% accuracy, and the laser was used to accurately adjust the end of spiral after it was hermetically sealed in a glass tube. A total of 50 resistors were trimmed, all to within 0.01%, with an average of four laser shots each.

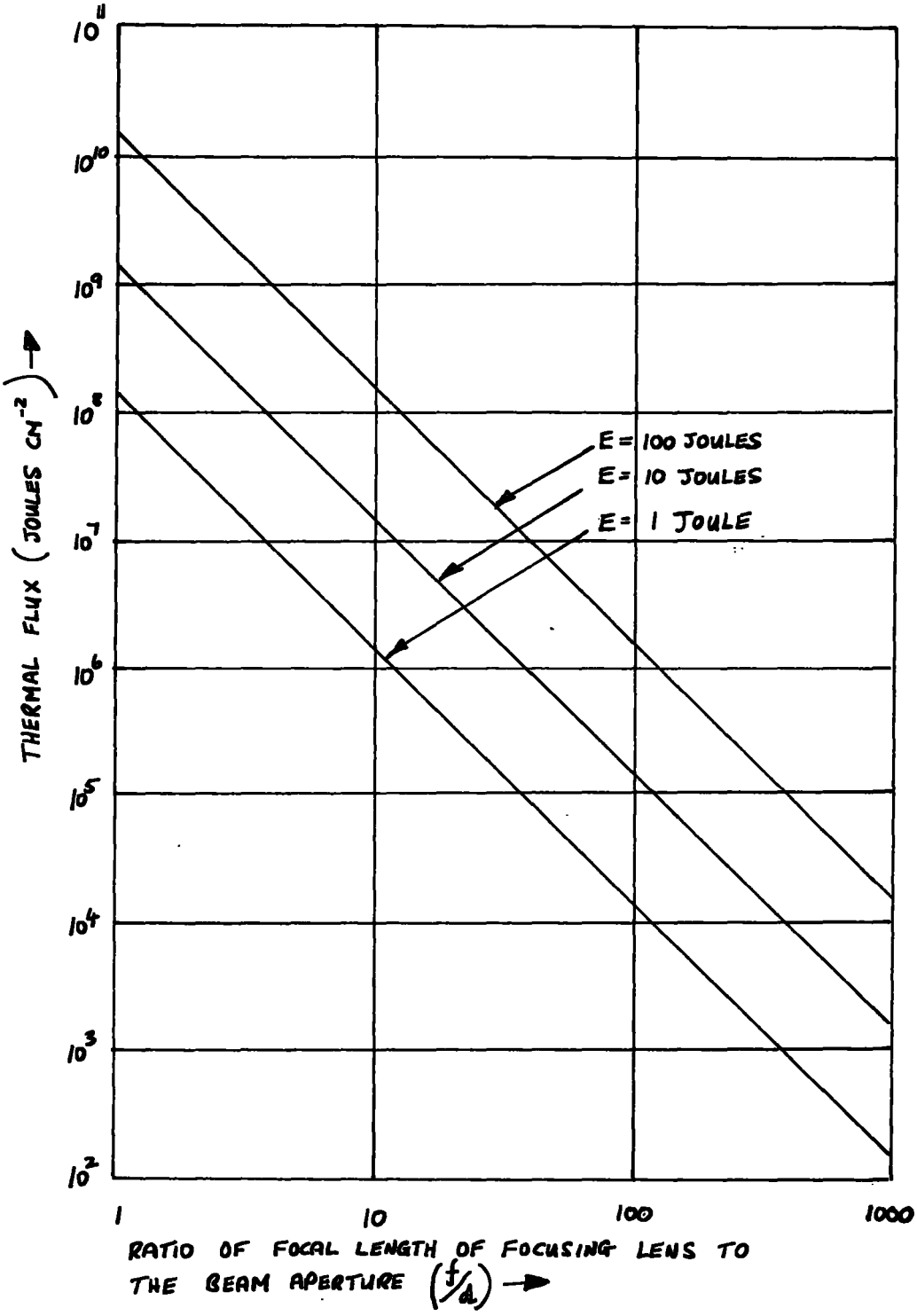

FIG 38 ATTAINABLE THERMAL FLUX FROM RUBY LASERS

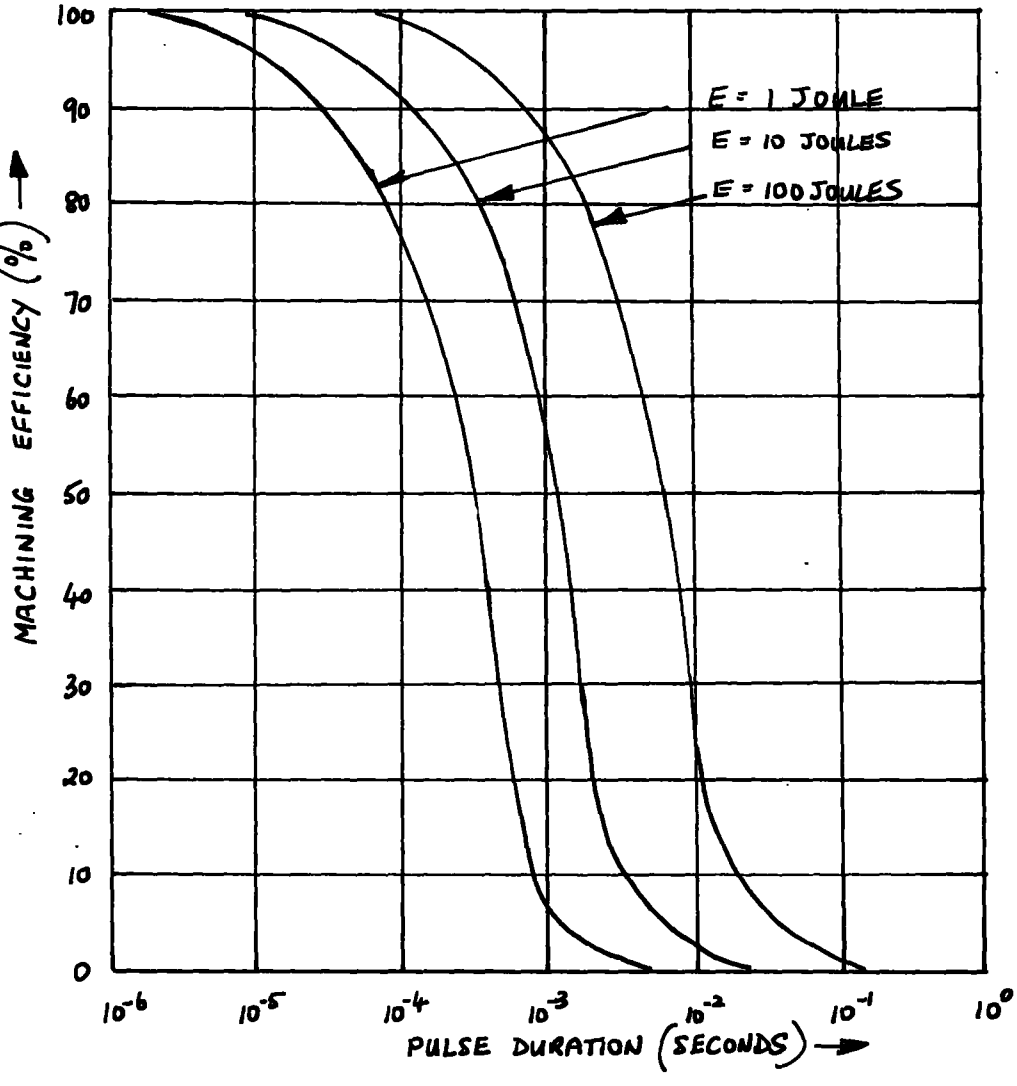

FIG 39 MACHINING EFFICIENCY AS A FUNCTION OF PULSE DURATION AND ENERGY FOR COPPER

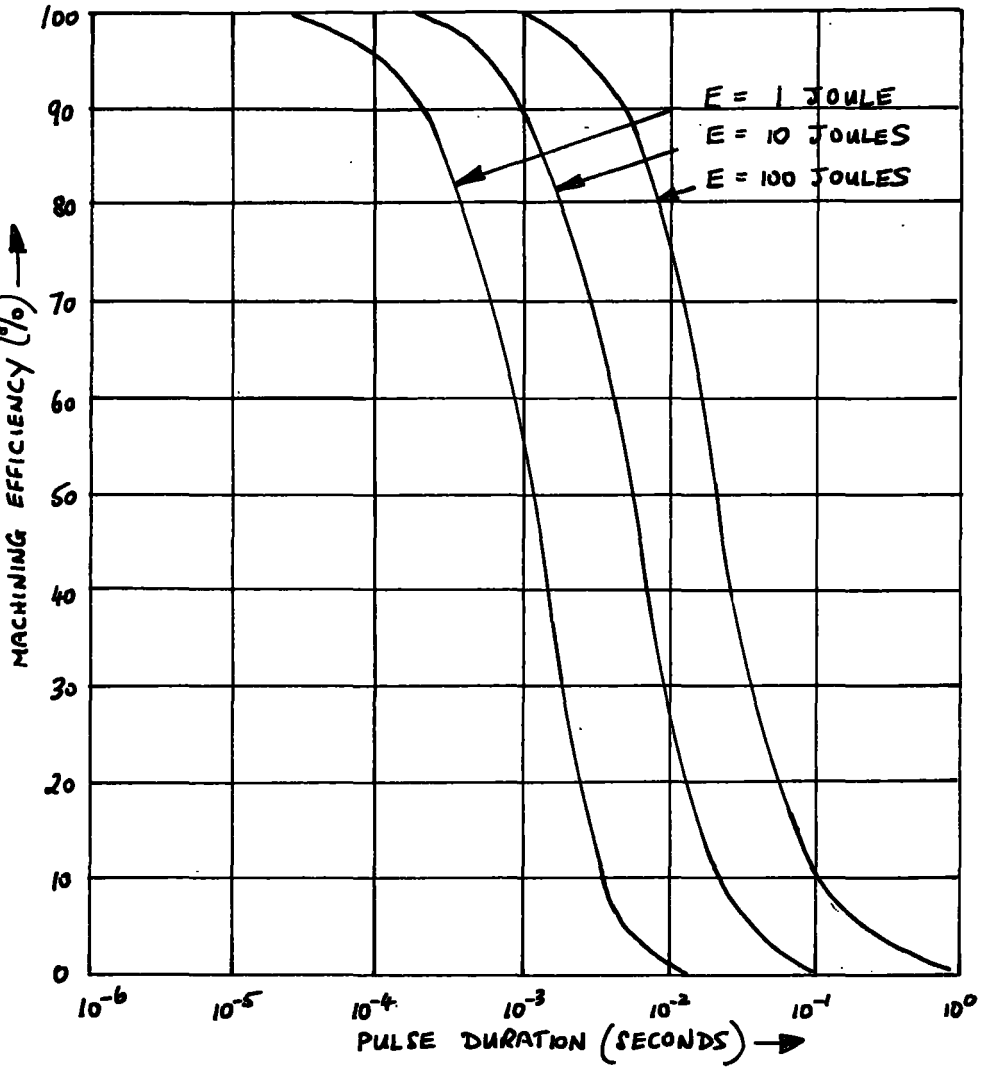

FIG 40 MACHINING EFFICIENCY AS A FUNCTION OF PULSE DURATION AND ENERGY FOR MILD STEEL

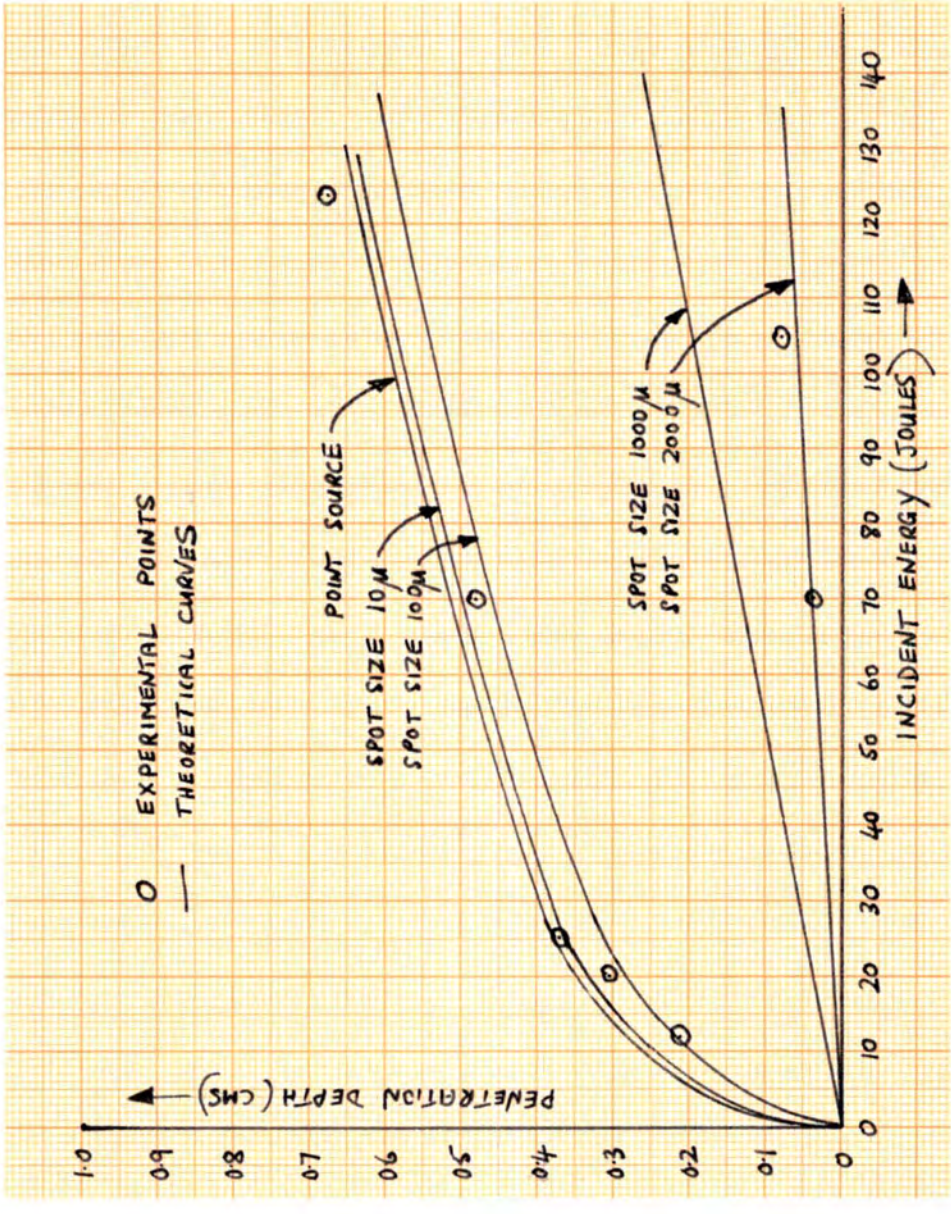

FIG 41 PENETRATION DEPTH AS A FUNCTION OF THE INCIDENT LASER ENERGY FOR COPPER.

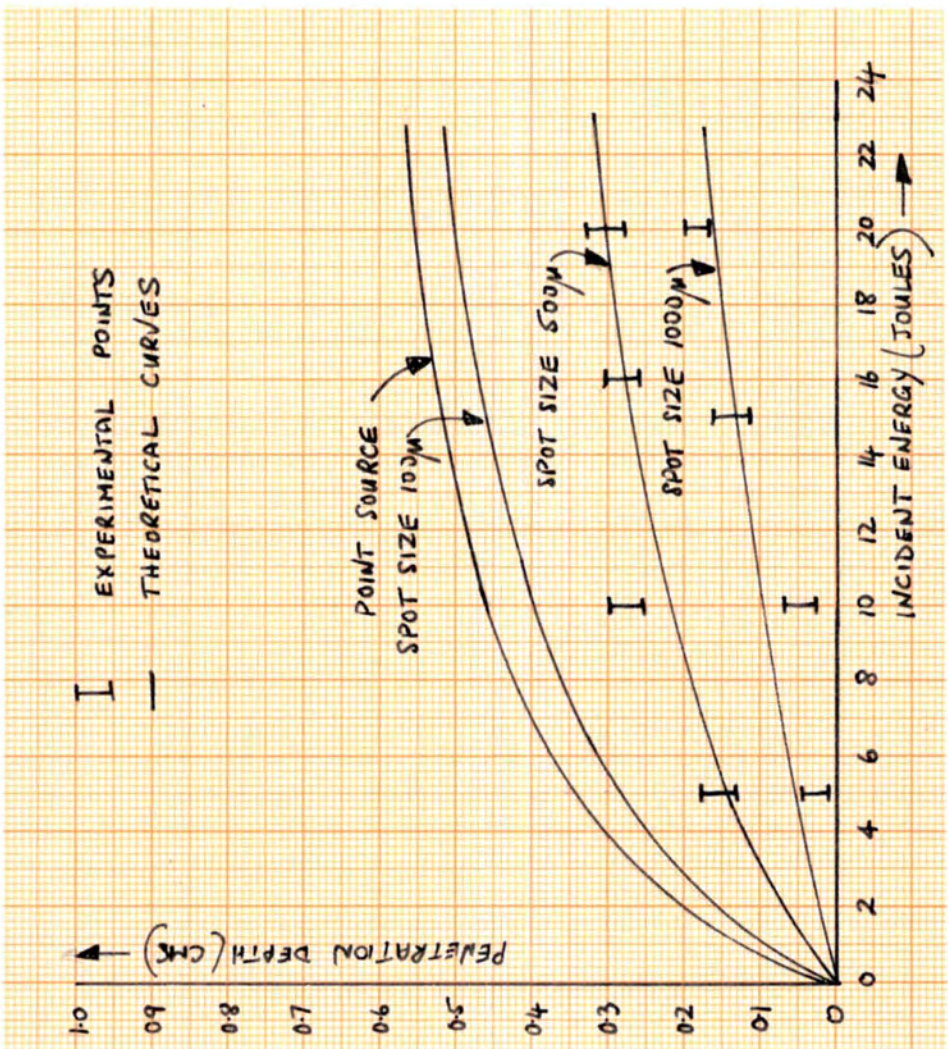

FIG 42. PENETRATION DEPTH AS A FUNCTION OF THE INCIDENT LASER ENERGY FOR LEAD.

FIG 43. LASER THERMOCOUPLE WELD

FIG 44. LASER WELDED POTENTIOMETER TAPPINGS

FIG 45 LASER WELDED TRANSISTOR

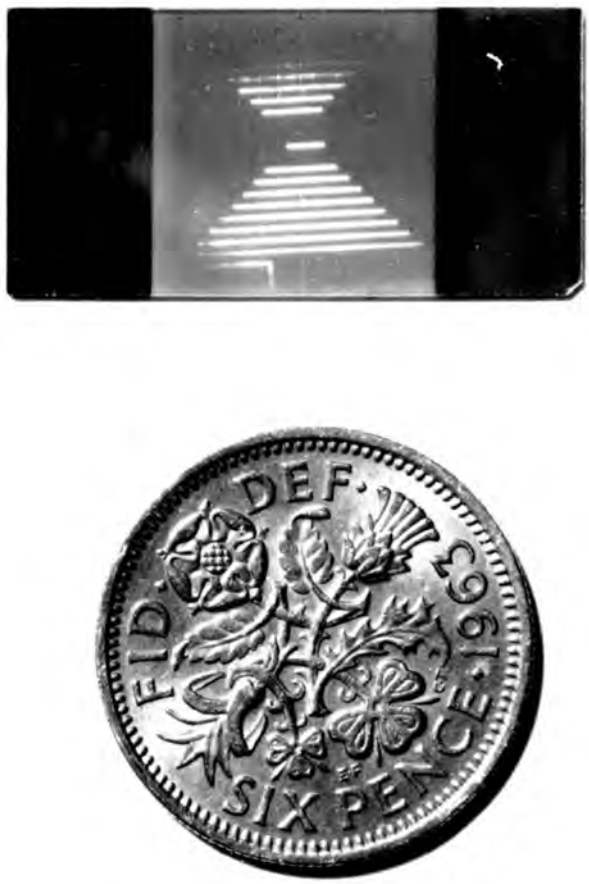

FIG 46. LASER ETCHED METAL FILM

FIG 47. LASER TRIMMED RESISTOR

REFERENCES.

BAHUN C.J. and ENDQUIST R.D.	Metals Eng. Quarterley 4 27 1964(a)
BAHUN C.J. and ENDQUIST R.D.	Journal of Metals 16 242 1964(b)
BASOV N. G. et al	Soviet Physics (J.E.T.P.) 1, 184, 1955
BROOKS R. E. et al	Proceedings Quantum Electronics Conf. Phoenix. To be published 1966.
CARSLOW H.S. and JAEGER J.C.	Conduction of Heat in Solids. Clarendon Press 1959.
CIFTON M. et al	Proc.Inst. Radio Eng. 49, 960, 1961
COLGATE. S.A.	Advance Quantum Electronics. Columbia University Press. pp 288. 1961
COLLINS. R.J. et al	Phys. Rev. Letters. 5, 303. 1960
COLLINS S.A. and WHITE G.R.	Laser and Applications. O.S.U. Press pp 96, 1963.
CONGLETON. R.S. et al	Quantum Electronics III Columbia University Press Vol. I pp 817. 1964
DE MARIA. A.J.	J. A. P. 34, 2984. 1963.
DEVLIN. G.E. et al	App. Opt. 1, 11. 1962
DEXTER. D.L.	Solid State Physics. 6, 653. 1958
EINSTEIN. A.	Phys. Zeit. 18, 121. 1917.
FAIRBANKS R.H. and ADAMS C.M.	Welding Journal 43, 975. 1964.
FRANKEN P.A. et al	Phys. Rev. Letters 7, 118. 1961.
GIORDMAINE J.A. and KAISER W.	J.A.P. 35, 3446. 1964.
GONCZ J.H.	J.A.P. 36, 742. 1965.
GORDON J.P. et al	Phys. Rev. 99, 1264. 1955.
GROVER F.W.	Inductance Calculations Von Norstrard. 1947.

~~HAIMAN T.H.~~	~~Phys Rev. 123, 1151. 1961~~
HALL R.N. et al	Phys. Rev. Letters. 9, 366. 1962.
HALL R.N. and CHURCH.	App. Opt. 2, 451. 1963.
HANNA D.C. et al	Quantum Electronics Conference. Phoenix 1966. To be published.
HELFRICH	J.A.P. 34, 1000. 1963
HELLWARTH R.W.	Advances in Quantum Electronics Columbia University Press. pp 334. 1961
JAVAN A. et al	Phys. Rev. Letters. 6, 166. 1961.
JOHNSON. L.F. et al	Phys. Rev. Letters. 11, 138. 1963.
KAFALAS P. et al	J.A.P. 35, 2349. 1964.
KECK P.H. et al	App. Opt. 2, 827. 1963.
KISS Z.J. et al	App. Phys. Letters. 2, 93. 1963.
KLEINMANN D.A. et al	Phys. Rev. 128, 1761. 1962.
LAX B. et al	Phys. Rev. Letters. 8, 166. 1962.
LENGYAL B.A.	An Introduction to Laser Physics John Wiley. 1966.
MAIMAN T.H.	Nature. 187, 493. 1960
MAIMAN T.H. et al	Phys. Rev. 123, 1151. 6. 1961
McCLUNG F.J. et al	J.A.P. 33, 3139. 1962.
McCLUNG F.J. and HELLWARTH R.W.	J.A.P. 33, 828. 1962.
McCLURE D.S.	Solid State Physics. 9, 400. 1959.
McEWAN G.	Private Communication To be published 1966.
McKENNA J.	App. Opt. 2, 303. 1963.
MISSIO D.V.	Machine Shop. P.318 July 1964.

NATHAN N.I. et al	App. Phys. Letters. 1, 62. 1962.
NELSON D.F. and COLLINS R.J.	Advances in Quantum Electronics Columbia University Press. pp 79. 1961
NORTHEND C.A. et al	Rev. Sc. Inst. 37, 393. 1966.
OHTSUKA Y.	Jap. J.A.P. 5, 74. 1966.
OPPENHEIM A.K. et al	Proc. Roy. Soc. 291, 279. 1966
PERLMAN D.E.	Rev. Sci. Inst. 37, 340. 1966.
QUIST J.M. et al	App. Phys. Letters 1, 62. 1962.
SCHAWLOW A.L.	American Quantum Electronics. Columbia University Press. pp. 288. 1961.
SCHAWLOW A.L. and TOWNES C.H.	Phys. Rev. 112, 1940. 1958.
SCHAWLOW A.L. and TOWNES C.H.	Advances in Quantum Electronics. Columbia University Press. pp 553. 1960.
SCHULDT S.B. and AAGARD R.L.	App. Opt. 2, 509. 1963.
SCHWARTZ H.	J.A.P. 35, 2020. 1964.
SOOY W.R. et al	Quantum Electronics III Columbia University Press. Vol. 2, pp 1103. 1964.
STEVENSON M.J. et al	J.A.P. 34, 500. 1963.
TERHUNE R.W. et al	App. Phys. Letters 2, 54. 1963.
VERNON-INGRAM H. et al	Brit. Med. Journal 1, 823. 1965.
WEBER J.	Rev. Mod. Phys. 31, 681. 1959.
WENZELL J.H.	'Lasers and Applications' O.S.U. Press ... p 115 (1966)

REFERENCES (CONTD)

WHITEMAN P.	Proceeding Conference on 'Fastening and Jointing Techniques' P.E.R.A. 1965 (a)
WHITEMAN P.	Proceedings of Conference on 'Machinability'. The Iron and Steel Institute. 1965 (b)
WHITEMAN P. and WILSON G.W.	Nature 208, 66. Oct. 2nd 1965.
WITTKE J.P.	J.A.P. 22, 2333. 1962.
YARIV A.	Proc. IEEE. 51, 1723. 1963.